FINAL REPORT

High Speed, Low Cost Fabrication of Gas Diffusion Electrodes for Membrane Electrode Assemblies

Contract Number: DE-EE0000384 BASF Fuel Cell, Inc. 39 Veronica Avenue Somerset, New Jersey, 08873	**Project Director:** Emory S. De Castro, Ph.D. Phone: (848) 209-3509 E-mail: Emory.DeCastro@BASF.com **Co-Authors:** Yu-Min Tsou, Ph.D., Zhenyu Liu, Ph.D.
Subcontractor: Dr. Vladimir Gurau Case Western Reserve University, Cleveland, Ohio	**Project Start Date:** July 1, 2009 **Project End Date:** June 30, 2013

Executive Summary

Fabrication of membrane electrode assemblies (MEAs) depends on creating inks or pastes of catalyst and binder, and applying this suspension to either the membrane (catalyst coated membrane) or gas diffusion media (gas diffusion electrode) and respectively laminating either gas diffusion media or gas diffusion electrodes (GDEs) to the membrane. One barrier to cost effective fabrication for either of these approaches is the development of stable and consistent suspensions. This program investigated the fundamental forces that destabilize the suspensions and developed innovative approaches to create new, highly stable formulations.

These more concentrated formulations needed fewer application passes, could be coated over longer and wider substrates, and resulted in significantly lower coating defects. In March of 2012 BASF Fuel Cell released a new high temperature product based on these advances, whereby our customers received higher performing, more uniform MEAs resulting in higher stack build yields. Furthermore, these new materials resulted in an “instant” increase in capacity due to higher product yields and material throughput. Although not part of the original scope of this program, these new formulations have also led us to materials that demonstrate equivalent performance with 30% less precious metal in the anode.

This program has achieved two key milestones in DOE’s Manufacturing R&D program: demonstration of processes for direct coating of electrodes and continuous in-line measurement for component fabrication.

Contents

Goals, Objectives, and Achievements

- Reduce cost in fabricating gas diffusion electrodes (GDE) through the introduction of high speed coating technology, with a focus on materials used for the high temperature MEAs that are used in combined heat and power generation (CHP).
    - Increased throughput for cloth based materials ~4x compared to target of 3x
    - Decreased labor cost by ~75%
    - Achieved DOE Manufacturing R&D Milestone (1.6); demonstrate processes for direct coating of electrodes on gas diffusion media
- Relate manufacturing variations to actual fuel cell performance in order to establish a cost effective product specification.
    - Dramatically increased uniformity and decreased defects by an order of magnitude so as to allow statistical process control

  - Used “six sigma” methodology to establish a product specification compared to pre-program selection of high performing lots or “cherry picking”.
- Use advanced quality control methods previously developed to guide realization of these two objectives.
  - Developed an on-line X-ray fluorescence analyzer to scan platinum loading and distribution on the web during the application step
  - Achieved DOE Manufacturing R&D Milestone (6.6); demonstrate continuous in-line measurement for MEA component fabrication.

Introduction

The basis of this project is to create gas diffusion electrodes at a far lower cost than those currently available. GDEs are critical components of membrane electrode assemblies and represent the highest cost subcomponent of the MEA. Cost reduction will be accomplished through development of a higher throughput coating process, modeling the impact of defects due to the higher speed process, and overcoming these limitations and providing a six-sigma manufacturing specification that relates performance to defects. The main focus of the effort is creating next-generation inks through advanced additives and processing methodologies. As part of our approach, we will also develop on-line QC methods such as determination of platinum concentration and distribution during the coating process. The on-line mapping of platinum will guide the ink development process and provide feedback on uniformity.

Approach

Gas Diffusion Electrodes are comprised of a gas diffusion layer coated with catalyst. The gas diffusion layer is simply carbon cloth or a non-woven carbon that has been coated with carbon black and serves as a current collector for the catalyst. For both the carbon black and catalyst, a hydrophobic binder is added to achieve critical porosity and hydrophobicity in the final structure. Of the carbon black, catalyst, or hydrophobic binder none are soluble in aqueous solutions. Aqueous solutions must be used as solvents since the use of organic solvents with a highly active catalyst is too dangerous in a production environment. Also, the hydrophobic binder is shear-sensitive, meaning it becomes less stable when pumped or subjected to shear forces in the coating applicator. Thus, the challenge in this program is overcoming the inherent physical limitations in these materials through advanced formulations and processing.

Our approach to solving this challenge begins with identifying key quality GDE metrics that relate directly to ink performance, develop an understanding of the forces behind ink stability, and introduce solution measurement methods that relate ink performance to the quality metrics. With more stable ink formulations, we have shown we were able to coat longer and wider webs at higher speeds. Since the ink can be made more concentrated and remain stable we can use less application passes and save cost. The ink development process is supplemented by two other activities that

ultimately lead to lower cost GDEs. We developed a model that will predict the impact of manufacturing variations on MEA performance, and used this model to determine the level of coating quality needed to maintain consistent current and voltage. Also, we created an on-line analyzer to tract the distribution of precious metal catalysts and guide more precise coating processes.

Results

Continuous in-line Measurement

Due to its cost, the single-most important on-line measurement when fabricating gas diffusion electrodes is platinum distribution and loading level. We selected XOS (X-Ray Optical Systems) as the subcontractor to construct the X-Ray Fluorescence (XRF) engine to be mounted on a motion-control rail. XOS has an XFR optic technology that facilitates high data acquisition rates. For example, a typical commercial hand-held XRF unit accumulates signals from 10-90 seconds, and more typically within 60 seconds. Considering a web moving from 3-6 linear meters per minutes, a 60 second data acquisition time would imply a spatial resolution of approximately 3-6 meters! The XOS engine signal accumulation target was 250 milliseconds, which could provide a spatial resolution of approximately 2.5 cm at the higher coating speed. This higher speed for data collection is due to the special optical technology of XOS. The XRF head features an innovative X-ray focusing device that collects large solid angle of X-rays and focuses them onto a small spot. This allows a high-intensity excitation beam to be achieved with a low power, air-cooled X-ray tube. When combined with the state-of-the-art detector technology as used in the system, it allows a fast and accurate mapping of the catalyst coating levels of the GDE materials.

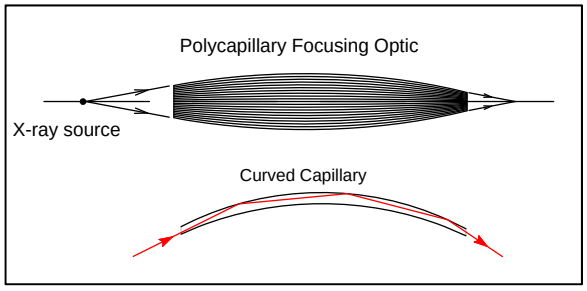

Figure 1. Illustration of control of X rays using polycapillary focusing optics.

A polycapillary optic consists of an array of curved glass capillaries that transmit X rays by multiple total external reflect. Figure 1 illustrates how a polycapillary focusing optic collects a large solid angle of X rays from a microfocus X-ray source and redirects them to the output focus. The hollow capillaries guide X rays effectively as long as the grazing incident angle at the interior surface is less than the critical angle θc, which is approximately equal to 30 mrad / E (keV). Such an optic typically has hundreds of thousands of channels with diameters ranging from a few micrometers to a few tens of micrometers. Small channel diameters are especially critical for efficiently transmitting higher energy X rays. The picturesin Figure 2 shows the typical size of the polycapillary optics and the structure of the cross-section.

The fabrication process began at XOS with assembly and preliminary testing of a discrete XRF unit ("XRF Engine") that was delivered to an engineering subcontractor (Progressive Machine and Design, Victor, NY) and incorporated onto a sliding rail unit with National Instrument's Labview software control (to form the Electrode Scanning System, or ESS). The ESS was evaluated on samples of gas diffusion electrode that were in static mode, i.e., not moving roll to roll. Various control algorithms were verified such as edge detection and splice detection, evaluation of any leakage radiation above State and Federal guidelines (none found), as well as preliminary calibration of the XRF signal. Having passed initial design specifications, the unit was then dismantled and installed on BASF's coating line.

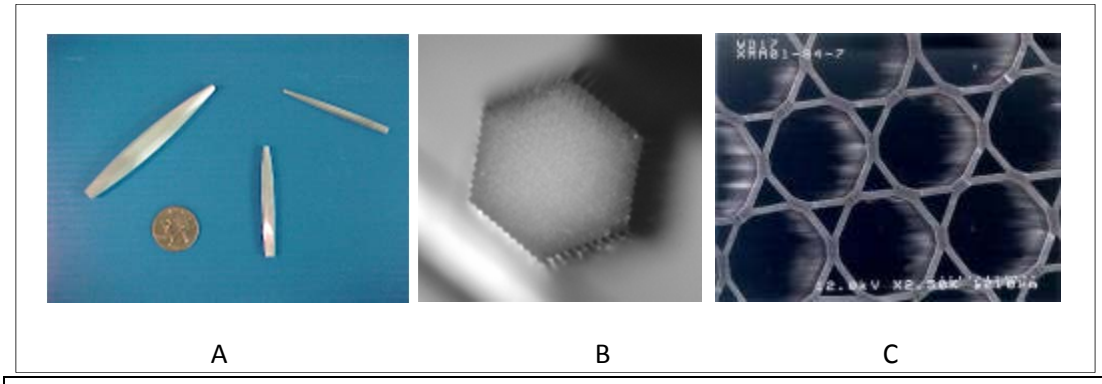

A B C

Figure 2.Photographs showing the typical size of polycapillary optics (A), an alignment jig that holds an optic assembled in a stainless steel enclosure (B), and SEM images showing the cross-section of a polycapillary optic (C)

Figure 3 is an image of the unit on-line. Starting with following the application of platinum catalyst on the GDL ("anode" for MEA), we have verified all safety modes of operation and debugged various software interface issues between either the unit control or interface with the control system of the coating machine. Table 1 summarizes the design goals and achievements of the system. We consider the signal accumulation time the most critical achievement: from this we are able to acquire a high data-density on a moving web through to the higher speeds that are a goal of this program. Similarly, the rail scan rate effectively determines the angle of the transect on the moving web: the higher the rail scan rate, the more "side to side" data can be obtained. We have achieved the capability to obtain <45^{o} transects at the listed rates. Finally, the lower detection limit as listed is more determined by the material that was being coated.

Figure 3. On-line XRF unit

Table 1: Summary of Design and Achieved

Characteristic	Design Point	Achieved
Signal Accumulation Time	25ms	10ms
Rail Scan Rate	10meters/s	20meters/s
Detection Limit	<1 gm Pt/m^2	1.7 gm Pt/m^2
Variation	+/-2.5% full scale	<+/- 1%

As part of the start-up plan, we followed a long-roll platinum-coating run with the XRF analyzer. Figure 4 and Figure 5 illustrate the importance of visualizing platinum distribution.

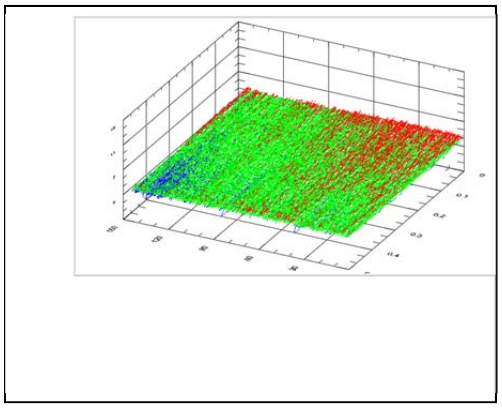

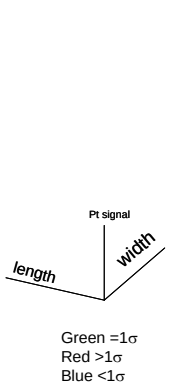

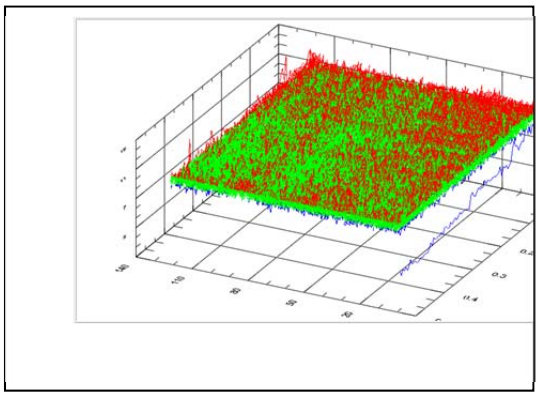

Figure 4. Initial set-up application of platinum catalyst

Figure 5. Adjust applicator

Following the legend, the red color represents a platinum loading >1 σ in distribution, while blue represents <1 σ. Figure 4 shows the initial application of platinum was higher across the web (transverse direction) with higher concentrations along the edge (red) and lower at one of the ends of the web (blue). Figure 5 demonstrates how the on-line XRF can then act as a guide for correction in setting the applicator: we were able to compensate through adjustments to the applicator and more evenly distribute catalyst (see red in Figure 5).

Another example is noted in Figure 6. For this example we show the output of the on-line analyzer as a function of the length of the roll and a serious of successive applications of catalyst. Two events are noted. The event noted as (1) was artificially induced and consisted of disengaging the applicator and leaving a section of the GDL uncoated with platinum. One notes in Figure 6 that this uncoated section can be identified even after subsequent applications of catalyst are applied. Event (2) consisted of an unplanned anomaly. In this example a coating defect began during early applications and was promulgated / amplified during subsequent applications. We are using this data-scan as part of our root-cause analysis for this coating non-uniformity.

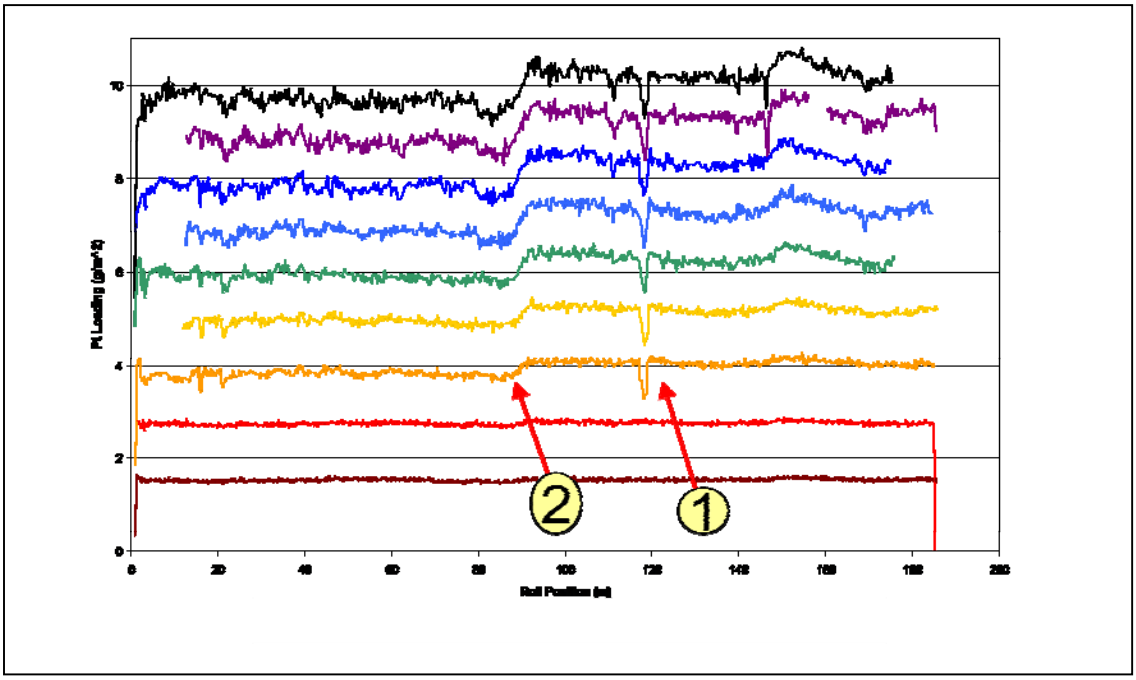

Figure 6. Output of Electrode Scanning System (ESS), on a coat by coat basis.

Model for variation sensitivity

Case Western Reserve University was provided with detailed characteristic data on membrane thickness, conductivity, electrode structure, etc. and using CFD constructed a model whereby the output is a polarization curve. We first constructed a baseline case to support the defect study.

Baseline performance of Celtec® -P1000;

The model parameters have been initially fitted to match the baseline of a Celtec® -P1000 MEA in a fuel cell operating at atmospheric pressure and 160°C with dry hydrogen and air at 1.2 and 2.5 anode and cathode stoichiometric ratios (Figure 7). Since this study focuses on the cathode catalyst layer operation, when fitting the model parameters to the experimental baseline, particular consideration was given to the parameters affecting the activation and ohmic regions of the polarization curve (parameters in the charge transfer and Butler-Volmer equations). The best fit to the experimental baseline was obtained for the model parameters shown in Table 2.

The model values for the Tafel slope and the thermodynamic open circuit voltage in Table 2 represent theoretical values at 160°C. The model value for the membrane proton conductivity is significantly lower than the value measured at 160°C in reference [1]. The measured value [1] corresponds to a membrane with a doping level of 32 mol phosphoric acid (PA) per polybenzimidazole (PBI) repeat unit that results from the sol-gel process before hot-pressing it into the membrane electrode assembly (MEA). During hot-pressing, some PA is squeezed out of the membrane into the adjacent GDEs and the resulting membrane conductivity reduces after assembly. It is reasonable therefore that the fit value for the proton conductivity in the present model is equal to the actual conductivity of a membrane in the MEA.

Table 2: Model parameter corresponding to a pristine MEA (fit values vs. measurement results)

Parameter		Model	Measured
Tafel slope for ORR, *b*		86 mV/decade	90 mV/decade (Ref. [2])
Thermodynamic open circuit voltage, E_0		1.15 V	-
Reference exchange current density times effective catalyst area per unit volume, aj_0^{ref}	5.5E-04 A/cm^3	-	
Membrane proton conductivity, σ	0.135 S/cm	0.225 S/cm (Ref. [1])	

Figure 7 shows good agreement between the numerical and experimental polarization curves in the activation and ohmic regions, with a small deviation in the highest current density region. This discrepancy is attributed to the mass transport limitations induced by the particular flow-field used in the model, having dimensions different from the undisclosed flow-field dimensions in reference 1.

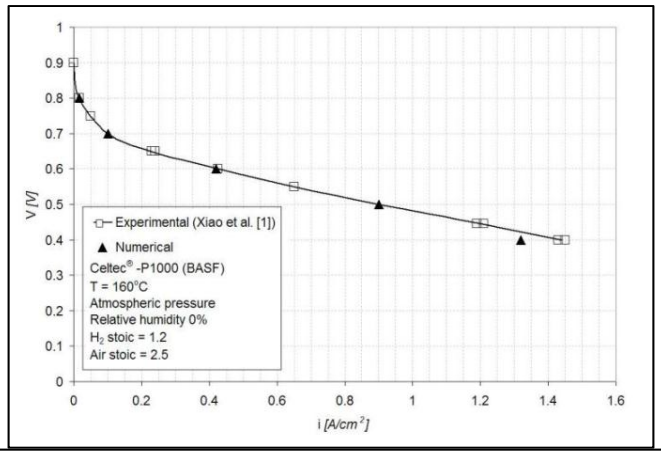

Figure 7. Numerical (this work) and experimental (ref. [1]) polarization curves for a Celtec® -P1000 MEA operated at ambient pressure and 160°C with hydrogen and air at 1.2 and 2.5 stoichiometric ratios

The calculation point for the subsequent analysis was selected at 0.5V (0.9A/cm^2) which corresponds to a relatively high power density and which exhibits good agreement between model and experimental results.

Study of agglomerate distribution or uncoated area in the cathode catalyst layer that would cause a 10% drop in performance;

During the catalyst layer fabrication process, the C/Pt-PTFE mixture organizes itself into clusters with a bimodal pore-size distribution in which the PTFE binder covers a fraction of catalyst sites. Only the Pt sites covered by PA are accessible by proton bearing complexes and are electrochemically active. The catalyst layer fabrication process results inherently into a number of defects consisting of agglomerates of the order of 1 µm, in which the Pt sites cannot be accessed by PA. To predict performance variation caused by manufacturing tolerances and defects in the cathode catalyst layer, a pristine catalyst layer was compared numerically with a hypothetical one prepared from an identical C/Pt ink (same Pt wt %) and having same catalyst loading (mg Pt/cm2), but exhibiting defects which cause a drop in performance. To achieve this, the effective catalyst area per unit volume (cm^2/cm^3) was changed in the Butler-Volmer equation until a 10% drop in performance was obtained at the calculation point. When the defects are much smaller than the characteristic size of the catalyst layer and when they are uniformly distributed, the total volume of defects that cause the performance decay can be calculated as:

$$V_d = \frac{a - a_d}{a} V \tag{1}$$

where a is the effective catalyst area per unit volume of the pristine catalyst layer (Table 3), a_d is the corresponding value for a catalyst layer with uniformly distributed defects and V is the catalyst layer volume. Note that while the reference exchange current density - j_0^{ref} is usually not deconvolved in calculations from the effective catalyst area per unit volume - a, it represents a constant which reduces in equation (1). Table 3 compares the effective catalyst area per unit volume for the pristine and defected catalyst layers, the total volume of defects and the number of defects per unit active area that induce a 10% drop in performance at the calculation point. The total volume of defects that cause a 10% performance drop at 0.5V would represent 39% of the total catalyst layer volume. The number of defects per unit active area in Table 3 was calculated as

$$\frac{n}{A_{act}} = \frac{\frac{a - a_d}{a} t_{cl}}{V_{1d}} \tag{2}$$

where n, A_{act}, t_{cl} and V_{1d} represent the number of defects, the catalyst layer active area, the catalyst layer thickness and the volume of a single defect respectively. The value in Table 3 was calculated based on a 30µm thick catalyst layer having spherical defects of 1µm diameter.

Table 3: Total volume of defects and number of defects per unit active area that cause a 10% performance drop at 0.5V.

	Reference exchange current density times effective catalyst area per unit volume, aj_0^{ref} $[A/cm^3]$ x10^{-4}	**Volume of defects** [% of total catalyst layer volume]	**Defects per cm^2 of active area**
Pristine catalyst layer	5.5	0%	0
Catalyst layer causing 10% performance drop at 0.5V	3.35	39%	46.6E+06

From these results we can conclude that only a very large defect, such as the disengagement of the applicator noted in Subtask 1 would cause a significant loss in performance. However, this model does not address the long term impact of this defect for durability.

Link actual defects to beginning of life performance;

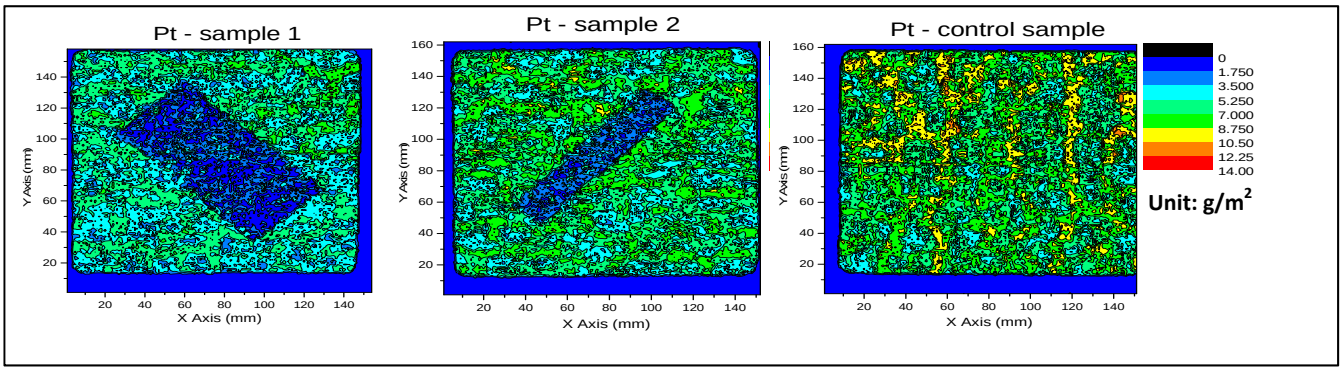

Figure 8. Anode Gas Diffusion Electrodes with 25% (Sample 1), 10% (Sample 2) and 0% (control) catalyst loss as measured by high resolution x-ray fluorescence. Catalyst loss area controlled through a template. Provided by X-Ray Optical Systems, Albany, NY. 1g/m^2 = 0.1mg/cm^2.

For this phase of the task, we intentionally introduced a surface defect on a gas diffusion electrode, characterized the defect with a high resolution XRF map, assembled a MEA, and evaluated this MEA for performance loss. Figure 8 is a comparison of the XRF maps for the control (no defect), a 10% catalyst coating loss, and a 25% catalyst coating loss. Figure 9 is the resulting polarization curve when these materials are incorporated into a high temperature MEA and run with the defective GDEs as a cathode. One notes that at 0.2A/cm^2, the current typically employed for micro combined heat and power (μ-CHP), the loss in power is 1.1% for a 10% defect and 2.4% for a 25% defect. The defect model above is in agreement with these results at under 0.4A/cm^2. Although a hypothesis at this time,

we attribute this robustness to coating loss a function of the dry state of the high temperature MEA, and not having to eliminate water, i.e., all water at the cathode is a vapor.

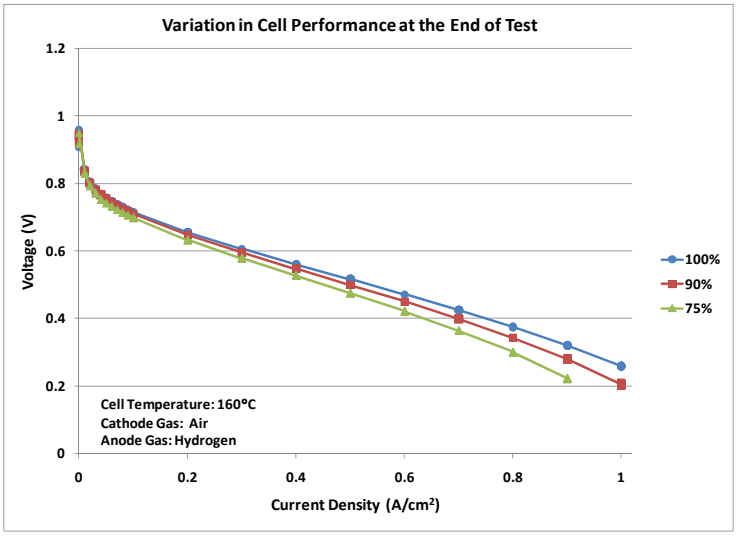

Figure 9. Polarization of control (100%), 10% defect (labeled 90%), and 25% defect (labeled 75%) at 160°C, Air/Hydrogen 2/1.2 stoichiometric flow, after 100 hours on line.

Full Length Roll Coating: Ink Stability

(1) Ink Compositions and Stability Issue

Electrode inks for high temperature Celtec® MEAs are primarily composed of carbon supported catalyst and PTFE, differing significantly from typical low temperature electrodes (inks) by the absence of ionomer. The necessity of PTFE provides both an advantage by being able to adjust and control hydrophobicity and porosity of the electrode structure and a disadvantage in having to develop an ink using colloidal suspension of PTFE. In addition to the tendency of agglomerate precipitation from component interaction in PTFE-containing inks, shearing forces in the coating environment such as slot die, gravure, or spraying can also lead to fibrillation of the PTFE with formation of extended agglomerates composed of PTFE or PTFE and catalyst. The need to coat longer rolls or higher line speeds requires us to have thorough understanding of n the nature of aqueous inks of carbon or carbon supported catalyst and PTFE.

(2) Initial Trial Runs with Existing Inks

Our initial approach to full length coating was to apply the pre-existing cathode ink formulation over an entire length (>240 linear meters at 0.5m across, as supplied) and assess the surface quality by counting the frequency of agglomerates (see Figure 10). Using prior QC criteria agglomerates were counted over a certain size. From this accounting we create a statistical profile of number of agglomerates per each 0.5m^2 GDE sheet that is reduced to average number of agglomerates per square meter. For ~ two full length rolls we averaged 18 agglomerates per square meter, which would lead to an unacceptable level for material yield once cut into pieces varying from 10 cm^2 to 1000 cm^2. For the anode inks and full roll coating, we ranged from 9 to 12 agglomerates per square meter (~ 4 full rolls).

Figure 10. Agglomerates

(3) Fundamental Colloidal Science Understanding of Ink Stability

There are two general approaches to stabilizing the ink suspension of PTFE and catalyst. The simplest is employing additives that increase the viscosity of the ink effectively increasing the settling time. Another is probing the forces that lead to instability and designing an ink composition that mitigates these forces. In either of these approaches, our selection of additives is guided by one simple rule: any additive must be largely removed/decomposed during the PTFE sintering step (>300^oC) and not interfere with catalyst activity. We began our efforts with probing the forces that lead to instability through measurement of the ink zeta-potential.

A short summary of zeta potential can be found in Wikipedia (http://www.wikipedia.org/) and is summarized here.

" Zeta potential is an abbreviation for electrokinetic potential in colloidal systems. From a theoretical viewpoint, zeta potential is the electric potential in the interfacial double layer (DL) at the location of the slipping plane versus a point in the bulk fluid away from the interface. In other words, zeta potential is the potential difference between the dispersion medium and the stationary layer of fluid attached to the dispersed particle.

A value of 25 mV (positive or negative) can be taken as the arbitrary value that separates low-charged surfaces from highly-charged surfaces.

The significance of zeta potential is that its value can be related to the stability of colloidal dispersions (e.g. PTFE and carbon supported catalyst). The zeta potential indicates the degree of repulsion between adjacent, similarly charged particles (catalyst) in a dispersion. For molecules and particles that are small enough, a high zeta potential will confer stability, i.e. the solution or dispersion will resist aggregation. When the potential is low, attraction exceeds repulsion and the dispersion will break and flocculate. So, colloids with high zeta potential (negative or positive) are

electrically stabilized while colloids with low zeta potentials tend to coagulate or flocculate." {phrase "PTFE and carbon…." inserted by author}

Since carbon or carbon-catalyst surfaces often contain oxygenates that contribute a charge, and some of these oxygenates can be protonated / deprotanated under our ink pH, we evaluated the impact of pH and zeta potential. Comparison of the pH vs zeta-potential plots for typical anode inks (platinum on carbon) to cathode inks (platinum-alloy on carbon) confirms the fundamental difference and stabilities of these inks. Figure 11 details the anode ink, and one observes that under the operational pH's, a zeta potential of -16mV to -20 mV is obtained, which is consistent with some stability of the ink. The measurements of the cathode ink of Figure 12 stands in contrast to Figure 11. Here the operating pH is at a charge that will lead to instability of the dispersion and flocculation: the visual agglomerate statistics cited above (18 vs 9 agglomerates per square meter) confirm this relationship.

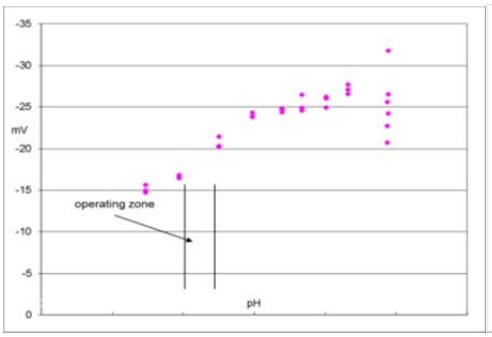

Figure 11. Zeta potential (mv) vs. pH of anode ink

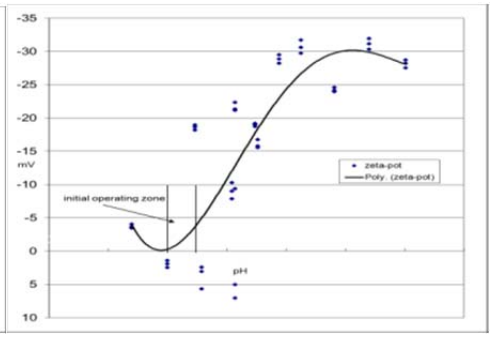

Figure 12. Zeta potential (mv) vs. pH of cathode ink (Pt-alloy/C)

When agglomerates formed during coating processes were analyzed, we also observed phenomenon that was consistent with the theory based on zeta-potential: significantly more agglomerates were collected for cathode ink than anode ink; and also the percentage of cathode catalyst in the collected ink was much higher than the corresponding percentage of catalysts in the ink solid content.

(4) Development of 1st Generation of Cathode Ink with Improved Stability

Armed with this insight, we began a search for an additive that would move the cathode ink to higher pH's, but not be so high as to destroy the alloy's integrity. Several potential additives were tried; of these, one additive demonstrated was able to control pH sufficiently to operate at absolute values of the zeta potentials consistently greater than 20mV and of a low enough pH to not damage the platinum alloy. Small scale replicate coating runs of ~40 linear meters each using our developmental coating machine were performed to assess average agglomerate and test for performance in a single cell. Under highly controlled conditions, the average agglomerate count was reduced to 1.2 per square meter! The measured average zeta-potential was – 28.5 +- 2.9 mv. Moreover, the rheology/viscosity of the solution in the modified cathode ink is also more desirable and it leads to consistent catalyst coating, so the number of coats to achieve target catalyst loading

was constant throughout numerous coating runs. However, while the additive was removed during the sintering cycle, the efficacy of removing other pre-existing additives needed for the formulation (surfactants, etc.) during electrode sintering decrease substantially and led to reduced performance. We initiated a sintering optimization program whereby heating cycles were varied to find the best condition for full removal of residuals. Figure 13 demonstrates our success in that no performance difference is noted between standard cathode ink formulation and the new, improved formulation employing an optimized sintering cycle.

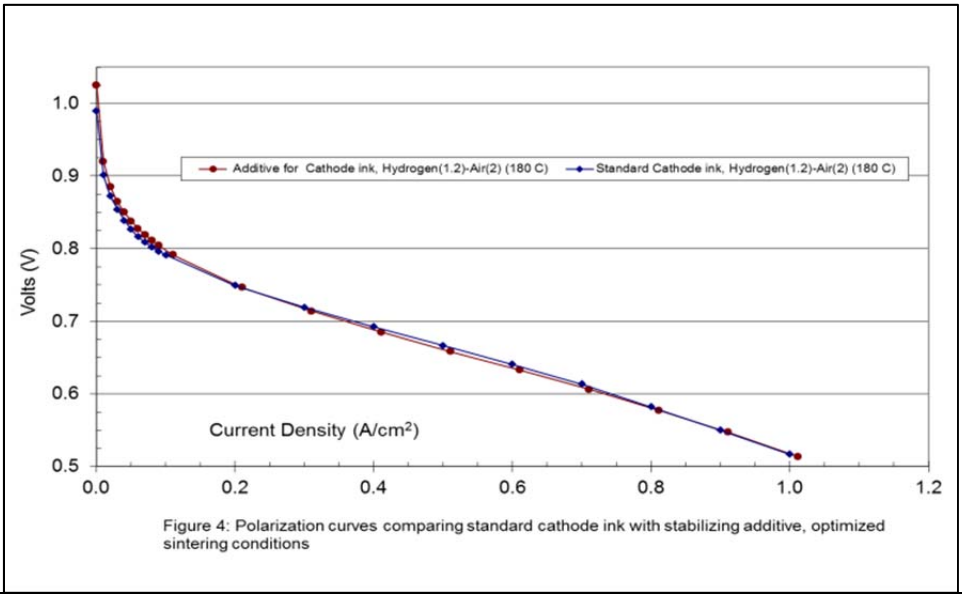

Figure 13. Polarization curves comparing standard cathode ink with stabilizing additive, optimized sintering condition

(5) Coating Runs with 1st Generation Improved Cathode Inks

The next test is to coat full length rolls using this new additive. We coated three cathode roles (>240 linear meters) and evaluated for surface agglomerates. Over these three separate runs we averaged 5.8 agglomerates per square meter, or a reduction of 68% in defects due to agglomerates.

(6) Catalyst Surface Property and Impurity on Ink Stability

During the course of the project, we found that one of the approaches to reduce catalyst cost was to use BASF infrastructure. One BASF site already had a large scale supply of electro-catalyst at the time, so we decided to explore this opportunity. After we qualified the anode catalyst made at that site, we then proceeded to qualify this catalyst in ink preparation.

We encountered an unexpected situation. As described above, we had concluded that, if a catalyst surface exhibits sufficient zeta-potential the catalyst ink should be stable. But for the ink prepared with the alternative anode catalyst from the aforementioned BASF site, this prediction was inaccurate. During the experimental coating runs with this catalyst, we collected many more agglomerates in the coating line than runs with BFC standard catalyst although a zeta-potential scan

suggested a well-charged suspension for this ink. After careful analysis we found the ink stability was caused by impurity in the alternative catalyst.

First we used TGA (thermogravimetric analysis) to determine the compositions of the agglomerates collected during the coating of the alternative anode catalyst ink and compared it to that for BFC standard anode catalyst. As Table 4 shows, for a well behaved BFC anode catalyst ink, a small amount of agglomeration (<<1%) is collected in the filter during coating and there is comparable amount of catalyst and PTFE. On the other hand, the agglomerate collected from alternative catalyst ink mainly contained catalyst. This observation led us to hypothesize the ink instability for alternative anode catalyst originated from the property of the catalyst. Therefore, we used TGA program to determine the amount of impurities in the catalysts. The water amount was determined by holding at 100 deg C and the organic content was determined by holding the temperature at 300 deg C under N_2. As Table 5 shows, there is a higher degree of residual water and more organic content in the alternative catalyst and the amount is much higher for the two alternative samples than typically found for the BFC standard anode catalyst. The alternative catalyst is only 92% of the total weight of the sample. The organics most likely originated from the reagents or solvents used in catalyst synthesis. After a treatment above 300 deg C, the water and organics were reduced to values even below that found in the current catalyst (Table 5) and the agglomerate problem was essentially eliminated (Table 4).

The electrochemical performance test of the anodes made from the heat-treated alternative catalyst showed similar performance to that of BFC standard. We suspect the organics probably weaken the interaction between the surfactant and catalysts so the dispersion capability of the surfactant is reduced and the catalyst particles are allowed to aggregate.

Table 4. The impact of removing organics on alternative anode catalyst ink stability as measured by collected agglomerate during coating

Anode Pt/carbon Catalyst	**Pt collected as % of total Pt in the ink**	**Cat/PTFE in agglomerate**
Alternative as-is anode catalyst ink	6.00%	8
Alternative as-is anode catalyst ink, after heat treatment of catalyst	0.10%	ND
Typical BFC standard anode catalyst ink	0.30%	0.97

Table 5. Water % and Organics % as determined from TGA

Catalyst	**Water**	**Organic impurities**
Alternative Pt/C #1, as is	3.73%	4.27%
Alternative Pt/C #2, as is	3.04%	4.64%
Alternative Pt/C #1, after heat treatment	0.61%	1.25%
BFC standard	<1.0%	<1.8%

(7) High energy dispersion methodology- 2nd Generation Improved Inks

Although we reduced the agglomeration problem in cathode catalyst ink by using zeta potential control to create negative charge on catalyst surface, it actually directed us to a lower throughput route- completely opposite to what this program was intended to achieve. That was because that in order to significantly reduce the agglomerate we needed lowering the catalyst concentration in the ink. In view of this, in order to overcome this dilemma, we have to modify the ink formulation an/ or process to achieve inks with both high solid content and low agglomerate defects in resulting electrodes.

From a fundamental point of view, the most efficient way to disperse the catalyst particles to increase surface areas for efficient uses of catalyst particles is to employ shearing dispersion. However, tiny particles from fine dispersion have high tendency to agglomerate. The finely dispersed particles usually have enormous surface areas and are more hydrophobic than the large particles before dispersion, due to some internal surfaces now becoming external surfaces and the internal surfaces having less catalyst contents (loadings). These hydrophobic carbon support surfaces have a high tendency to interact with PTFE to form precipitation (agglomeration). An innovative approach was developed during the course of this program: combining high shearing dispersion and zeta-potential adjustment. By imposing charges on these small particles they exert repulsion on one another even though they have certain percentage of exposed hydrophobic areas on the surfaces.

(8) High shear cathode ink formulation and optimization

(A) Lab Scale Experiments

The ink formulation needs a buffer agent to stabilize the cathode catalyst and dispersion agent for suspending PTFE particles. Other components include a leveling agent to allow even spreading of the formulation to the GDL for low defects (agglomerates). The final agent is a viscosity adjuster. All experiments were conducted with a GDL layer and a formulation. The formulation was applied to the GDL by an applicator in a fixed specific manner.

(i) Leveling agent

The goal of this experiment is to confirm there is no negative effect in using it. Figure 14 shows that there is essentially no difference in performance for adding a leveling agent. Actually at high current density, some performance improvement is observed in air /H_2 operation. This can be explained as more uniform current distribution from a more even coating with catalyst wet-proofing agent evenly distributed out for maximized 3-phase boundary areas. For H_2/O_2 operation, only catalyst utilization is the determining factor and no advantage is observed.

(ii) Effect of different concentrations of viscosity adjuster

The effect of viscosity adjuster in catalyst formulation has not been studied previously in this area. It is plausible to consider how the viscosity of the ink will influence catalyst particle packing and form a layer with some interpenetration of catalyst layer into the GDL (gas diffusion layer). We studied this

effect by preparing formulations of different viscosity with a viscosity adjuster for two levels of viscosities- high and low. Figure 16 shows the comparison of H_2/Air and H_2O_2 curves; and in **Figure 15** we decomposed the performance differences into catalyst utilization difference and the differences caused by air transport through the gas diffusion electrode.

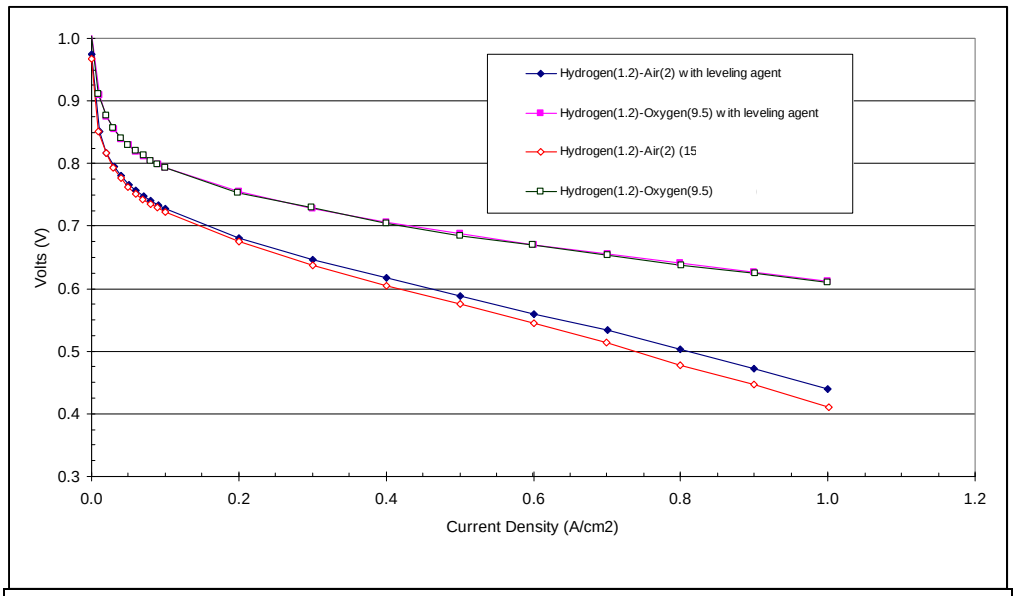

Figure 14. Effect of leveling agent in formulation on performance. 160°C, H_2/air stoich 1.2/2

Figure 16 indicates that the viscosity adjuster can improve the catalyst utilization and also mass transport. It is plausible to consider that higher viscosity can prevent the close packing of the catalyst layer and close packing can impede the penetration of electrolyte into the catalyst pores. Very close packing can also reduce the pores in catalyst layer. Also, the low viscosity can allow undesirable interpenetration of the catalyst layer and the GDL layer, resulting in reduction gas diffusion pore sizes. Moreover, catalyst particles in the hydrophobic GDL layer will have low utilization.

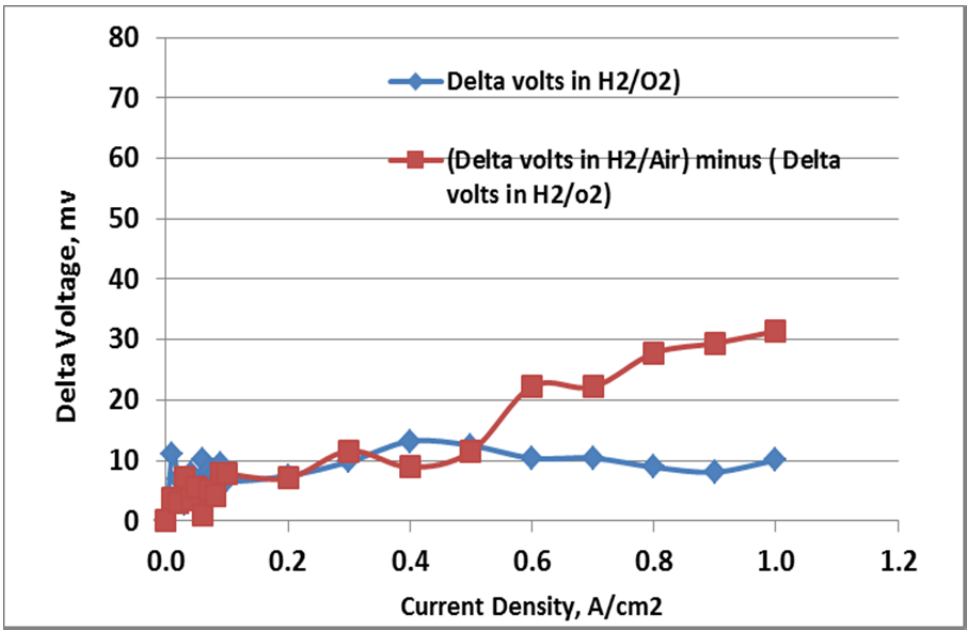

Figure 15. Analysis of performance difference in Figure 16 by decomposition into catalyst utilization (H_2/O_2 curves) and mass transport (difference in H_2/Air subtracted by difference in H_2/O_2)

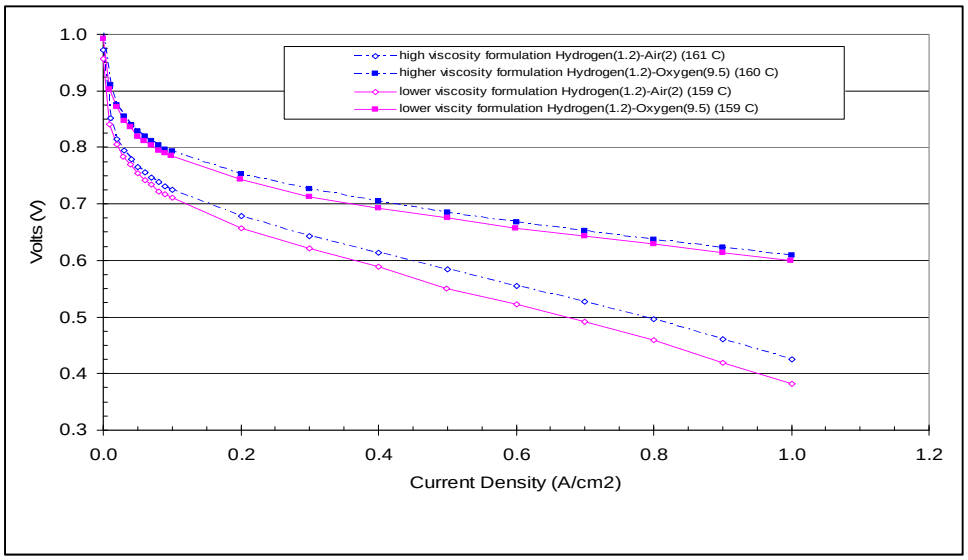

Figure 16. Effect of viscosity adjuster in ink formulation on performance. 160°C, H_2/air stoich 1.2/2

Formulation with appropriate viscosity can also lead to more consistent catalyst layer morphology, thus more consistent performance. Figure 17 on the next page shows the performance in H_2/Air. The average performances for the two formulations essentially the same, but the formulation with optimized viscosity showed smaller standard deviation, i.e., better consistence.

(iii) Effect of high energy dispersion of catalyst particles

As discussed above, one of the purposes to enlist shearing of the catalyst particles is to breakdown particles to lower end of size distributions that results in more total catalyst surface areas. We anticipated achieving better performances and that's what we actually observed. Figure 18 shows the comparison. Each curve is the average of five samples (different catalyst batches). Figure 19 shows the comparison of the cathodes made with only one type of catalyst whereby one is with the high energy shearing and the other one without high energy shearing. Figure 20 shows, for cathodes in Figure 19, at current density below 0.3 A/cm^2 the major contribution to the performance difference comes from catalyst utilization and above 0.3 A/cm^2 some mass transport advantage was also observed for well-dispersed catalyst. The catalyst utilization is expected from more total surface areas. Mass transport resistance could be attributed to some other ink formulation adjustment.

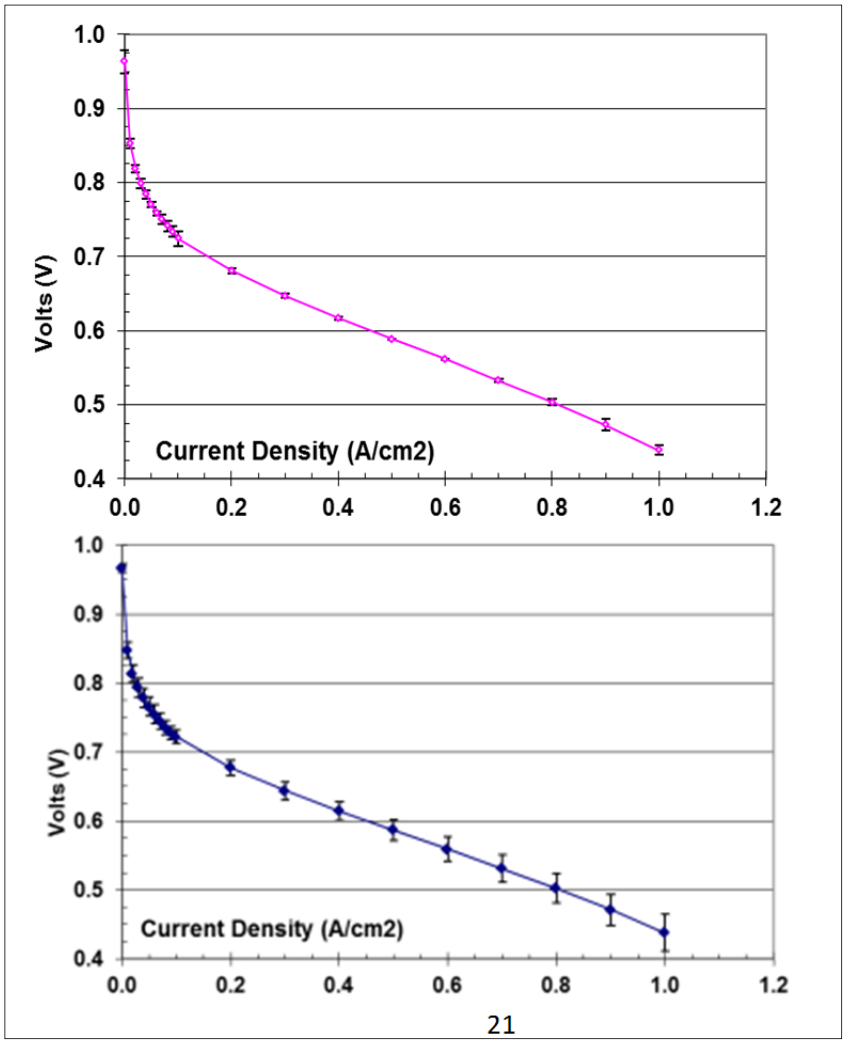

Figure 17. polarization curves for cathodes with formulations of different viscosity (Top) optimized viscosity; (Bottom) lower viscosity. 160^{o}C H_2/Air stoich 1.2/2

(iv) Catalyst/wetting agent ratio

The optimized catalyst/wetting agent ratio depends on many factors, like surface dispersion extent and surface quality demand and performance. When the catalyst dispersion step is applied we need to re-optimize the composition.

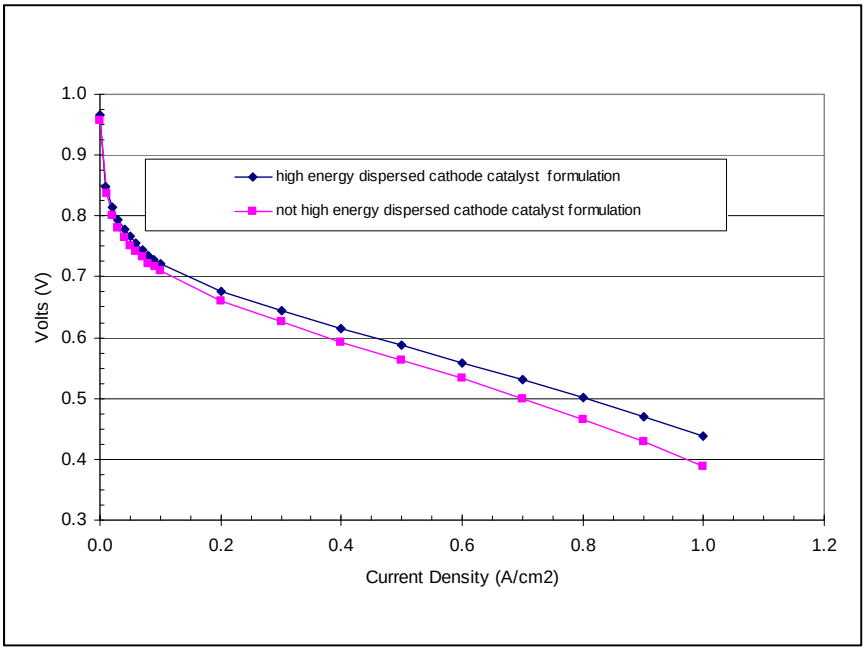

Figure 18. Comparison of polarization curves with two groups of cathodes (of various batches of catalysts) (1) blue markers, formulation contains shearing dispersed cathode catalyst particles; (2) pink markers ,formulation contains non-shearing dispersed cathode. 160^{o}C, H_2/Air stoich 1.2/2;

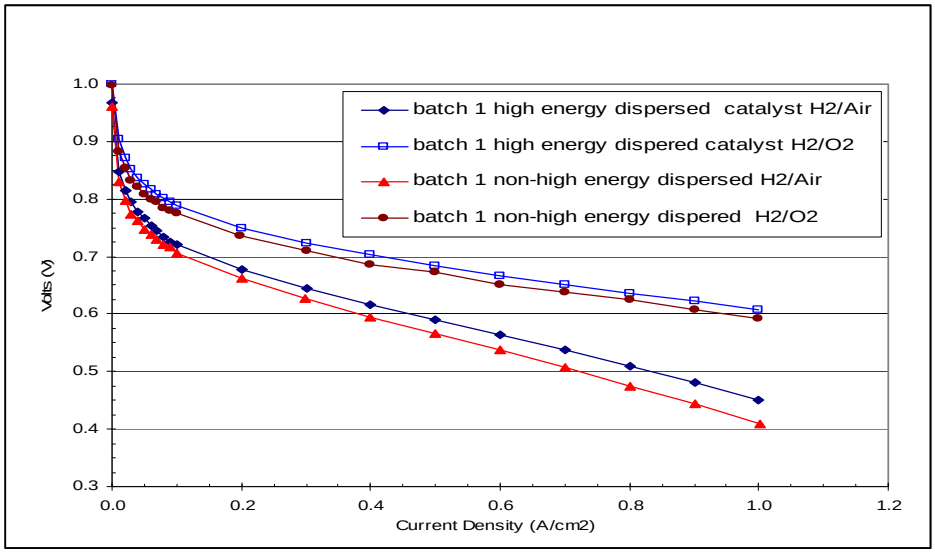

Figure 19. Polarization curve comparison for cathodes prepared from formulations with high energy dispersed and non- high energy dispersed, from same batch of catalyst. 160°C, H_2/Air stoich 1.2/2; H_2/O_2 1.2/9.5

Figure 21 compares two ratios, one is previous ratio and the other one optimized for the dispersed catalyst. Apparently with more surface area for dispersed catalyst and better surface quality, we can use a composition closer to optimization. The improvement from this adjustment comes mostly from catalyst utilization as Figure 22 shows.

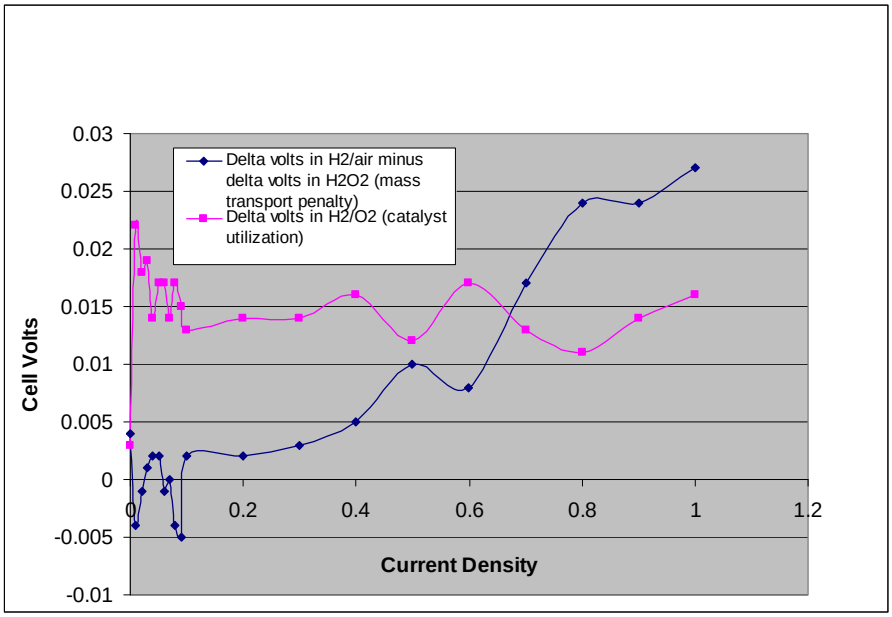

Figure 20. Analysis of performance difference in Figure 19 by decomposition into catalyst utilization (H_2/O_2 curves) and mass transport (difference in H_2/Air subtracted by difference in H_2/O_2)

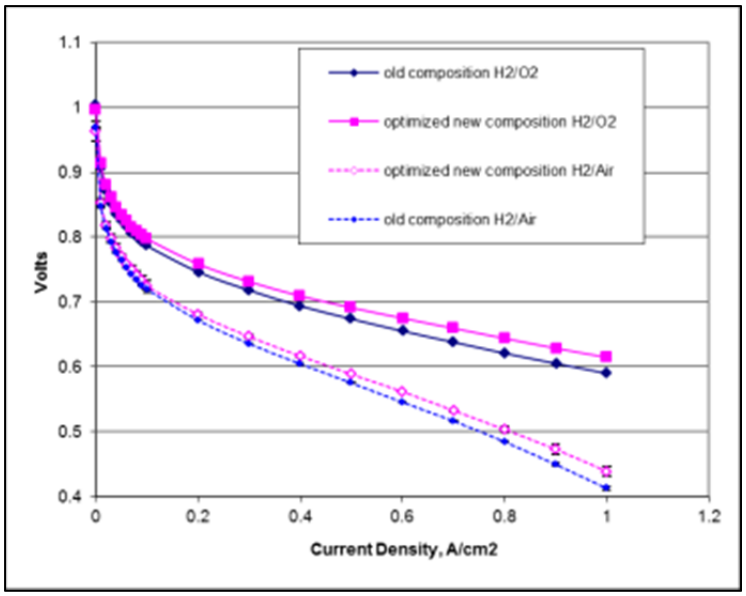

Figure 21. Performance comparison of cathodes from two different catalyst/wet agent compositions. Blue markers for previous compositions and pink markers for new optimized composition for high energy dispersed catalysts

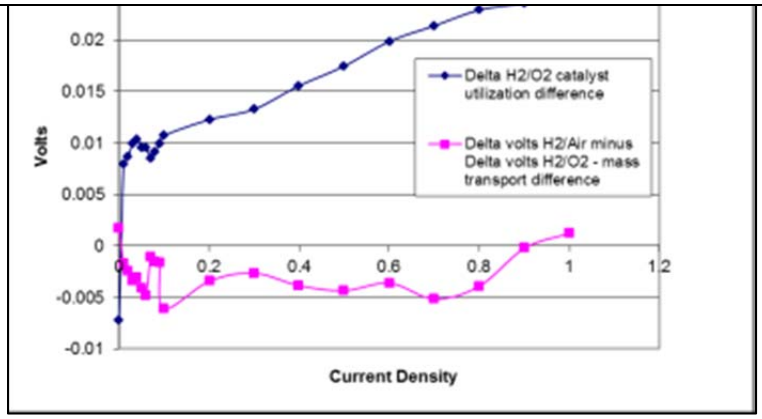

Figure 22. Analysis of Performance difference in Figure 21 by decomposition into catalyst utilization (H_2/O_2 curve) and mass transport (difference in H_2/Air subtracted by difference in H_2/O_2)

(v) Effect of surfactant property

After catalyst particles are dispersed by high energy shearing, some agents need to be added to the mixture to stabilize the suspension; and other agents are added to ensure good mixing of various components, such as catalyst particles that are usually more hydrophilic and wet-proof agents that are hydrophobic. Generally surfactants are added to make compatible components with very different hydrophobicity properties. If the surfactants are not tuned to mix the hydrophilic components and hydrophobic components, then the ink will not be applied uniformly or dried non-uniformly. The result is non-uniform distribution of electrode coating. Therefore, use of suitable surfactants for compatiblization of components with different hydrophobicity is crucial for uniform

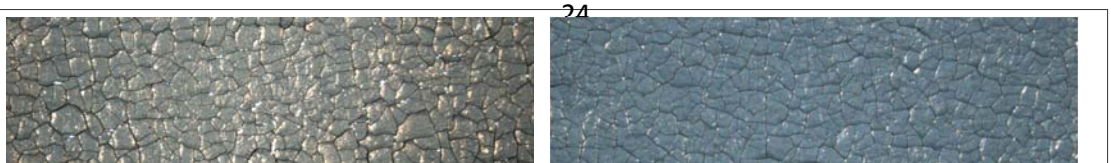

coating.

Figure 23 shows the surface quality comparison of two cathodes prepared with two high energy sheared cathode ink formulations. The one with surfactants for higher compatiblizing power clearly shows less cracking or surface irregularities. The catalyst loading distribution for (Left) has a standard deviation about 4-5 times of that for (Right), and (Left) and (Right) have about the same loadings. This less uniform catalyst loading distribution for (Left) is consistent with the observation that the formulation for (Left) dried non-uniformly resulting in more coating aggregations.

(B) Scale up of High Energy Dispersed Cathode Formulation from Lab Coater to Pilot Coater

The results discussed above were from cathode samples prepared on draw-down lab coater and the sample sizes were usually 10-20 cm in each dimension. With the good results of the experiments reported last quarter and that mentioned above, we decided to scale the formulations developed to trials $2m^2$ long using our continuous pilot coater. We have settled on a set parameters in the formulation, including new buffer agent, higher concentration of catalyst (1.5x of that in previous formulation with non- high energy dispersed catalyst), and optimized surfactant and viscosity adjuster concentrations. The ink formulations were prepared and small samples were coated with lab coater and then the same ink was used for pilot $2m^2$ coating. As a control a 2 m^2 pilot run was also coated with previous non high energy dispersed cathode formulation developed at the beginning of this program. The polarization curves are shown in Figure 24.

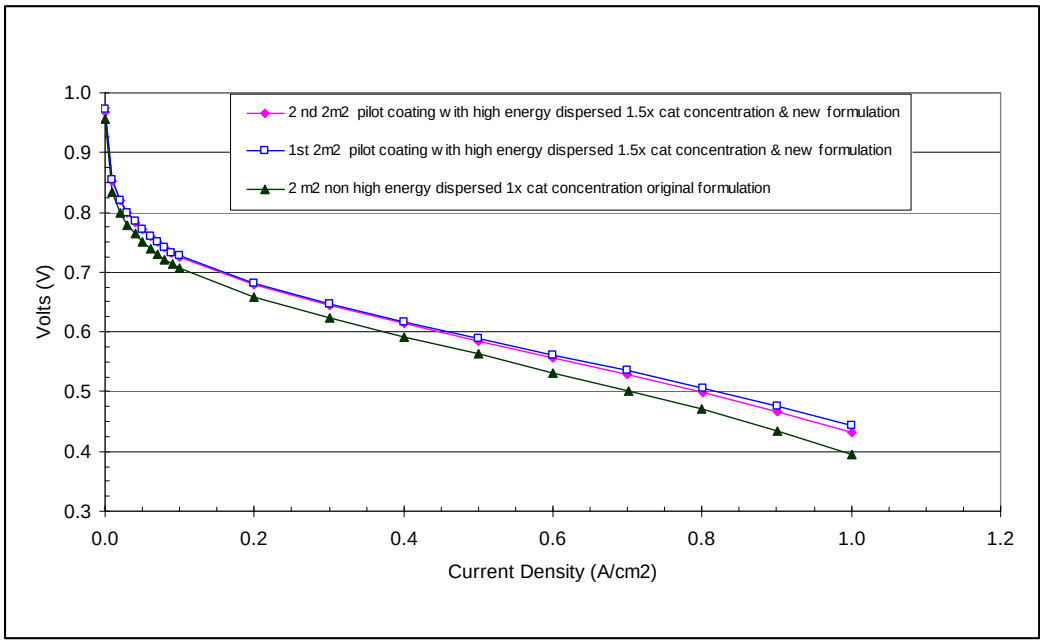

Figure 24. Performance comparison for two pilot coater runs with high energy dispersed cathode catalyst of 1.5x concentration & new formulation and the run with non-high energy dispersed catalyst of 1x concentration and original formulation

Figure 24 shows clearly the improvement. The improvement is believed from mainly the higher surface area created by high energy dispersion; however, some moderate improvement might come from better dispersant and leveling agent that leads to a more uniform coating and thus uniform current distribution during operation. The improvement is summarized in Table 6.

Table 6. Performance improvement in H_2/Air at 160°C for cathodes from high energy dispersed new cathode formulation over those from non-high energy dispersed original cathode formulation.

Volts at current:	**0.2 A/cm^2**	**0.5 A/cm^2**	**0.9 A/cm^2**
2m^2 pilot run of non-high energy dispersed original cathode formulation	0.658	0.562	0.434
Average of two 2m^2 high energy dispersed new cathode formulation	0.679	0.587	0.470
Improvement, mv	21	25	36

Besides improvement in performance, the cathodes prepared with the new formulation with high energy dispersed catalysts also showed less agglomerates per unit area. The ink with high energy dispersed catalysts showed about 2 agglomerates per 0.5 m^2 sheet and the typical number for the previously reported ink formulation with non-high energy dispersed catalysts was about 4 agglomerates per sheet.

Furthermore, because the increase in catalyst concentration in the ink by 50% combined with higher viscosity of the new ink, it took fewer coats to reach our target catalyst loading compared to the previously reported non high energy dispersed formulation. We employed 25-35% fewer coats to reach the target. Using a higher concentration of catalyst in non-high energy dispersed formulation usually has a higher tendency to cause extensive agglomeration formation on the electrode surface and this property has been an impeding factor for speeding up coating. The use of high energy dispersion has removed a very significant barrier.

(i) Areas for improvement

If we compare the performances of pilot samples with the high energy dispersed new formulation to those of lab coated samples with the same formulation we found a performance decrease for all current densities. In the range of 0.2 A/cm^2, the decrease is an average of 4 mv in both H_2/Air and H_2/O_2. This result indicated some blocking of catalyst site by most likely residues left during the step for additive heat removal. It's plausible that large scale processing of heat removal step might not be as complete as in carrying out the same process at small scale. The removal of all additives can be influenced by many factors, such as heat program as well as additives. One of the possible factors is the viscosity adjuster we added to optimize the penetration of catalyst into GDL layer, As discussed above, we have shown that without a viscosity adjuster, the severity of penetration can lead to both catalyst site blocking and gas pore blocking.

In the observations described above for performance lowering with scale-up, the loss could be most likely related to residue blocking in GDL. With this hypothesis in mind, we decided to conduct an investigation to optimize the concentration of the viscosity adjuster.

(ii) Optimization of viscosity adjuster concentration

In section (8) (A)(ii), we discussed about the effect of viscosity adjuster on cathode performance. From the results we constructed the following theory: higher viscosity can prevent the close packing of the catalyst layer and close packing can impede the penetration of electrolyte into the catalyst pores. Very close packing can also reduce the pores in catalyst layer. Also, the low viscosity can allow undesirable interpenetration of the catalyst layer and the GDL layer, resulting in reduction gas diffusion pore sizes. Moreover, catalyst particles in the hydrophobic GDL layer will have low utilization. On the other hand, the concentration of viscosity adjuster might have its optimization point, too high a concentration might cause some side effect. The side effect appeared to be related to the removal of additives. Higher concentrations of viscosity adjuster can lead to high total organic species that need to be decomposed becomes too high during heat-removal step, thus incomplete decomposition results.

A series of experiments were conducted in which all components were kept the same except the concentration of viscosity adjuster was varied from 1x to 3x. Moreover, judging from the success of 1.5x of catalyst concentration we decided to increase concentration to 2x catalyst for further reducing formulation preparation time and coating time. Performance measurements were taken at 160 deg C with H_2/air and H_2/O_2 operations, respectively. The results are shown in Table 7 and Table 8, and also plotted in Figure 25 Figure 26 with 2 standard deviations.

Table 7. Cathode Performances in 160°C, H_2/Air, 1.2/2 H_2/Air stoichiometry; all components in formulations the same except viscosity adjuster is varied.

H_2/Air, 160°C	**Volts at current listed**

viscosity adjuster concentration	0.2A/cm^2, avg	0.2 A/cm^2, std dev	0.5A/cm^2, avg	0.5A/cm^2, std dev	0.9A/cm^2, avg	0.9A/cm^2, std dev
1x	0.691	0.012	0.610	0.014	0.509	0.021
1.5x	0.694	0.004	0.610	0.004	0.504	0.003
2x	0.692	0.005	0.609	0.004	0.507	0.001
3x	0.688	0.009	0.600	0.024	0.484	0.061

At 0.2 A/cm^2 in H_2/Air, there is a moderate maximum around 1.5x to 2x of viscosity adjuster. However, this does not appear in H_2/O_2. To understand the cause for this difference we decompose the performance curves in H_2/Air into catalyst utilization and mass transport effect. Catalyst utilization data can be obtained from H_2/O_2 data, after taking the difference between the curves in H_2/O_2 and H_2/Air, we obtain the effect of mass transport. Catalyst utilization data can be obtained from H_2/O_2 data, after taking the difference between the curves in H_2/O_2 and H_2/Air, we obtain the effect of mass transport.

Table 8. Cathode Performances in 160^{o}C, H_2/O_2, 1.2/9.5 stoichiometry; conditions as in Table 7.

H_2/O_2, 160^{o}C						
viscosity adjuster concentration	0.2A/cm^2, av	0.2A/cm^2, std dev	0.5A/cm^2, av	0.5A/cm^2, std dev	0.9A/cm^2, av	0.9A/cm^2, std dev
1x	0.762	0.015	0.701	0.011	0.643	0.006
1.5x	0.767	0.003	0.703	0.003	0.645	0.000
2x	0.764	0.005	0.702	0.004	0.647	0.004
3x	0.765	0.003	0.703	0.006	0.646	0.010

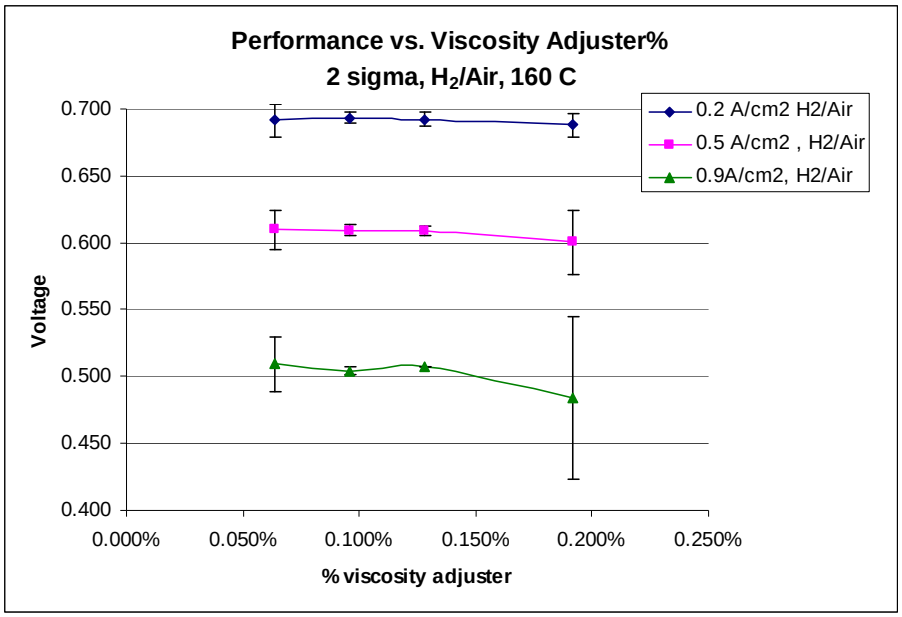

Figure 25. Graphs according to Table 7

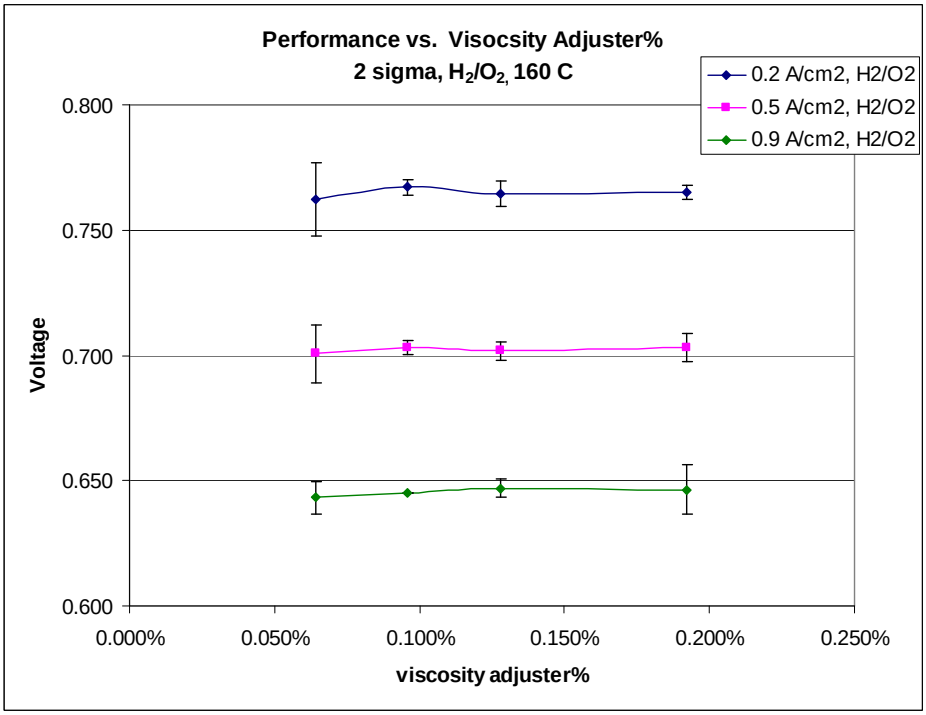

Figure 26. Graphs according to Table 8

For easy comparison, we use (define) the performance of cathode from ink with 1x viscosity adjuster as baseline, and compare cathodes from inks containing other concentrations of viscosity adjuster with this baseline. Table 9 summarizes the results. We note that cathodes with viscosity adjuster concentration higher than 1x, the utilization increase, presumably this is due to less catalyst will penetrate the GDL (gas diffusion layer). Catalyst penetrating deep into GDL layer will have a more hydrophobic environment and less wettable by H_3PO_4. In our previous study, we also find that

the deep penetration of catalyst into GDL can also lead to gas pore blocking and induce mass transport problem; however, this is not observed here, actually all cathodes prepared with higher viscosity adjuster concentrations show slightly poorer mass transport property, and cathodes from 3x concentration shows worst mass transport property (Figure 25). This trend suggests other factors are in play. Careful examining the performances at higher current densities, especially at 0.9 A/cm^2, it becomes even clearer that mass transport property is impacted by the high viscosity adjuster concentration. Not only the performance average is lowest but the standard deviation is also much larger for the performance with 3x concentration in the formulation.

The fact that this trend is clear in H_2/Air performance (Figure 25), but not in H_2/O_2 performance (Figure 26), indicates that there are some residues in the cathodes that blocking gas pores, but not catalyst sites. We believe that higher viscosity adjuster impede the complete decomposition of all additives and mostly in the GDL layers. To find a compromise for getting optimized penetration and minimize residues, we will use viscosity adjuster in the range of 1.5x to 2x.

Table 9. Utilization and mass transport differences for cathode samples with various amounts of viscosity adjuster concentrations in formulations.

Level of Viscosity Adjuster	**H_2/Air @0.2A/cm^2**	**H_2/O_2 @0.2A/cm^2**	**Utilization Gain vs 1X, mV**	**Mass Transport Gain vs 1X, mV**
1X	0.691	0.762	0	0
1.5X	0.694	0.762	4.6	-2.3
2X	0.692	0.764	2.0	-0.8
3X	0.688	0.765	2.5	-5.8

(C) Scale up of the Revised Formulation of High Energy Dispersed Cathode Formulation from Lab Coater to Pilot Coater and Production Coater.

(i) Confirmation of Revised High Shearing Cathode Formulation at Pilot Scale

With the optimization results mentioned above, we think we are in the position to scale-up this revised high shearing formulation and optimized viscosity adjuster concentration along with improved surfactant disperser. In the performance testing of 1st 2m^2 pilot runs of high shearing cathode formulation as shown in Figure 24, we used catalyst concentration at 1.5x of that for non-shearing cathode catalyst sink. For future reference we will redefine that high shearing cathode catalyst as normalized here as “1x”, so the old non-shearing cathode catalyst concentration (ref run) is normalized as 0.7x. In the meantime, the viscosity adjuster concentration in the high shearing cathode formulation in Figure 24 is normalized to 1x. By this normalization, in the revised high shearing formulation we used (normalized) 1.3x catalyst concentration and (normalized) 0.5 x viscosity adjuster concentrations.

Figure 27 shows the performance comparison along with that of the reference run with non-sheared catalyst. The improvement in performances for the revised cathode formulation over the previous versions is very clear.

(ii) Scale-up of Revised High Shearing Cathode Formulation to 20 m^2, 60 m^2 , and 120 m^2

After the successful run of 2m^2 pilot run with the revised high shearing cathode formulation, we further scaled up to 20 m^2 on the pilot coater and 60 m^2 and 120 m^2 on the production coater.

Figure 28 shows the average performances for each of these runs. For 60m^2 and 120 m^2 coating three and six sintering batches were conducted respectively. The performances of six sintering batches for 120 m^2 coating are shown in Figure 29. As shown in Figure 28, obviously all these runs show very similar performances that are far better than "current non-dispersed production cathodes", - actually in middle 2012, the "current non-dispersed production cathode" (P1000) was discontinued and replaced by the new technology described here.

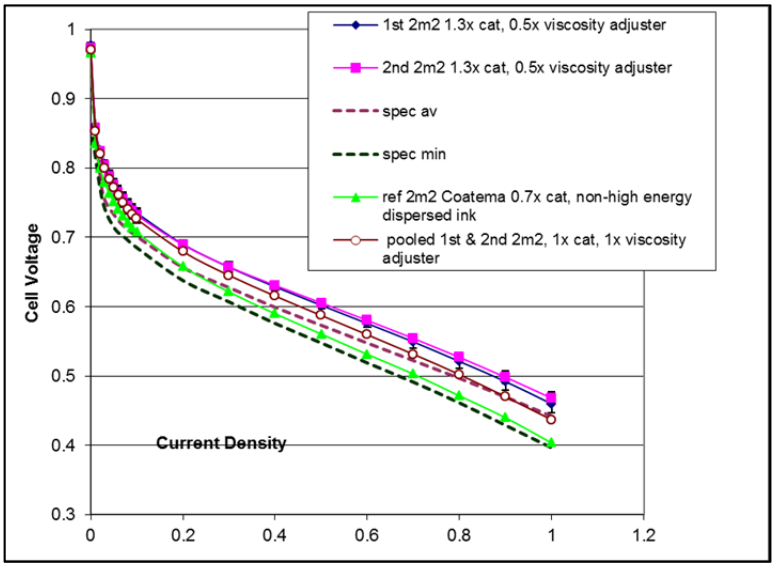

Figure 27. Performance comparison in 160°C, H_2/Air for revised version of high energy dispersed cathode ink with previous versions of high energy dispersed catalyst ink and non-dispersed ink. 2 Standard deviations are shown for some samples others are omitted

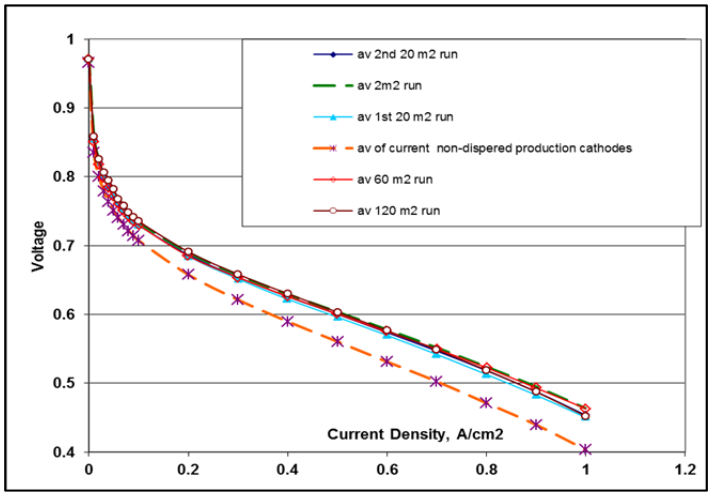

Figure 28. Comparison of performance for high energy dispersed cathodes at various scale-up stages (2 to 120 m^2). 160°C, H_2/Air, 1.2/2 stoich, standard anodes are used in all MEAs. Spec average and minimum for current production cathodes are also shown for comparison.

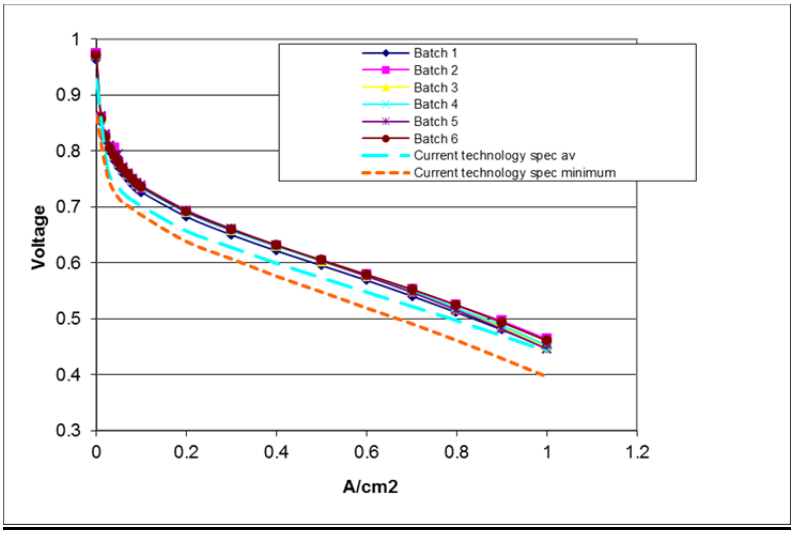

Figure 29. Performance at 160°C in H_2/Air (1.2/2 stoich), of six sinter batches sampled from 120 m^2 coated high energy dispersed cathodes. Spec average and minimum for current production cathodes are also shown for comparison.

For the new cathode formulation, the improvement at 0.2 A/cm^2 over current production baseline cathodes is about 30 m^2. This gain is equivalent to an increase in active surface area or utilization by 100%. Furthermore, the consistency of the performance demonstrated in Figure 29 with 6 sintering batches also testifies the quality consistence over a long roll (240 l.m) and the consistency of sintering process.

(D) Advantage of High Energy Dispersed Cathode Technology

Besides improvement in performance high energy dispersed cathode has also advantage in ink preparation and production rate. All advantages are summarized below.

(1) Improve performance by 25-30 mv at 0.2-0.5 A/cm^2

(2) Reduce ink preparation time by >50%

(3) Reduce coating passes by 40-50%

(4) Reduce defects per m^2 electrode from 6-7 to 2.5-2.6 at production scale

(5) Reduce catalyst loading variation to ¼ of standard variations

We describe each item in the list briefly below. One time-consuming process step is eliminated from current production ink to high energy dispersed ink, so more than 60% time is saved. With the combination of high energy dispersion and targeted additives, ink stability is vastly improved and we can employ higher concentrations of catalyst in the ink subsequently reducing the number of coating pass by 40-50%. The high energy dispersed ink contains uniformly dispersed catalyst particles and results in cathode uniformity increase. With on-line X-ray fluorescence we found the standard deviation of precious metal loading was reduced to one fourth of that for current production cathode. Finally with good uniformity and the use of leveling agent in the formulation, surface defect rate (QC rejected) is reduced by 60%. Table 10 summarizes the statistical data for the high shearing

cathodes prepared at pilot and production scale.

Table 10. Agglomerates per sheet of cathodes for $2m^2$, $20m^2$ pilot coater runs and $60m^2$ production coater runs.

Length of coating run	Incidents/sq m Average	Standard Deviation
$2m^2$	2.5	1.4
$20m^2$	2.5	1.6
$60m^2$	2.6	1.1

(9) High shearing anode ink formulation and optimization

(A) Lab Experiments

After the successful scale-up of high shearing cathode ink/coating we started to apply the same type of high energy dispersion methodology to anode ink formulations. With some critical modifications we are able to develop a new anode formulation. We improved not only the performance and its consistency but also reduced the ink preparation time and number of coating passes thus realizing an effective overall increase in process speed.

(i) Leveling agent change

In our initial anode ink development, using a formulation similar to that for high energy dispersion for the cathode ink resulted in poor performance. Careful examination revealed that the poor performance was caused by incomplete decomposition of the residues during the post-treatment step after coating. The incomplete decomposition was induced by a side reaction of the additives facilitated by the anode catalyst. By optimizing the generation 1 leveling agent this issue was mostly solved. Trial runs with high energy dispersed anode ink without leveling agent also resulted in poor electrode coating quality, so the discovery of the new easily decomposed leveling agent was crucial.

Figure 30 shows the comparison. With generation 1 leveling agent in the ink, although H_2/Air performance is acceptable and similar to anodes prepared from inks containing improved leveling agents, in reformate operation the anode prepared from ink containing generation 1 leveling agent shows very poor performance.

This phenomenon is generally observed because in H_2 operation the reaction and mass transport are facile, and the performance is not sensitive to the state of catalyst sites or utilization. However, in reformate operation even at higher temperature, sites can be occupied by CO, so the utilization or surface area is critical. Even small amounts of ink additive residues can significantly reduce available sites.

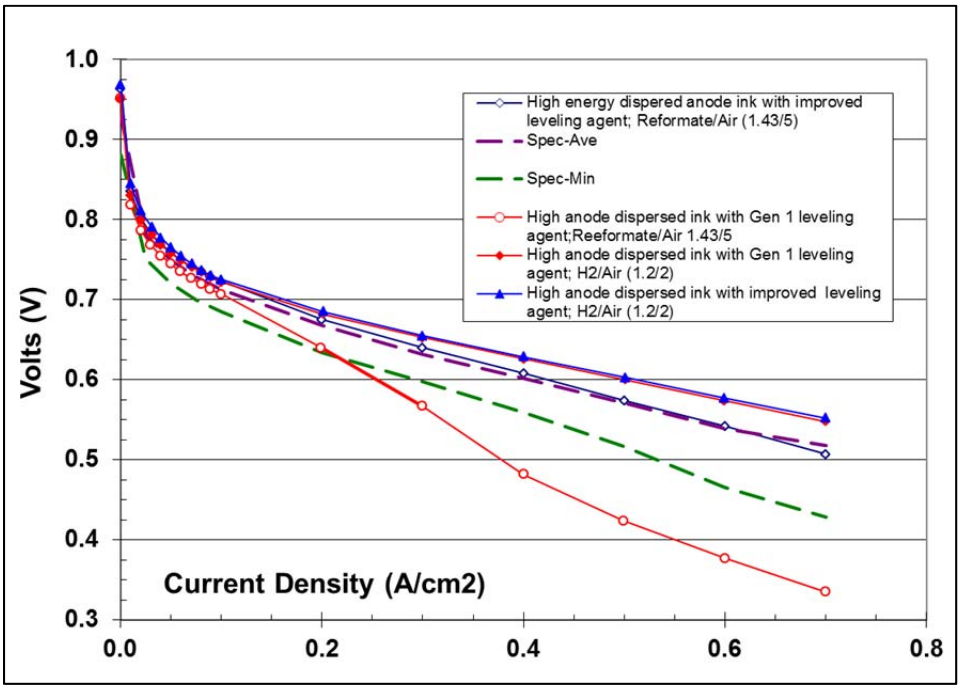

Figure 30. Performance comparison for anodes prepared from inks containing different leveling agents. Standard cathodes used in all MEAs. H_2/Air stoich 1.2/2; Reformate Stoich 1.43/5, 180°C.

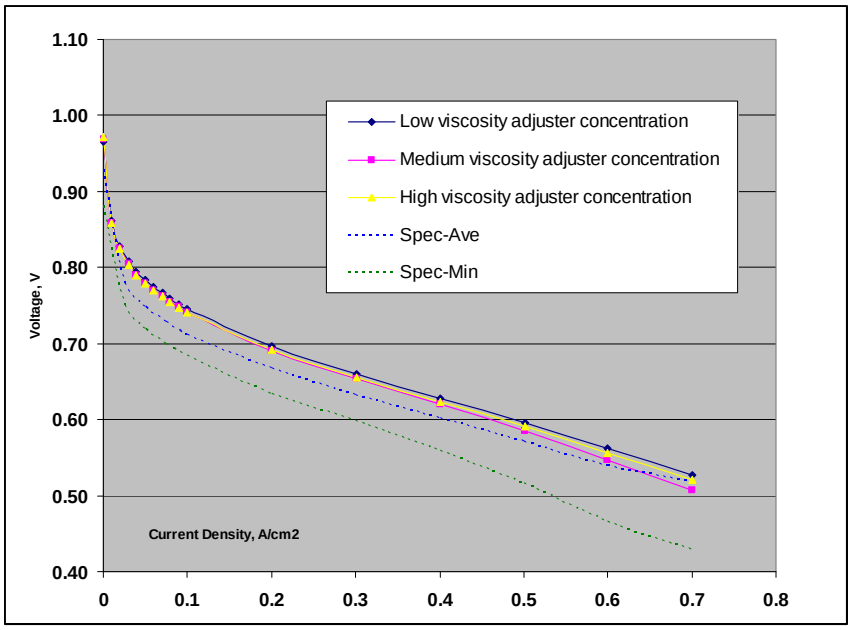

Figure 31. Effect of viscosity adjuster concentration on anode performance. Standard cathodes are used in all MEAs. Reformate/Air stoich 1.43/5, 180°C.

(ii) Viscosity Adjuster Concentration

Besides leveling agents, viscosity adjuster concentration was also studied. Previously we found that there is an optimized concentration for the viscosity adjuster because of the compensation to

minimize penetration of the catalyst layer into the gas diffusion layer (by higher viscosity) and complete decomposition of all additives. We carefully selected three viscosity adjuster concentrations and the data in reformate/air are shown in Figure 31 shows the performances of three anodes that are similar with the lowest viscosity adjuster to be slightly better than the other two levels. It appears that in this concentration range, the additive decomposition might be slightly more important. Based on the results in Figure 31, the low viscosity adjuster concentration is chosen as the standard for future anode ink formulation. Note all anodes showed significant better performances than that of current production anode with catalysts not dispersed with high energy in the ink.

(iii) Electrode Acid Wettability Adjustment

Introduction of high energy dispersion has the potential to change the physical state of catalyst. This change in catalyst morphology can impact the overall electrode structure including acid wettability. In reformate operation, especially the 2% CO typically employed with high temperature MEAs, electrode acid wettability can be very crucial. A proper balance of electrolyte imbruement and gas diffusion paths are the key factors. Available anode catalyst sites needs to be high due to the strong competition from carbon monoxide, but not so high as to impede the diffusion of hydrogen in reformate, especially when reformate with dilute H_2 is utilized.

As a methodology in developing ink formulation additives and high energy dispersion for the anode, we performed experiments to determine the optimized structure – acid wettability for anodes in reformate operation typical for μ CHP. Figure 32 shows the results. The previous structure was for non-dispersed catalyst and high energy-sheared catalyst appeared to require higher wettability to function properly. Not only average performance is influenced, but also the variability can also vary. Both medium and high wettability appear to improve performance. The anode with medium wettability structure also shows reduced variability. Medium acid wettability is chosen over high wettability because the coating process is more manageable and more reproducible.

(iv) Post-Treatment Optimization

In electrode manufacture all electrode coatings are subject to a post-treatment to remove additives and secure a final wet-proofing structure. However, the post-treatment process needs to be carefully controlled, otherwise inferior performance results. The residue formation described in the leveling agent section above is one example. Besides selection of appropriate additives in the ink, the procedure of post-treatment is also important. The undesired residues can be formed from side reactions in the post-treatment process. Therefore, a goal for post-treatment process development is to minimize the amount of residue formation while retaining acid wettability properties as well as gas diffusion pathways.

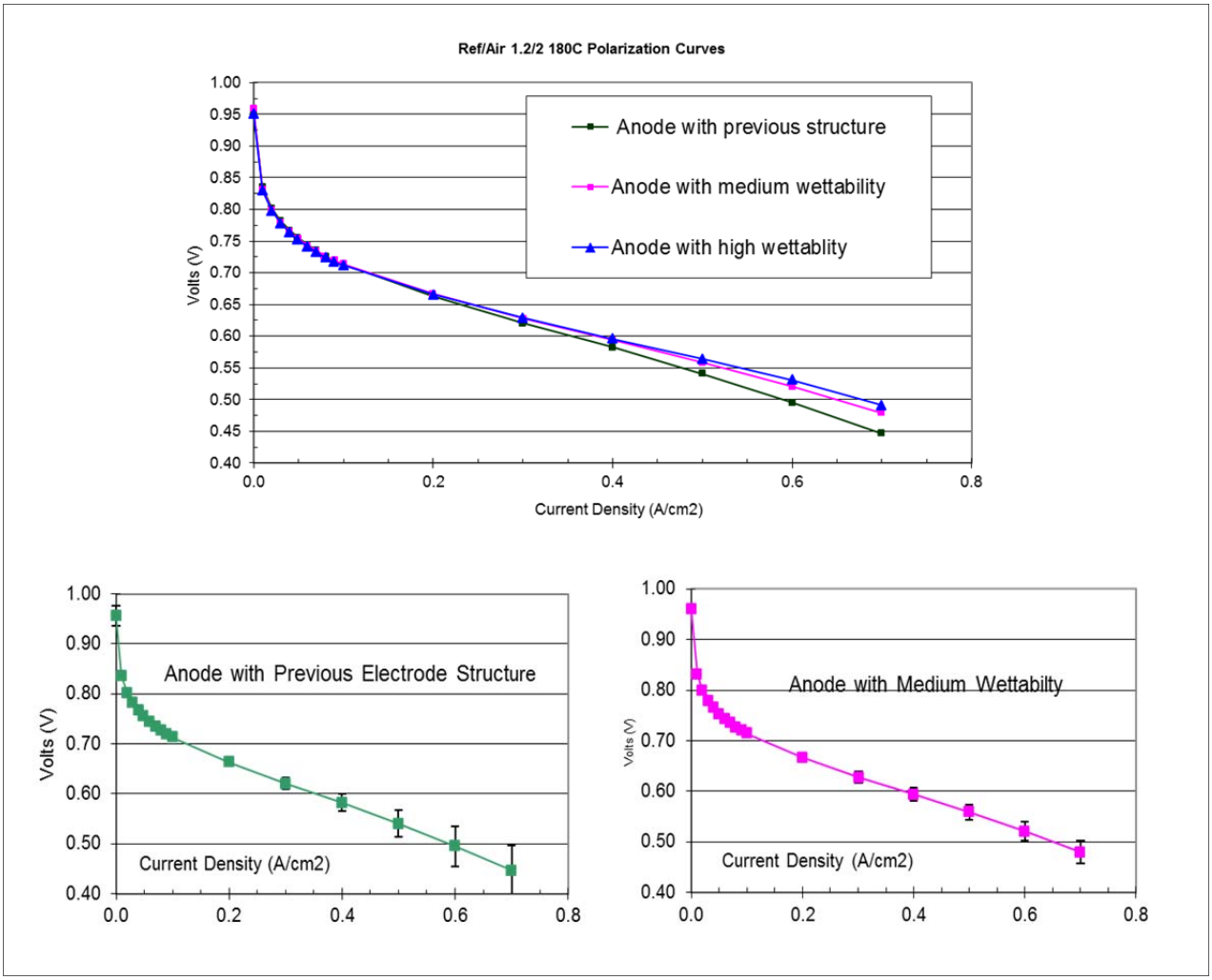

Figure 32. Performances of high energy-dispersed anode with electrode structures of various acid wettabilities. Reformate/Air 1.2/2, cathode is standard.

As mentioned above, high energy dispersion leads to more active catalyst with higher surface area, but as a consequence the rate of ink additive decomposition reactions are also increased, so we needed to adjust the treatment process to get optimum performance. We further examined this effect and found a set of process conditions that can lead to a further improvement in performance. Figure 33 illustrates this improvement. The 1st version program only included thermo process modification and the new advanced program includes both thermo and design change. In Figure 33 we also included the average performance and 2-sigma minimum for current production batches. The improvement is obvious and it far exceeds the level of current standard. The samples made from new advanced program shows better performance than those from 1st version improved program and anodes from both programs far exceed the performance of production batches. It is important to note that while typical µCHP operates at lower current densities (<0.2A/cm^2), the typical MEA for µCHP is >500cm^2, so any mass transport effects noted at the highly controlled 50cm^2 test cell are amplified in a full scale cell at the lower currents.

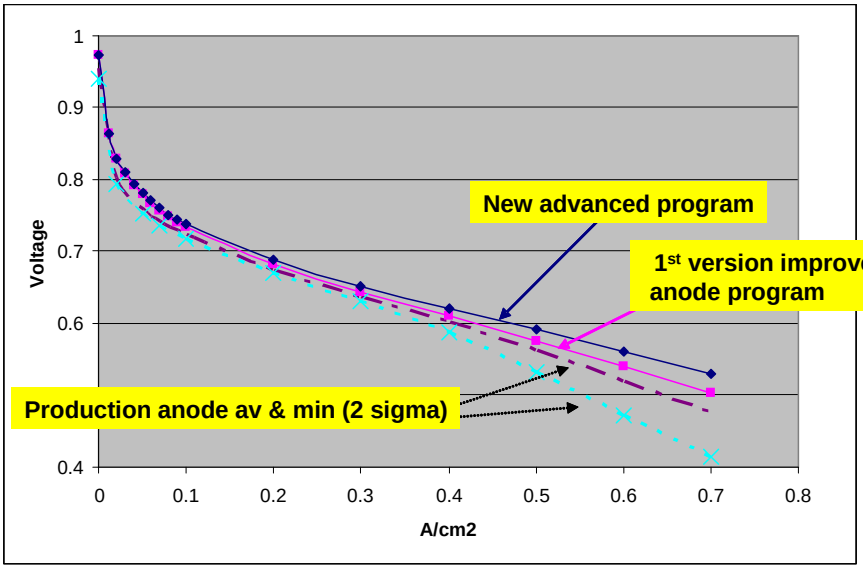

Figure 33. Anode performances for high energy dispersed anode by two different post-treatment programs, H_2/Reformate- 1.2/2, 180°C production anodes have non- high energy dispersed catalyst ink

(v) Post-treatment Uniformity

While the goal of this program is focused on inks and coating, a key ancillary part of this process is being able to post process full batches of GDEs in specialized ovens to set the hydrophobicity profile. Large batches of electrodes in the post-treatment chamber can change the extent of side reactions and lead to performance problems

These side reactions are particularly severe for the anode because the anode catalyst seems to be a more active catalyst for this class of reactions. To counter this effect, we worked on oven control sequences and thermal processes. Figure 34 shows one of the many improvements that we achieved. In Figure 35, post-treatment 1 led not only an improved average performance but also less variability.

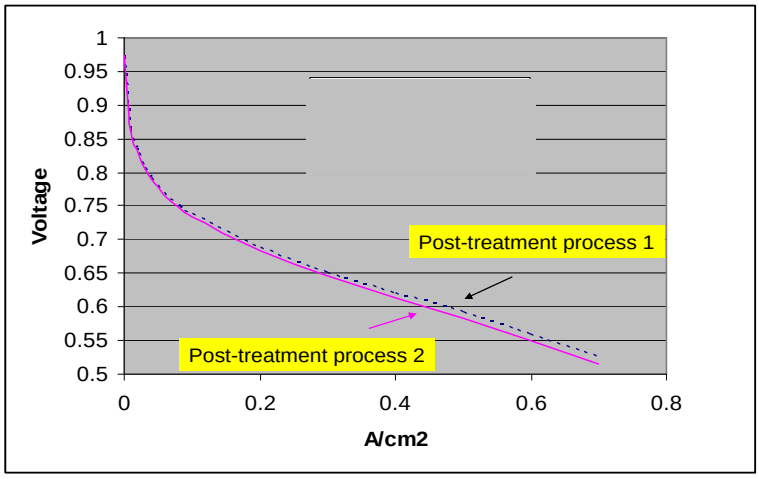

Figure 34. Average performance comparison for high energy dispersed anodes with two different post-treatment processes. Same conditions as Figure 33.

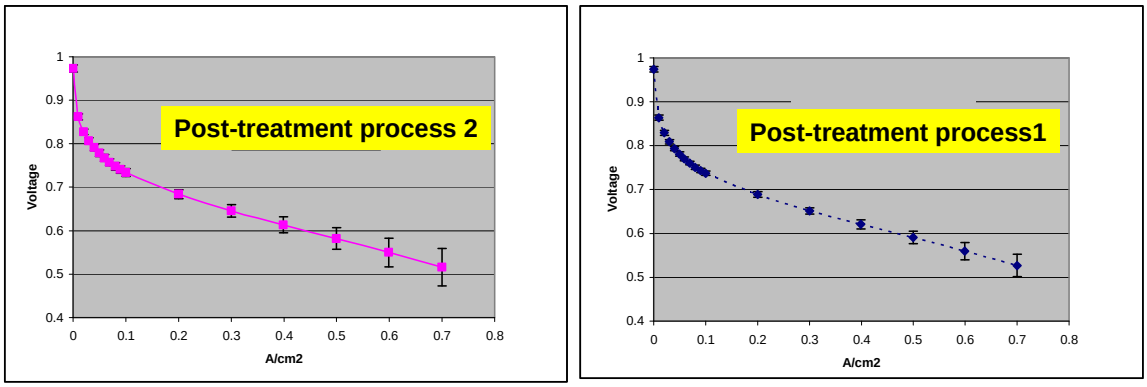

Figure 35. Performance variability of the anode post treatment 2 (left) and 1 (right). Error bar is for 95% confidence level.

If we concentrate on electrodes at a specific location in post-treatment chamber, even larger differences for the two post-treatments are observed. Figure 36 shows that the variation in performance for samples at location A for post-treatment 1 is much smaller than that for post-treatment process 2. It is important to note that any decrease in variability can be just as important, if not more so, than an increase in performance: the stacked nature of MEA-based fuel cells amplifies failure issues when lowest performing cell or cells are below specification or at the end of life specification prior to the other cells.

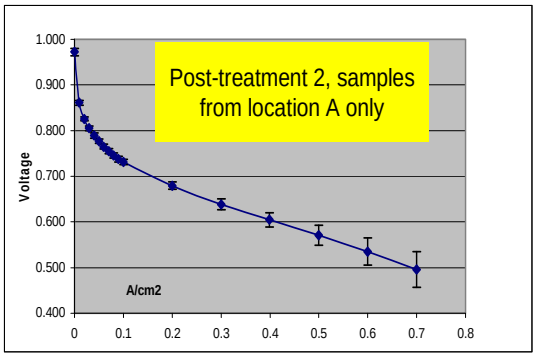

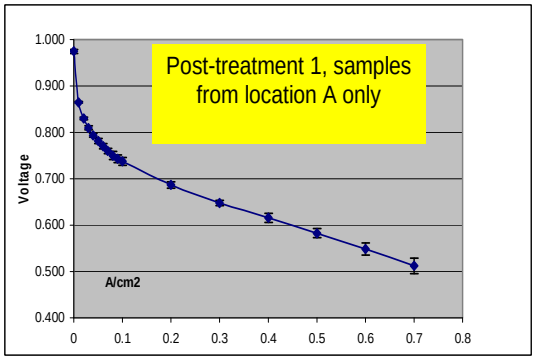

Figure 36. Same as Figure 35, but for samples from location A only.

(10) High Energy Dispersed GDL (micro-porous layer) Formulation Development

- Pilot Scale

Gas diffusion electrodes include at least two porous layers: the gas diffusion layer (also called the micro-porous layer) and the catalyst layer. To realize the higher gas diffusion electrode throughput goal of this program, special efforts were needed to improve the throughput of GDL coating. At the beginning of this program, gas diffusion layer formulation and application takes a far longer time to prepare than catalyst formulations. The challenge for gas diffusion layer formulation is higher than catalyst formulation because of the hydrophobic nature of the carbon used. The high hydrophobicity is needed for building durable "dry" gas channels to allow gases to diffuse to the catalyst sides on three-phase boundaries to undergo electrochemical reactions. However, because of the high hydrophobicity it is difficult to wet the carbon and disperse it to small particles for building highly porous coatings.

At the beginning of this program, the production process for gas diffusion layer formulation uses a rather lengthy process to prepare the formulation. The majority of time is spent on getting the carbon powders wet and sufficiently dispersed. Compared to the carbons used for catalyst supports, the base carbon for the MPL tends to form tightly bound extended agglomerates that need very high dispersion energies to initially break apart, and more importantly, tend to re-agglomerate quickly after being broken apart. The general approach is to identify a class or classes of additives that can both bind to the hydrophobic carbon black and quickly stabilize the dispersion but not interfere with the critical porosity and hydrophobicity attributes needed in the GDL. We identified five additives with high potential to solve this issue.

(A) Selection of Hydrophobic Carbon Dispersion Agent

Starting with a very high energy dispersion, all five potential candidates facilitated the stabilization of the carbon black suspensions at concentrations five times more concentrated than benchmark formulations at the beginning of the program. These inks were then processed with other

additives using the methodology of our earlier cathode ink efforts for coating with BASF Fuel Cell's standard procedures on carbon cloth. The first task is performance evaluation. From our past experience, good dispersing agents usually have some functional groups that are difficult to decompose and the performance can be impacted because of blocking catalyst sites or gas diffusion pores. Four high energy dispersed cathode formulations were coated on gas diffusion layers prepared from formulations containing four different dispersants, respectively. The average performances in 160°C H_2/Air of two samples each of cathode with one dispersant, respectively are shown in Figure 37.

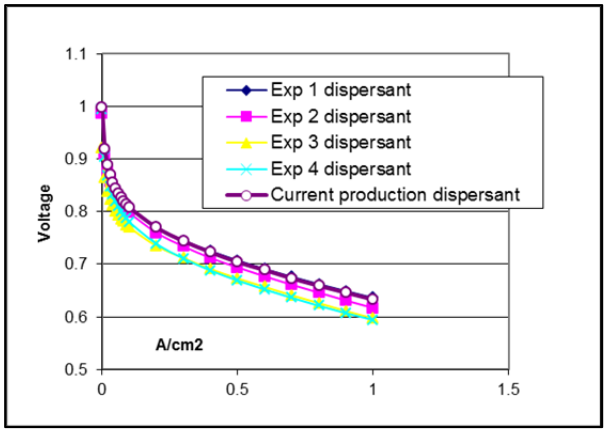

H_2/O_2

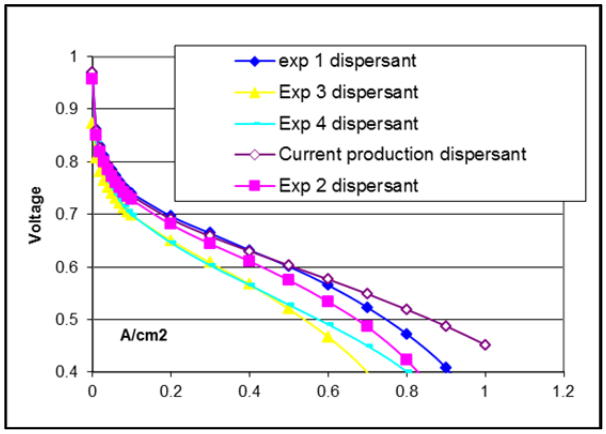

H_2/Air

Figure 37. H_2/Air and H_2/O_2 performance at 160°C for high energy dispersed cathode coatings on gas diffusion layers made from inks containing four different experimental dispersants.

Figure 37 indicates that in H_2/O_2 operation where gas diffusion is not an important factor, a lower performance is most likely related to less active catalyst sites presumably due to blocking by residue from post-treatment. Samples with dispersant 1 showed almost no performance loss, followed by samples from dispersant 2. We believe these dispersants infiltrated into the catalyst layers from interpenetration of the gas diffusion layer and catalyst layer. All cathodes showed performance loss in H_2/Air operation, which is understandable since the greater load of carbon dispersants are in the gas diffusion layer so most residues from post-treatment originate in this layer. Dispersant 1 was very

promising because only at higher current density (>0.6 A/cm^2) the performance starts to fall below that of cathodes with current production gas diffusion layer. Therefore, dispersant 1 was chosen for further study. The drop in H_2/Air performance at high current densities for cathodes on gas diffusion layer with dispersant 1 was most likely associated with post-treatment process, so it can be corrected by modifying process. This was later confirmed and a solution was found.

(B) Viscosity Behavior of Gas Diffusion Layer Formulation

At the beginning of this program the production gas diffusion layer formulation showed shear thinning behavior – i.e., viscosity decreases with shear rate. Although the exact cause is not clear, we believed it might be related to weak shielding of carbon by the dispersant, so a morphological structure is disrupted by shearing action. This behavior can cause two problems in formulations and coating: (1) the ink does not have good flow behavior for even coating presumably because the shearing action at applicator head can cause uneven random flow on the substrate and result in uneven coating; (2) unstable ink – shearing can detach dispersant from the carbon particles and repetitive shearing cycling then cause carbon to re-agglomerate. From this point of view a more Newtonian flow behavior – i.e., viscosity independent of shearing rate is more desirable because we believe this can lead to even coatings and stable inks.

As shown in Figure 38, all the formulations containing experimental dispersants in this study showed close to Newtonian behavior and the viscosities are lower compared to the production ink at the beginning of this program even with much high carbon concentrations (in the range of 3x of carbon as that in the production ink at beginning of this program). Our hypothesis is that Newtonian viscosity behavior might be related to a complete and stable shielding of hydrophobic carbon from surrounding aqueous phase, so the shearing action causes rotation or translation of the morphological structure as a whole.

Dispersant 1 was chosen as dispersant for further study. The dispersion power of dispersant 1 is much better than that in the production ink at beginning of this program as evidenced by employing a far lower ratio of dispersant to carbon.

The rheological behavior of the formulations with dispersant 1 is very close to Newtonian, Figure 39 shows the data for several examples. The viscosity behavior for the benchmark formulation at the beginning of this program, usually shear thinning, is also included for comparison. For this benchmark formulation, as we tried to increase the carbon concentration (important for reduction in number of application passes) the shear thinning behavior becomes even more so and with concomitant higher viscosity leads to inferior coatings.

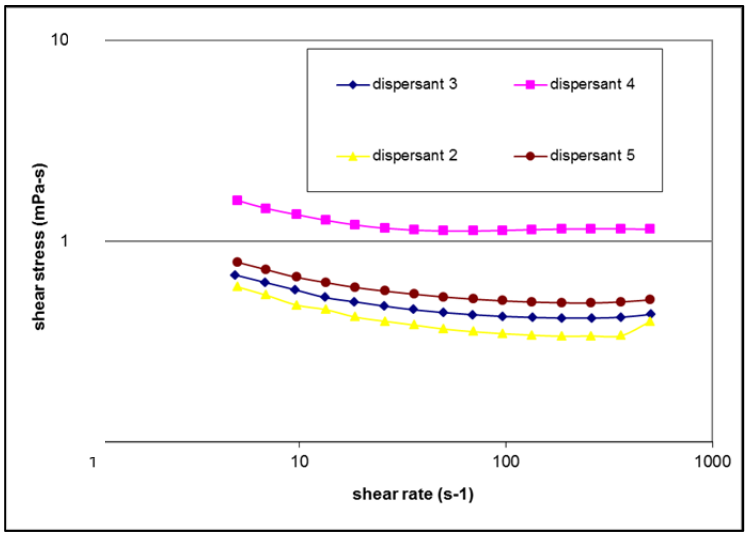

Figure 38. Viscosity behaviors of gas diffusion layer formulations containing various experimental dispersants. Carbon concentrations in the range of ~3x that in the current benchmark formulation.

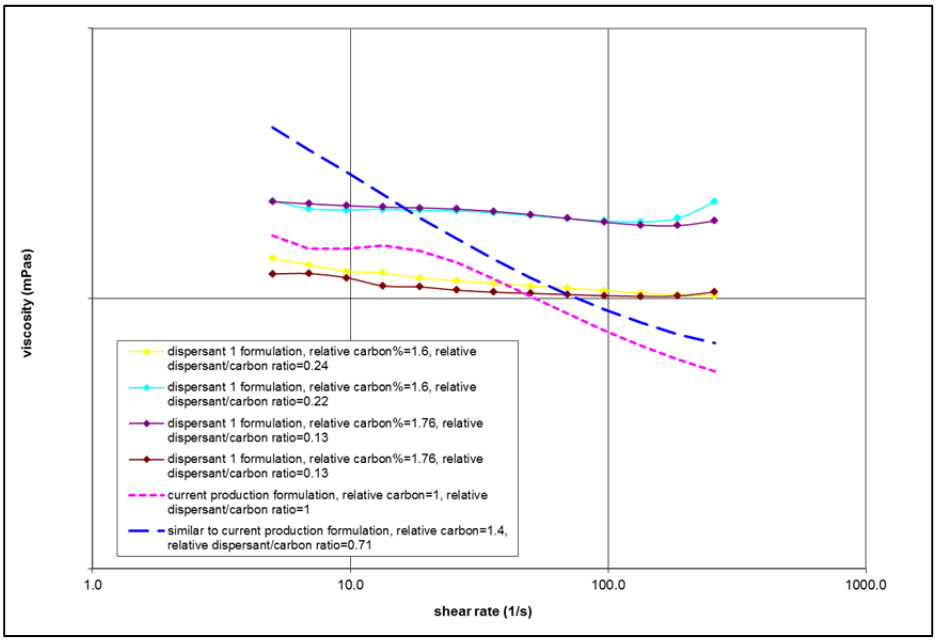

Figure 39. Viscosity behaviors of several gas diffusion layer formulations containing dispersant (1). Benchmark ("current") production formulation and its higher carbon concentration version are used as reference.

(C) High Energy Dispersed Cathode Coating on Gas Diffusion Layer with Dispersant 1

- *Electrode Trial Runs at Pilot Scale*

With the encouraging results of viscosity behavior of the gas diffusion layer formulation containing dispersant 1, we tried to combine the high energy dispersed cathode catalyst coating and the new gas diffusion layer. Pilot scale 1-2m^2 runs were conducted and the results are shown in Figure 40, in which the average performance of the 240l.m. (120m^2) run of high energy dispersed cathode coating on the ("current") benchmark production gas diffusion layer is used as a comparison. Figure 40 confirms that cathodes made on the new gas diffusion layer exhibit similar performances to that of the 120m^2 reference samples with benchmark production gas diffusion layer (at the time).

Springing from the success of the pilot 1-2 m^2 gas diffusion layer with dispersant 1 and new formulation, our next step was scaling-up new gas diffusion layer formulation to production scale, i.e., >150kg batch formulation scale-up.

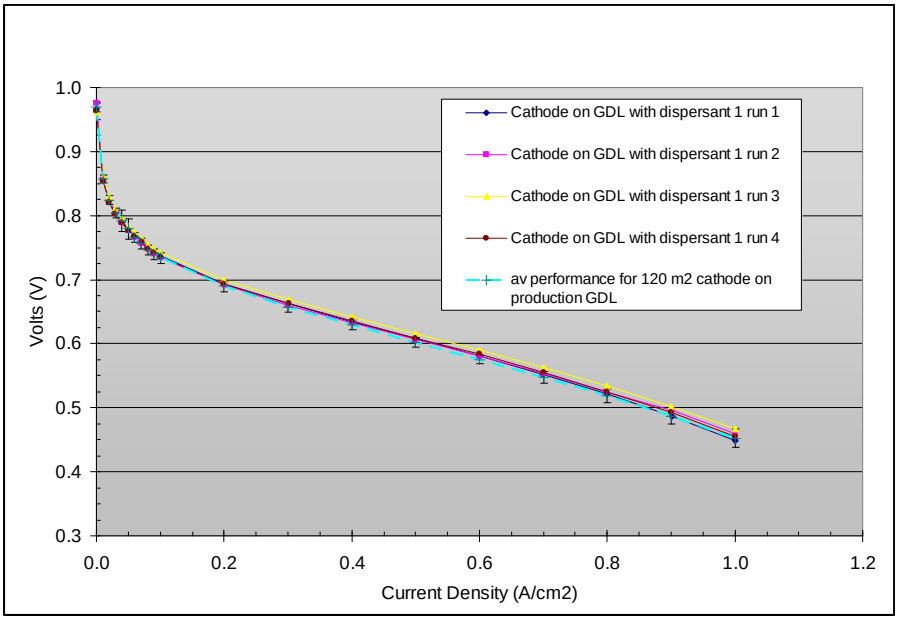

Figure 40. Performances at 160°C H_2/Air for high energy dispersed cathodes on new gas diffusion layer formulation with dispersant 1. Blue dotted line is the reference (120m^2 cathode on benchmark production GDL at the time of development).

Increase GDE Throughput

(1) Production Scale, Single Width Cloth (0.5 m)

High Energy Dispersed Cathode Coating on Gas Diffusion Layer with Dispersant 1

As discussed in section (A) Dispersant I showed excellent dispersion power for the graphitized hydrophobic carbon in gas diffusion layer formulation. It allowed us to increase carbon concentration by ~80% and in the meantime the dispersant concentration was reduced to only 1/3 of the concentration of the previous dispersant used in baseline formulations. Moreover, the carbon dispersion time decreased by more than 70%. At this time we were ready to scale up the new ink preparation to production scale of >150 kg.

(A) Challenge of Gas Diffusion Layer Ink Preparation at Large Scale

As part of the additive suite a defoamer is used along with dispersant I in the 1-2 m^2 pilot scale run of high energy dispersed cathode coating on gas diffusion layer with Dispersant 1, described above. The need for a defoamer came from incorporation of massive amount of trapped air from high energy dispersion. The hydrophobic carbon compounds this effect by providing a "hydrophobic phase" for gases to reside. These gas molecules cause a sharp increase in viscosity to the extent that the agitation of the carbon suspension becomes extremely difficult. However, after the discovery of defoamer I and successfully demonstrated utility at the pilot scale, we encountered difficulties as we increased the batch size of ink to production scale.
This problem led to further adjustments in the formulation.

(B) Defoamer Fundamental

To solve the problem associated with gas-induced viscosity increase at large scale preparation, we explored the use of defoamer. As described in Wikipedia, http://en.wikipedia.org/wiki/Defoamer,

Generally a defoamer is insoluble in the foaming medium and has surface active properties. An essential feature of a defoamer product is a low viscosity and a facility to spread rapidly on foamy surfaces. It has affinity to the air-liquid surface where it destabilizes the foam lamellas. This causes rupture of the air bubbles and breakdown of surface foam. Entrained air bubbles are agglomerated, and the larger bubbles rise to the surface of the bulk liquid more quickly. In brief, the defoamer is used to compete with air molecules for the interfacial areas around lamellas in a foam structure. A good defoamer has high affinity for interfacial areas, so gas bubbles can be driven out.

We found the solution viscosity can be very effectively reduced with the chosen defoamer I. As shown in Figure 41. Viscosities at 10 sec^{-1} shear rate can be used as a good indicator for extent of dispersion. Without the defoamer, the viscosity of the carbon dispersion can reach several hundred MPa with a low extent of carbon particle break-down.

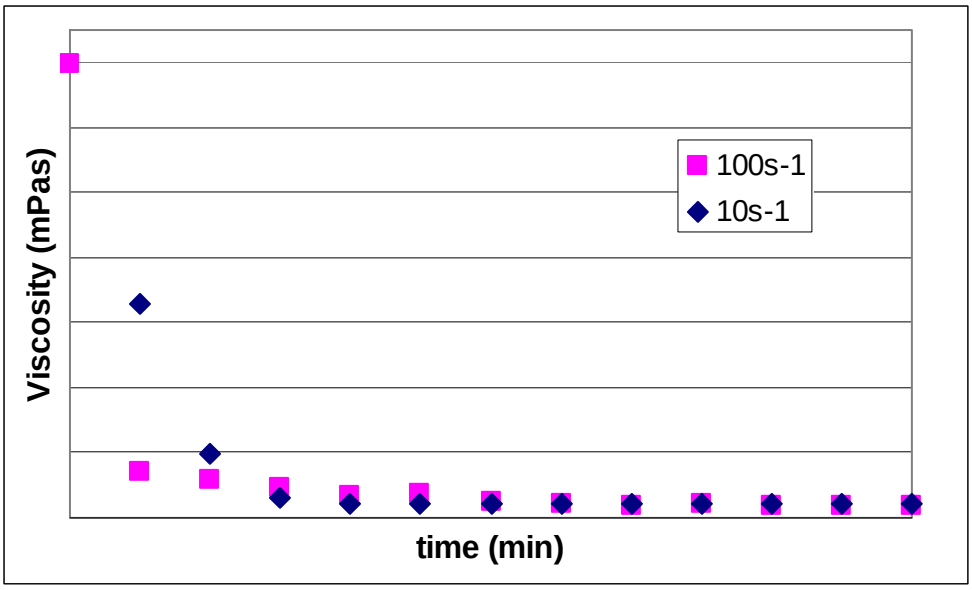

Figure 41. Dynamic Viscosities at shear rate 10 s-1and 100 s-1 for dispersed carbon suspension containing dispersant I and defoamer I.

The resulting ink formulation is Newtonian over a wide range of shear rates. Due to the Newtonian behavior, the ink formulation coating is consistent and uniform with good coating quality. Figure 42 compares the pinhole defects of GDLs with production baseline formulations at the time and that with the new GDL formulation described in this report. The new formulation with dispersant I and defoamer I apparently lead to gas diffusion layers with much less pinhole defects.

(C) Scale-up to Production Scale of Gas Diffusion Layer and Cathodes

In order to take the full advantage of new formulations for increasing the throughput of electrode production we next scaled-up these formulations to production scale with the goal to preserve the performance, higher throughput, and shorter ink preparation time seen at the pilot scale. Full length coating (>240 l. m) on the production coater with double wide cloth (>1m) needs over 100Kg of ink for the gas diffusion layer.

Figure 42. Photo micrographs of Gas Diffusion Layers prepared with new (experimental) formulations and that from baseline formulations (lighting is underneath the GDLs). Scale bar is 1mm.

In addition to developing the suite of additives for the ink formulations, we also had to design a system to process larger quantities of graphitized carbon that is in compliance with BASF's Environment, Health, and Safety guidelines. After review, it was determined that the carbon delivery/transport system needs to be properly designed to minimize the air bubble trapping that can lead to the viscosity increase as described above.

(i) Defoamer Adjustment at Production Scale

As mentioned above a defoamer was needed to drive out gas molecules trapped in the ink formulation for the gas diffusion layer. Defoamer I was efficient at pilot scale and lab scale ink preparations (< 20 Kg). For production scale ink preparation, the larger high energy dispersion unit introduced significantly more air bubbles into the formulation. Thus, defoamer I became inadequate and a more efficient defoamer was essential for successfully scaling the preferred ink formulation.

The portfolio of potential compounds was analyzed using the same selections rules used for defoamer I. Defoamer II has a similar molecular structure, but with modifications that created a more appropriate surface property. The difference is that defoamer II can occupy a larger interfacial area between air and liquid lamellas, so it is much more efficient at gas removal. Fortunately defoamer II did not show any negative effect on performance as Figure 43 shows. In Figure 43, H_2/Air performances of high energy dispersed cathodes on various gas diffusion layers were compared. Also included is high energy dispersed cathode on benchmark production GDL at the time, which was post-treated with the old process; all other cathodes were post-treated with a new process as described in section (b) below . After this test defoamer II replaced defoamer I in the gas diffusion layer formulation with all other components unchanged. Figure 43 clearly shows that all high energy dispersed cathodes on the new GDL with either defoamer I or II exhibit the same performances and they are all higher than the same cathode on baseline production GDL. The improved performance is believed to be from the new post-treatment process that can remove additives more completely.

From that point on, Defoamer II has been used in all GDL materials for both anode and cathode on the production machine as well as pilot scale trials.

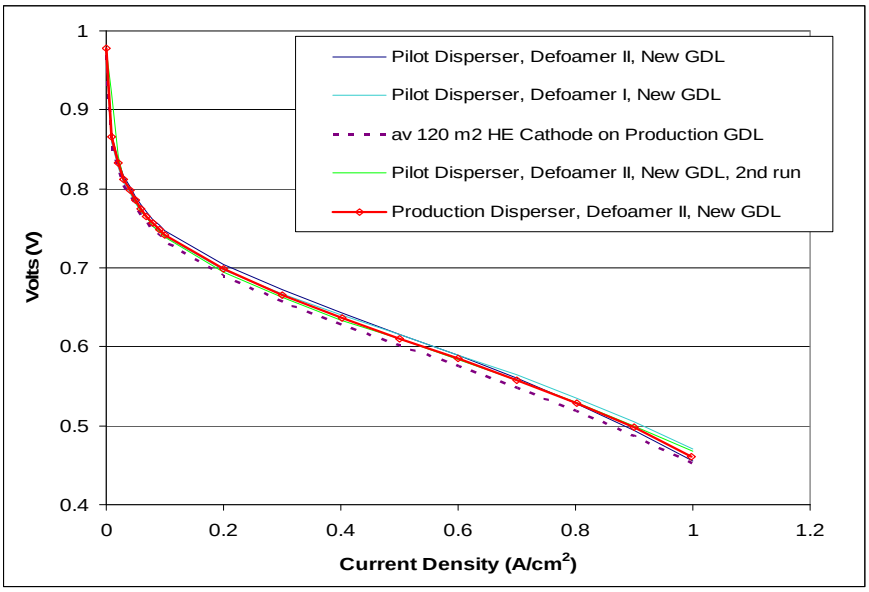

Figure 43. 160°C H_2/Air Performances for high energy dispersed cathodes on various GDL coatings (HE=high energy dispersion). All MEAs have standard anodes and membranes.

(ii) Post-Treatment Optimization

As Figure 40 and Figure 43 show, the new high energy cathode inks when coated with the Pilot coater over 1-2m^2 of the new GDL material, performed similarly to the benchmark GDL with these new high dispersion energy cathode inks at a production scale of 120m^2. However, these new GDL experiments were conducted with small batch sizes during post-treatment. Usually larger batches undergoing post-treatment can be significantly more challenging due to the larger processing volume of electrode.

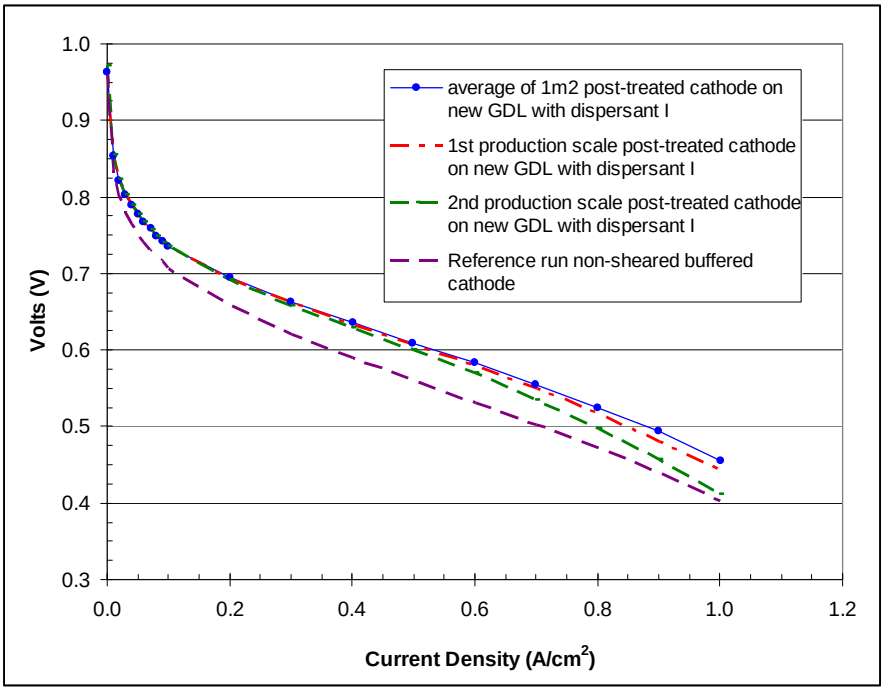

Figure 44. 160°C H_2/Air Performances for high energy dispersed cathodes on GDLs prepared from ink formulation containing dispersant I

Indeed this problem surfaced as we scaled-up the post-treatment batch size to "production post-treatment size". Figure 44 shows the comparison for the performance of high energy dispersed cathodes prepared on the same roll but post-treated at small and large batch sizes. The large batch shows obviously lower performance at high current densities – so called bending down behavior, indicating a mass transport issue that is most likely related to incomplete additive (in the new GDL ink) removal. This issue was resolved by optimizing the post-treatment process.

Figure 44 shows with the green curve the cathode performance of a high energy dispersed cathode on the gas diffusion layer with the new formulation (dispersant I). This batch was coated on the pilot coater (long roll) and post-treated in full production batch size. This green curve shows bending down behavior at high current densities. We then performed an analysis as shown in Figure 45 to determine the cause for this performance problem at high current densities. Figure 45 shows the comparison of samples from $1m^2$ coating/post-treatment (blue curve in Figure 45) and that from pilot scale coating/post-treatment (green curve in Figure 44). Since the two samples have almost the same H_2/O_2 performance we concluded that the difference was caused by the diffusion layer impeding mass transport. From our past experience this is most likely caused by incomplete additive removal in the new GDL ink. Based on this evidence we adjusted the post-treatment process to improve performance.

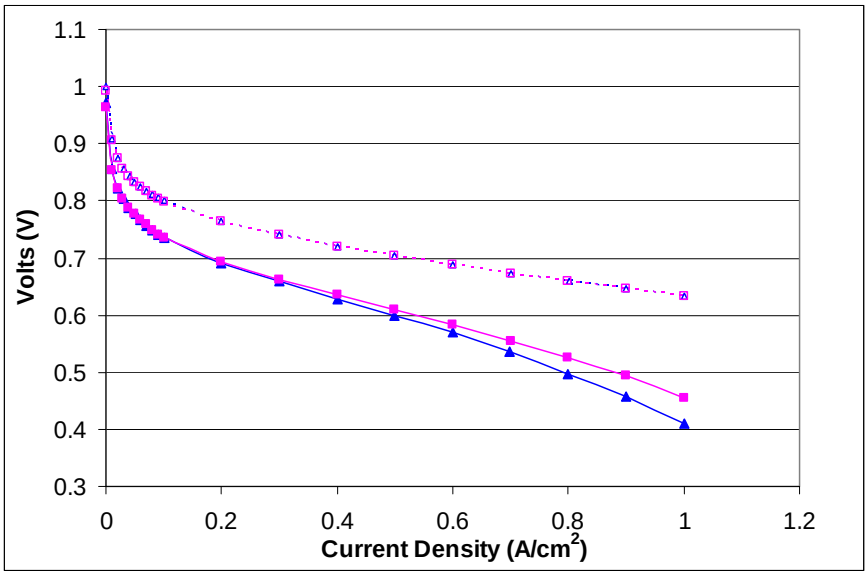

Figure 45. 160°C H_2/Air Performances for two cathodes. Blue (triangles) curve is for the sample corresponding to green curve in Figure 44; pink (squares) curve for samples corresponding to blue curve in Figure 44. Dotted line is same in H_2/O_2.

Figure 46 shows the large effect of manipulating the post-treatment process in which we presume a more complete removal of new additives thus leading to a significant improvement in performance at higher current density. The performance was raised to a level above that for the same high energy dispersed cathode layer on the benchmark production GDL (dotted line).

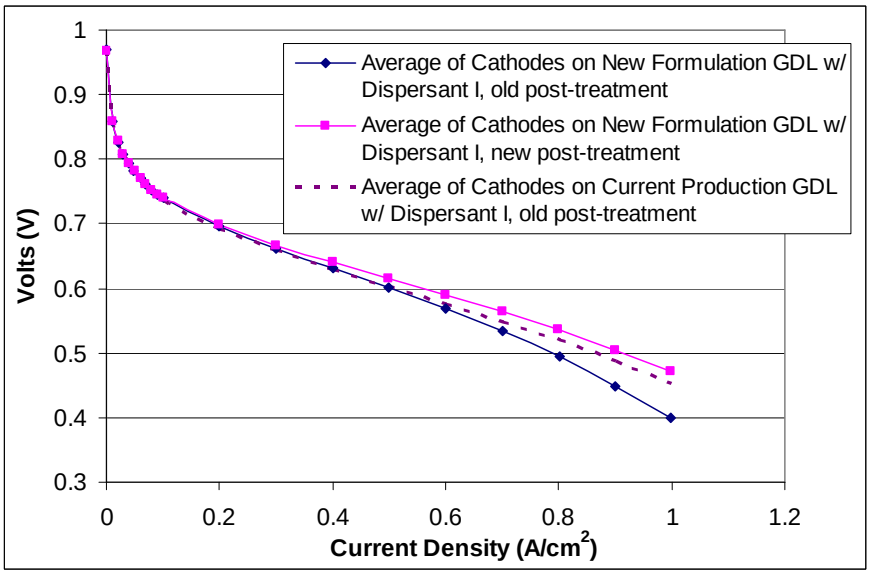

Figure 46. 160°C H_2/Air Performances for cathodes with different post-treatments

(2) Production Scale, Double Width Cloth (1.17 m)

High Energy Dispersed Cathode Coating on New Gas Diffusion Layer

As described previously, we have successfully developed cathode, anode, and gas diffusion layer ink formulation methodology that combines high energy dispersion and a series of additives to stabilize inks. This methodology has allowed a decrease in the time to prepare an ink, and more importantly, significantly decreased the number of applicator passes needed to obtain the target weight of carbon for the case of the MPL and anode/cathode catalyst for the GDE. By being able to both shorten ink preparation time and decrease application coats for the MPL and cathode/anode GDE we effectively decrease the overall time to prepare GDEs and substantially increased the overall throughput.

With the effort to increase throughput, we also scaled up the gas diffusion layer ink to >100 kg. After scaling the carbon ink, it became apparent that the cathode/anode ink batch was the new bottleneck for the whole electrode production. In the initial stages of this program, we have been using ink formulations prepared at the lab scale for making high energy dispersed cathode and anode. However, as we scaled-up coating to double width (1.17 m) with ~300 m long, the small scale ink preparation becomes the bottleneck to limit the electrode throughput. We decide to scale-up the ink volume in one batch with a target of nine-fold scale-up.

(A) Scale-up High Energy Dispersed Anode Cathode Ink Formulation

This scaling-up includes an increase in the scale of high energy disperser employed as well as ink handling equipment. All the preparation steps have been kept the same. Figure 47 shows that for both high energy dispersed cathode and anode the scale-up was successful without performance loss

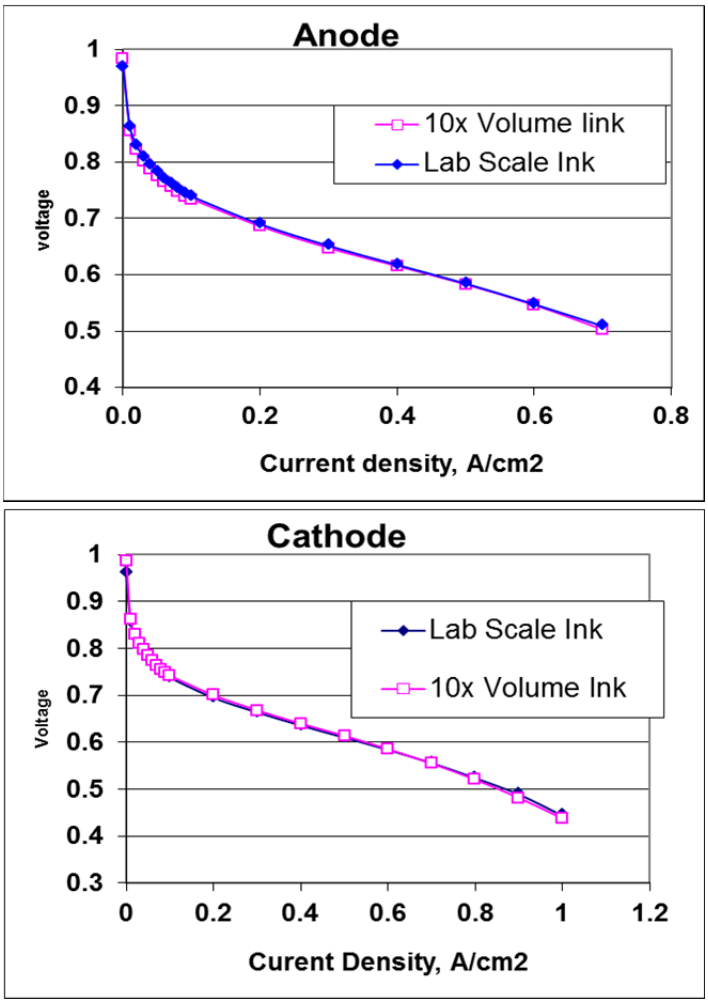

Figure 47. Performance Comparison for Cathodes at 160°C H_2/Air (1.2/2) and for Anodes at 180°C Reformate/Air (1.2/2) employing lab scale and ~10x scale up in preparation.

(B) Coating of Double Width Cloth Roll

Gas diffusion layer ink (>100 kg batch) was coated on ~240 m length of cloth with 1.17 m width- the production cloth width at the time of development was 0.5 m width. This provides not only an effective >2x in material throughput but just as importantly provides wide latitude in minimizing scrap losses due a mismatch between the native web size and the final MEA GDE size. One portion of the GDL layer was coated with high energy dispersed cathode ink (9x batch size), and one portion with high energy dispersed anode ink (9x batch size). The cathode and anode were then post-treated at production scale (new post-treatment process described in the session right above this one was used) and the performance was evaluated.

Figure 48 shows the scale-up from pilot to 280 m^2 run of GDL is successful without any performance loss. Both are better than the high energy dispersed cathode on baseline production GDL with baseline (old) post-treatment process. All these cathodes are improved over the benchmark production cathode at the time.

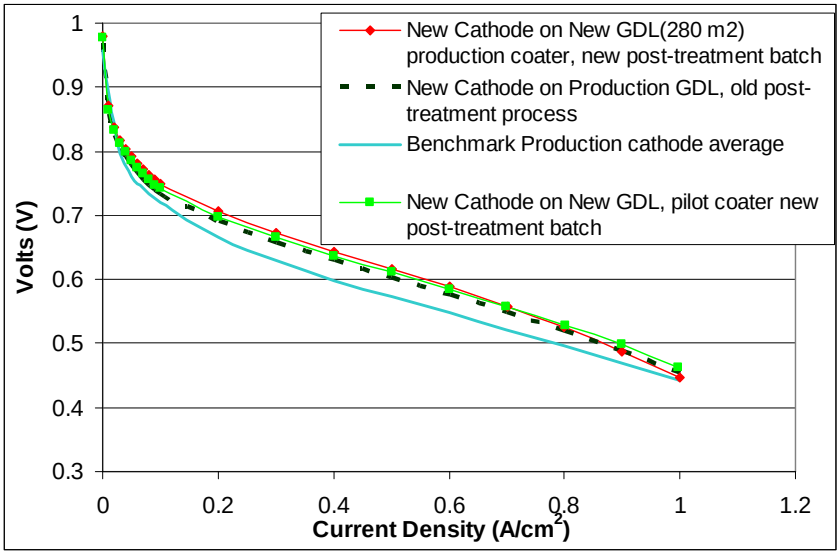

Figure 48. 160°C H_2 /Air performance comparison of high energy dispersed cathodes on new GDL (280m^2 on production coater)- red (diamonds) line, and same cathode on production (baseline) GDL- dotted line. Also included are pilot scale run corresponding to green (squares) line and current baseline production cathode and GDL layer technology (light blue line). All MEAs use standard membrane and standard production anode.

Figure 49 shows the same comparison for the anode. These results indicate that the scale-up from pilot scale to production scale is successful. The performances are also significantly better than the benchmark production anode at the time.

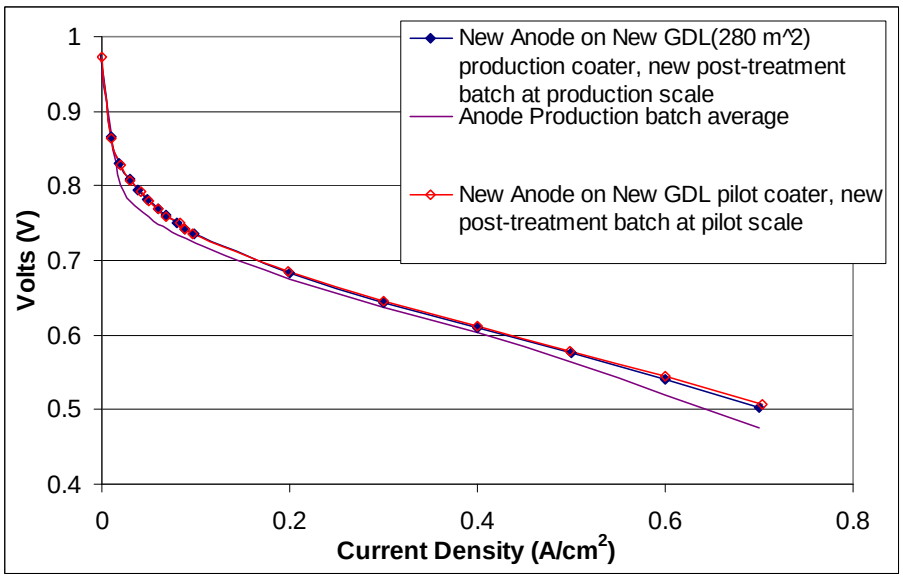

Figure 49. 160°C Reformate /Air Performance Comparison of High Energy Dispersed Anodes on New GDL (280m^2 on Production Coater)- blue line and corresponding pilot run- red line. Also included are benchmark production anodes with benchmark cathode and GDL layer.

(C) Summary of Advantages of New Electrode and Carbon Ink Formulations Employing High Energy Dispersion, Advanced Formulations, and Post-Treatment

The advantages of high energy dispersed anode ink formulation are similar to that for corresponding cathode. They can be summarized as follows:

High energy dispersed cathode/ anode

(1) Reduce ink preparation time by 50-67%

(2) Reduce coating passes by 30-40%

(3) Reduce surface agglomerate defects by 60%

(4) Improve performance (cathode in air; anode in reformate)

(5) Reduce catalyst loading variation to ¼ of standard variations of benchmark

There are many advantages for the new gas diffusion layer ink formulation based on new disperser, new defoamer, and new process. It leads to a vast improvement in operation efficiency and product quality:

(1) Improve MEA performance by 25-30 mv at 0.2-0.5 A/cm^2

(2) Reduce ink preparation time by >80%

(3) Reduce coating passes by ~40%

(4) Reduce GDL rejection rate

(3) Electrode Thickness Adjustment

In many commercial fuel stacks the individual cell sealing/assembly is controlled by a fixed design. Therefore, the useable MEA thickness range is limited. If the MEA is lower than the low limit, insufficient contact between MEA and flow field can occur and result in higher contact resistance and lower performance. Contact resistance can be measured easily by AC impedance at 1000-3000 hertz frequency. For high temperature PBI cells, 85-100 mohm-cm^2 is considered the typical range. AC impedance significantly higher than 110 mohm is an indication of insufficient contact. Thicker MEA can present problems associated with blocking of gas flow and difficulty in complete sealing.

Although re-design or re-molding of cell stack is an option, current commercial stack design is not flexible enough to allow for these modifications in a cost-effective manner. Therefore, the practical way is to adjust MEA thickness through adjustment of cathode and anode thickness. We carried out a short project to adjust the anode and cathode thickness through adjusting the GDL thickness, so our customers could take full advantage of the new product containing gas diffusion layer and catalyst layer prepared with high energy dispersed and advanced formulations, along with advanced post-treatment.

(A) Experimental Design

We adjusted the thickness of cathodes and anodes by choosing three levels of micro porous layer loadings. A series of GDL weights of the three levels were applied to the cloth base material and the thickness was measured after post treatment. Afterwards cathode and anode coating was applied to the GDL coating and subjected to post-treatment and thickness was measured again.

(B) Thickness and Weight Gain

Figure 50 shows the thickness and base weight of GDL, cathode, and anode. There were three runs and apparently the data was quite consistent and indicates the coating is under control. The standard deviation for cathode thickness with X=2 coating is 0.5% of the average and the corresponding value for anode was 2%. The MEAs made with the cathode and anode on GDL1 preparation show thickness close to the average or slightly higher than the revised target based on feedback from stack evaluations.

(B) Electrochemical Performances for Electrodes with GDLs of Different Thicknesses

As Figure 51 (below) shows for all cathodes on different GDLs the performances were almost the same. Only a very slight lower performance for X+3 layer GDL1 at >0.9 A/cm^2 was observed. The specification average and minimum is for standard materials.

As shown in many sections mentioned above, the new cathodes from high energy dispersed cathodes always show much better performance than current production cathodes (formulation without high energy dispersion). From this study we selected the X+2 level of micro porous layer weight to scale to the production coating trials.

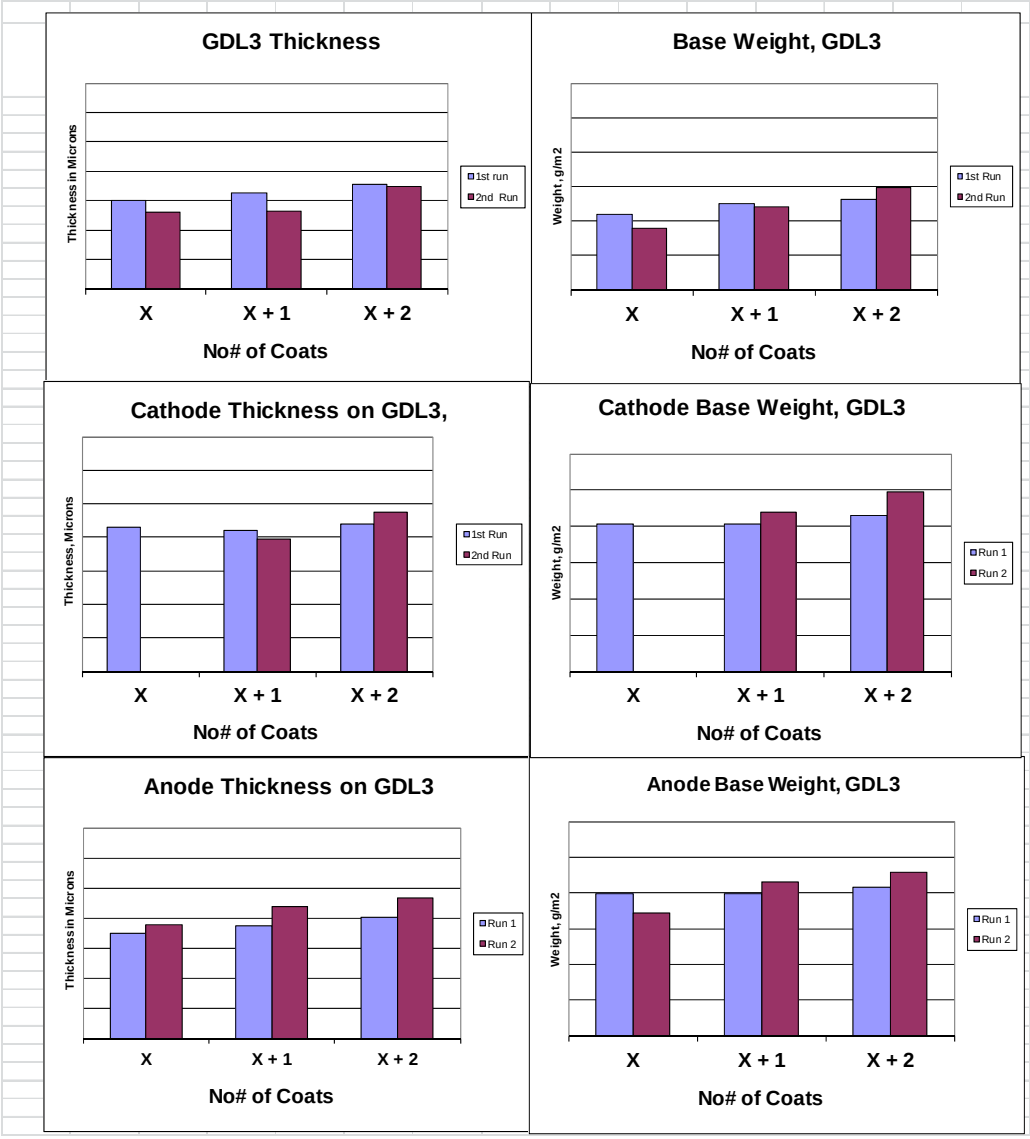

Figure 50. Thickness and Base Weight for GDL1, Cathode, and Anode Prepared with High Energy Dispersed Ink Formulation and Advanced Dispersant I (for GDL).

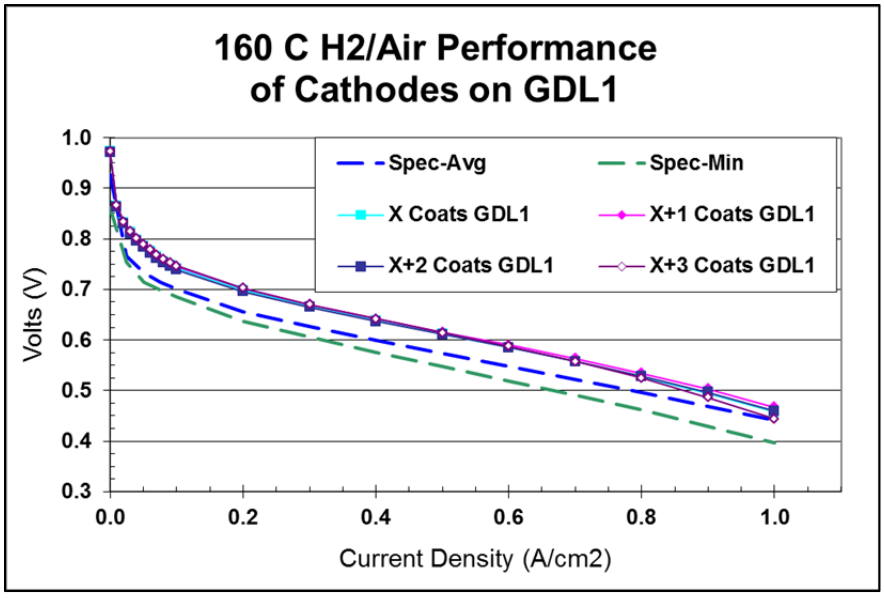

Figure 51. 160°C H_2/Air performances of High Energy dispersed cathodes on GDL1 of Different Thicknesses. Standard membranes and standard anodes were used.

(C) Effect of GDL Thickness on Pore Size Distribution

Figure 52 shows the pore size distribution for several batches of GDLs of X and X+2 coats measured by mercury intrusion porosimetry. In Figure 52 there is a clear trend of decreasing pore size distribution for GDLs with X+2 coats, and the distribution maximum shifts larger to smaller pores (X+3 not shown). The implication of the pore size distribution decrease in GDL layer is a resistance to gas diffusion. This is consistent with the results we presented in the last report: the cathode performance at very high current density, >0.8 A/cm^2, is lower for the cathode with X+3 layered GDL, where the pore size distribution is further shifted to lower values.

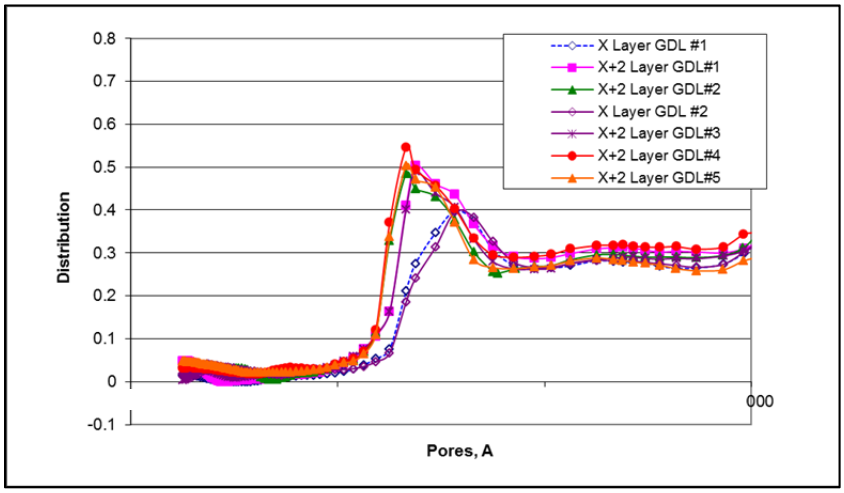

Figure 52. Hg intrusion porosimetry of gas diffusion layers of different build parameters.

The implication of the pore size distribution decrease in GDL layer is a resistance to gas diffusion. This is consistent with the results we presented in the last report: the cathode performance at very high current density, >0.8 A/cm^2, is lower for the cathode with X+3 layered GDL, where the pore size distribution is further shifted to lower values.

Decrease cost through platinum thrift

At the 2011 DOE Annual Merit Reviews, Reviewers inquired on the possibility of reducing platinum content in the MEA due to the higher catalyst utilization structures created by the new inks developed in this program. Although platinum thrift is not the focus of this program, the superior uniformity of the inks led us to believe some reduction in platinum is possible. Furthermore, the uniformity of the ink gave us potential to create new structures previously unattainable with the old formulations. This section summarizes BFC's achievement on platinum thrift by the approach of innovative electrode structure control.

(1) Concept

In typical steam reformed fuels there are ~70% H_2 and 1-2% CO with balance being CO_2. The poisoning of catalyst by CO effectively decreases the available catalyst sites for binding and for oxidation of hydrogen. The 70% H_2 in reformate usually does not lead to significant mass transport problems. Therefore, anode performance in reformate depends mainly on number of available active catalyst sites. To maximize the performance one should create an electrode structure whereby the number of engaging Pt catalyst sites is highest. For Pt sites to be involved in electrochemical reactions, they need to be accessible to both hydrogen ions (from H_3PO_4) and hydrogen gases, i.e., positioning at three-phase boundary with low proton transport and mass transport resistance. According to this principle, we worked along the line of modifying the porous structure of anode to build more sites positioning at accessible three-phase boundaries. This includes modifying the property of carbon support surface and catalyst particle morphology.

(2) Experimental Results

A series of anodes with the new structure were prepared on the pilot coater. Also, a series of standard P1100W anodes based on this program (P1100W is the new product released from this program: see section on "Developing Specification based on six sigma concepts") were also made on the same coater for comparison. As Figure 53 shows, one can see anodes with the new structure exhibiting a clear advantage over the existing P1100W anode in 160^{o}C reformate operation at all four loading ranges. The loadings are as follows: A1 = 0.33 mg Pt/cm^2, A2 = 0.51 mg Pt/cm^2, A3 = 0.75 mg Pt/cm^2, and A4 =1.0 mg Pt/cm^2. A4 is the current standard loading for P1100W anode. Figure 53 shows that for an anode with the new structure, even the A3 loading performance is better than the P1100W with standard structure and A4 loading. Reduction of loading from A4 to A3 is about 30%.

Operation at 180^{o}C reformate as shown in Figure 54 reveals smaller differences between anodes with standard structure and those with the new structure. For P1100W standard, only when the

loading is decreased to an A2 level is a significant performance drop observed; for anodes with the new structure, the loading has to be decreased to A1 level before encountering serious performance drop.

This observation above is consistent with the trend reported in a literature by employing meta-PBI and post-incorporated H_3PO_4, (also called "dip and soak") instead of BASF's *in-situ* formed para-PBI from PPA (polyphosphoric acid, also called the "PPA process"). The authors showed that the performance drop in operation from 200°C to 175°C is negligible but a very significant drop was observed from 175°C to 150°C. The fundamental principle is that there is a big change in Pt-CO bonding mechanism/strength around 160-170°C. (Ref 3).

Since fuel cell components degrade faster at higher temperature, we recommend stack operation at around 160°C, so the improvement observed here with the new structure(s) is very significant.

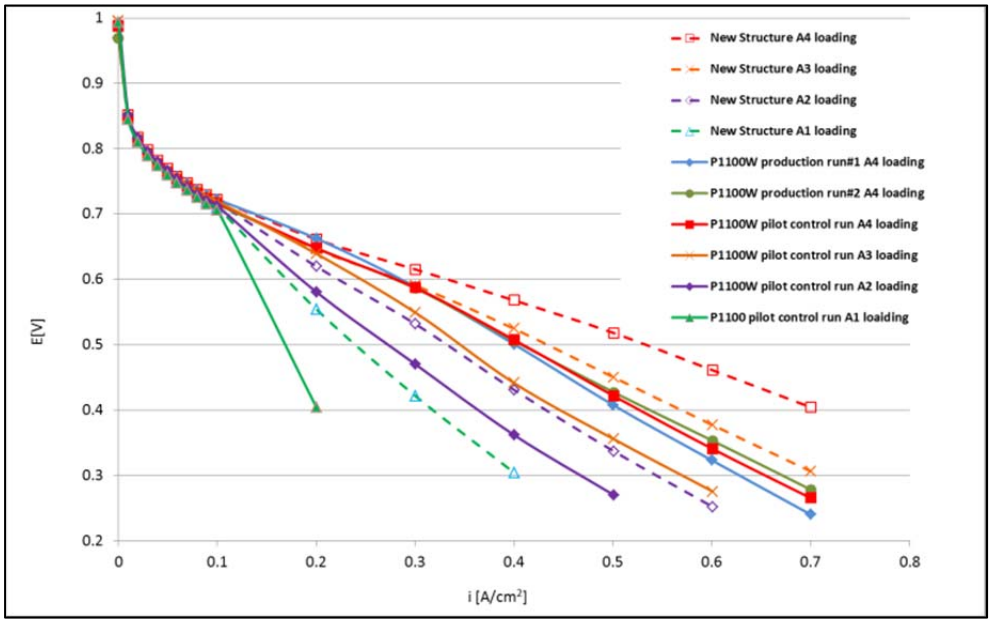

Figure 53. New Structure Anodes –dotted lines vs. P1100W Standard Anodes – solid lines (from this program), 160°C Reformate/Air, 1.2/2, pressure=1 bara.

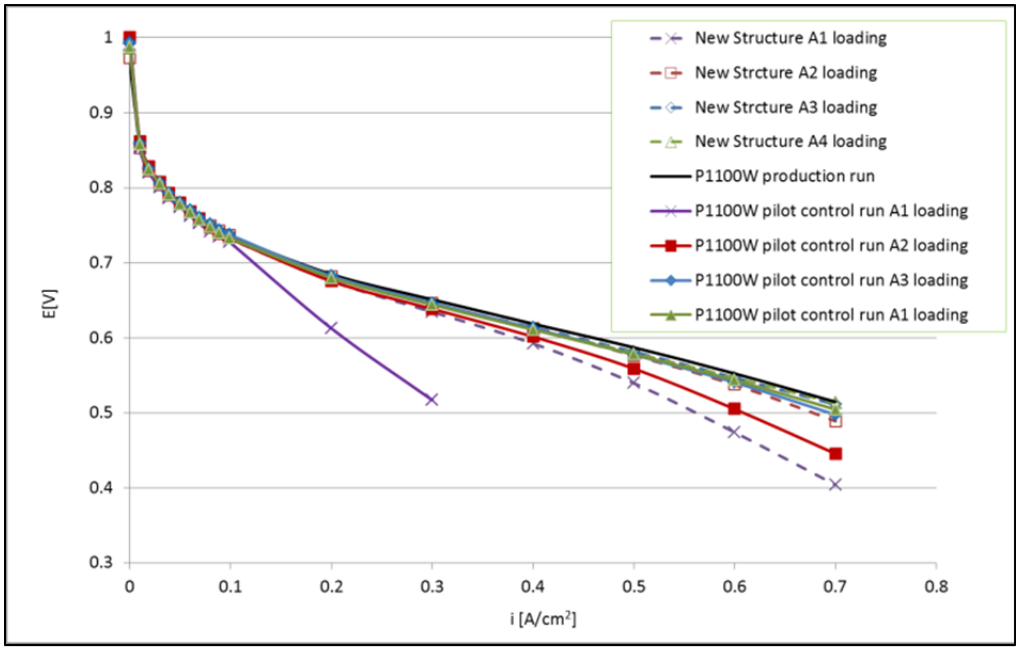

Figure 54. New Structure Anodes –dotted lines vs. P1100W Standard Anodes – solid lines (from this program), 180°C Reformate/Air, 1.2/2, pressure=1 bara.

(3) Fundamental Understanding on Performance Improvement: New Anode Structure

Performance Dependence on Mass Specific Current Density

As we showed in section (2), because of high utilization of anode catalysts in the new structure, we observed large improvement in performance in 160°C reformate operation. To further understand the factors controlling the reformate performance, we analyze the current density dependence of the performances in reformate. In order to be able to compare the performances of anodes with different loadings, we normalize all performances to the mass specific current A/mg Pt. This value is obtained by dividing current density by the loading of the anode: A/cm^2 divided by mg Pt/cm^2 = A/mg Pt. Therefore, the comparison will be the performance for unit Pt metal used in the anode. This property can reveal the efficiency of the catalyst utilization regardless of the surface property or degree of dispersion for the catalyst. Figure 55 and Figure 56 show such comparisons. Moreover, the cathode influence on reformate performances is also eliminated by taking the difference between Reformate/Air and H_2/Air performances at 160° C and 1.2/2 (anode gas/cathode gas stoich)

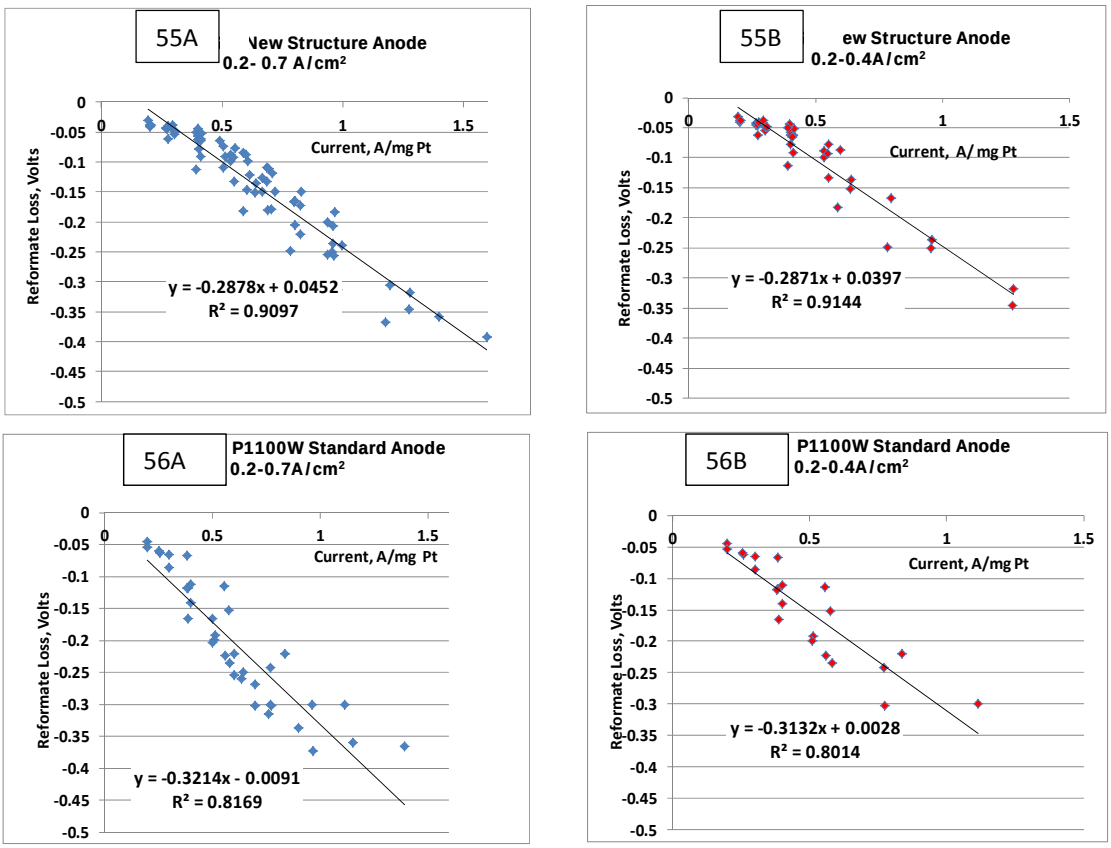

Figure 55. Reformate Loss vs. Mass Specific Current Plots for New Structure Anodes with Various Loadings. Comparison of linear correlation.

Figure 55A. 160°C Reformate Loss vs. Mass Specific Current New Structure Anode Samples "high current" (over 0.2-0.7A/cm^2)

Figure 55B. 160°C Reformate Loss vs. Mass Specific Current New Structure Anode Samples (over 0.2-0.4A/cm^2)

Figure 56. Reformate Loss vs. Mass Specific Current Plots for P1100W Anodes. Comparison of linear correlation.

Figure 56A. 160°C Reformate Loss vs. Mass Specific Current P1100W Standard Anode Samples "high current" (over 0.2-0.7A/cm^2)

Figure 56B. 160°C Reformate Loss vs. Mass Specific Current P1100W Standard Anode Samples (over 0.2-0.4A/cm^2)

Figure 55A shows the reformate loss for new structure anode vs. mass specific current. The correlation is very good with R^2 about 0.91 for the full current density range of 0.2-0.7 A/cm^2 and the slope is 288 mv per A/mg Pt. When only data points in 0.2-0.4 A/cm^2 are plotted, one gets almost the same slope and also the same R^2 correlation (Figure 55B). The analysis indicates that for over the whole current density range and anode loading ranges, a linear correlation is found between anode performance and Pt loading. This result points to the same electrochemical reaction mechanism throughout the ranges of current density and loading, and also a rather consistent and uniform anode structure and wetting of catalyst. Moreover, there is no detectable influence of mass

transport as indicated by no bending down behavior observed at high current density as one usually observed for cathode performance in air (Figure 55A). When a similar analysis is conducted on the P1100W anode as shown in Figure 56A and Figure 56B, we observe a somewhat linear correlation but with more scattering, R^2 is around 0.80-0.82. Moreover, the slope is slightly higher at around 310-320 mv per A/mg Pt. The higher slope for P1100W anode implies a higher tortuosity for H_2 (in reformate) to find a reaction site and the larger data scattering (high R^2) for P1100W points to a less uniform morphological structure for the P1100W anode. The difference in intercepts for Figure 55A and Figure 56A, ~35 mv represents a rough estimation of difference in "available catalyst sites" in terms of voltage penalty (or advantage). This means that for the same Pt loading, there is a 35 mv advantage for new structure anode, and leads the way to reduction of precious metal content.

(4) Electrode Pore Structure Study

As discussed above, an electrode with better performance in reformate operation is most likely associated with more available sites (for hydrogen gas and acid) in the electrode for same amount of total catalysts. This is presumably related to a more open or loosely packed electrode structure for anodes with the new structure. To further understand how manufacturing methods and procedures impact total pore volumes associated with anodes, we conducted electrode hydrophobicity tests. In this test we also gained more information about pore volumes in the electrodes.

Electrode pore volume test is conducted by equilibrating an electrode with various solvents containing a mixture of water and low alcohol with different ratios. The absorbed solvents at different ratios are weighed. The test was originally developed and applied to low temperature structures under a prior DOE program (DE-FC04-02AL67606) but has utility here as well. The weight gain vs. percent alcohol in a mixture of water/ alcohol for anodes with loadings A3 and A4 and with the standard and new structure, respectively, are shown in Figure 57. From our previous report, A3 = 0.75 mg Pt/cm^2, and A4 =1.0 mg Pt/cm^2, the current standard loading for the P1100W anode.

In Figure 57, the plateau regions are associated with the catalyst layer and the rising regions at higher alcohol content are associated with the gas diffusion layer. The Figure shows the rising part for catalyst layers in new structure anodes and standard P1100W anodes occur at about the same solvent composition, so hydrophobicity of catalyst layer is not the factor for observed performance. On the other hand, it clearly shows at the same loading, either A3 or A4, new structure anodes have larger pore volumes associated with catalyst layers (higher weight gains). This result is in consistent with our hypothesis of looser packing through the new manufacturing process/inks.

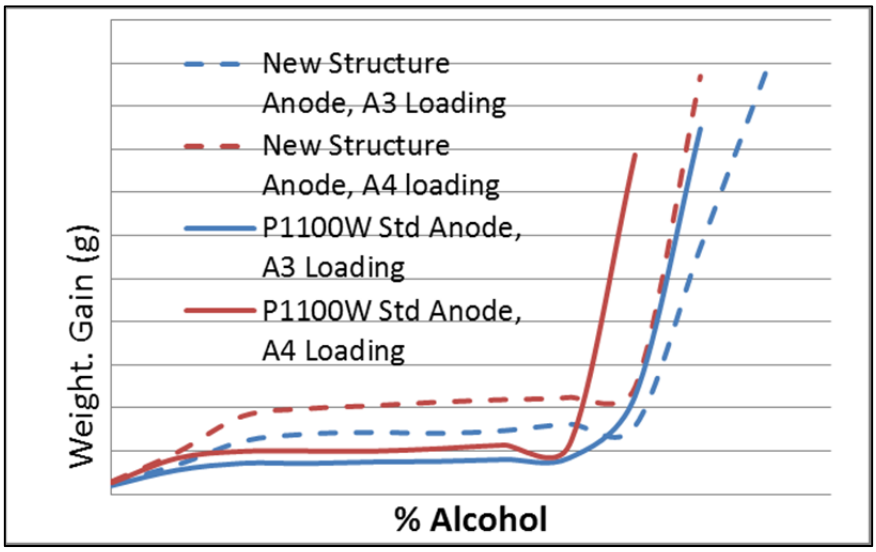

Figure 57. Electrode Hydrophobicity Test for Anodes with New Structure and Standard P1100W Anodes.

(5) New Cathode Structure and Durability Test

The same approach for improved anode structure has been also applied to the cathode side. Figure 58 shows the performance of MEA with cathode with new electrode structure and standard P1100W anode and standard membrane. The performance of an MEA with all standard components is included for comparison.

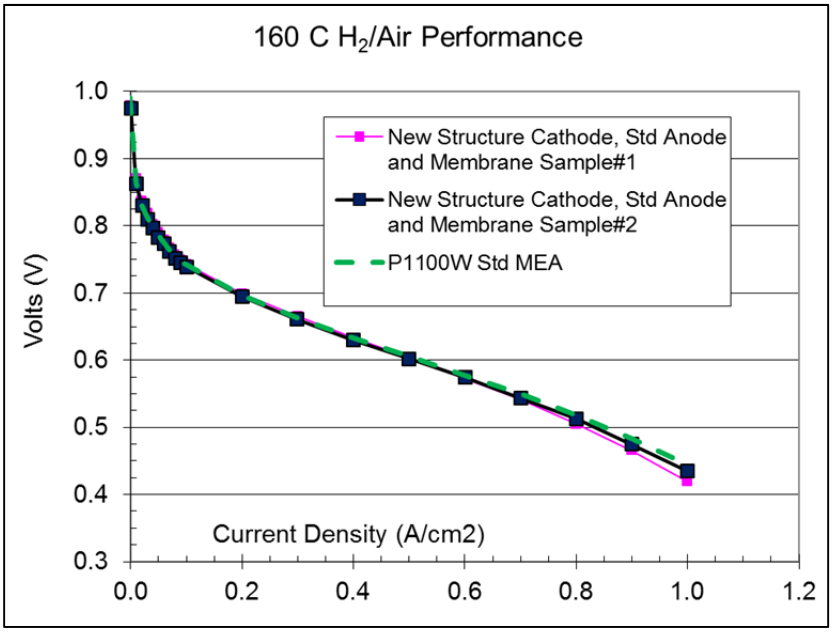

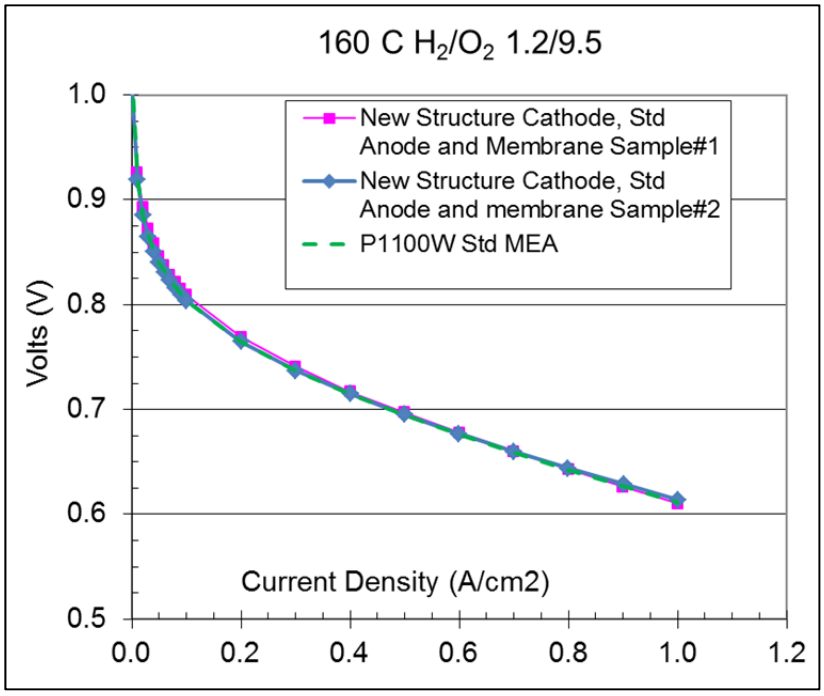

Figure 58. MEA Performances of MEAs with New Structure Cathodes vs. Standard MEAs. Top H_2/Air, Bottom, H_2/O_2.

The performances of MEAs with new structure cathodes are essentially the same as the standard P1100W MEA. However, we found durability advantages for the electrode with the new structure. When the MEA showing performance in Figure 58 was allowed to run continuously, the MEAs with new structure cathode showed much better stability with a lower degradation rate for initial 150 hours.

In view of this encouraging result, we started lifetime test for an MEA with both anode and cathode with the new structures, and compared it with the standard P1100W MEA. As shown in Figure 59, these MEAs show lower degradation rates than the standard P1100W MEA. A control with lifetime on only the new structure anode and standard cathode was not performed so the degree of contribution to stability from anode or cathode was not determined. However, continuation of this test was interrupted by Hurricane Sandy.

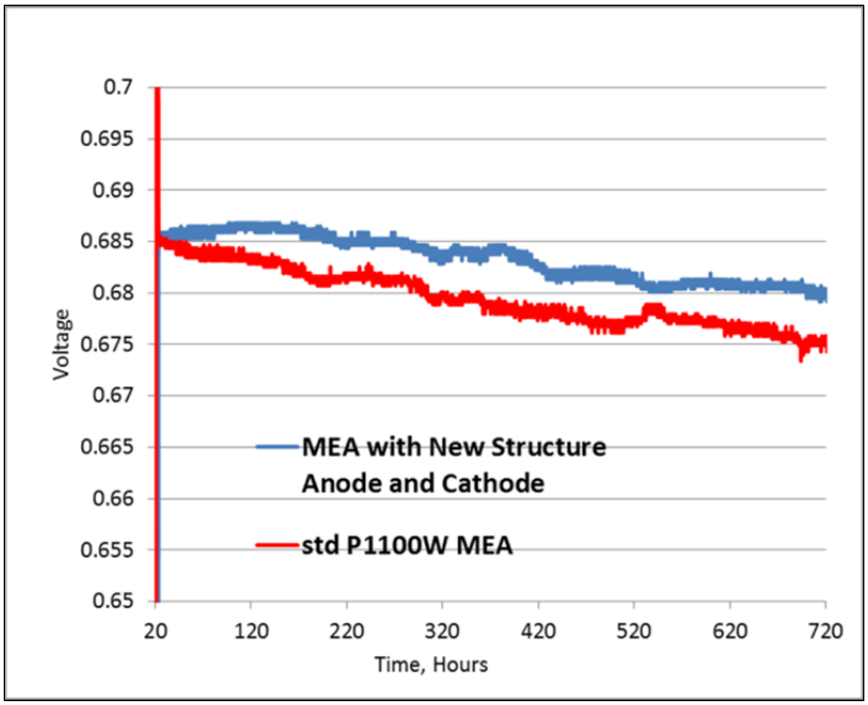

Figure 59. Comparison of MEA with new structure Cathode/Anode vs. standard P1100W MEA. Performance at constant current density (0.2 A/cm^2) and 160^{o}C H_2/Air; cells have been broken-in 20 hours.

(6) Scaling-up New Structure Anode

A 65m^2 roll of anode with newly modified structure was coated on the production coater with the same precious metal loading as P1100W anodes. P1100W is our commercial designation for materials that were developed through work in this program. A 65m^2 coating length is roughly 1/5 a full roll but believed to be representative for the stability and quality expected from a full roll. The ink formulation is essentially similar to what was developed for P1100W anode except using modified catalyst and surface structure. The same electrode post treatment as for P1100W anode was used. MEAs were prepared with standard reference membranes and cathodes.

Testing results in 160^{o}C reformate/air (1.2/2 stoich) are shown in Figure 60 along with the statistical data for P1100W anode. Figure 60 clearly shows the performance advantage for the new structure anode (16 sample average) in 160^{o}C reformate operation. Table 11 summarizes the average values and standard deviations for new structure anode and standard P1100W anode (data taken from production batches). The advantage at 0.2 A/cm^2 is 14 mv, and increases to 65 mv and >87 mv at 0.5 A/cm^2 and 0.7 A/cm^2, respectively (some lower values for P1100W anodes were not included in data acquisition). Not only the average values are increased, but the standard deviations are also reduced by about 40-50% as shown in Table 11.

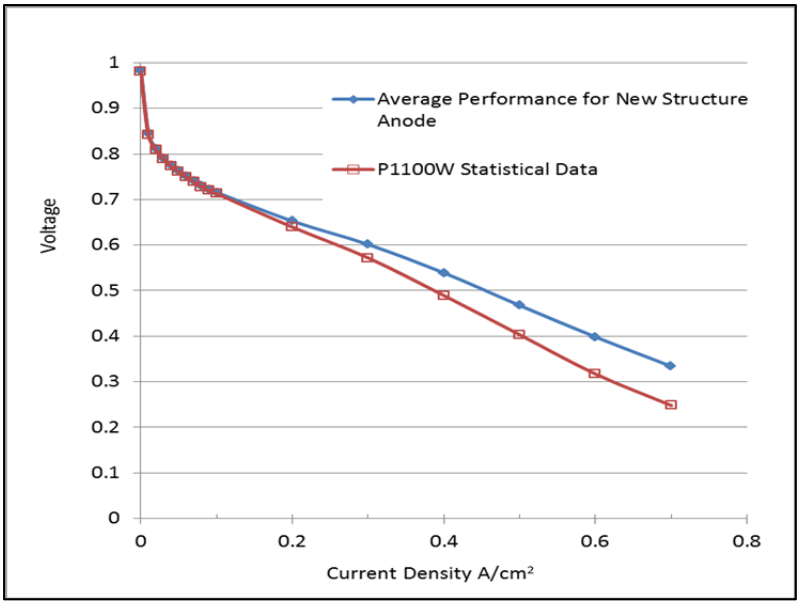

Figure 60. Performances for Anode with new structure and P1100W Standard Anode. Anode made on production scale coating machine. 160°C Reformate/Air (1.2/2).

Table 11. Performances for Anodes with New Structure and P1100W Standard Anodes. Average and Standard Deviations at 160°C Reformate/Air (1.2/2)

	Standard			**New Anode Structure**	
A/cm²	**Avg Volts**	**Std. Dev.**		**Avg. Volts**	**Std. Dev.**
0.2	0.639	0.014		0.653	0.007
0.5	0.403	0.040		0.468	0.019
0.7	0.248	0.032		0.335	0.020

As we moved to the comparison for 180°C reformate operation as shown in Figure 61, the differences between anodes with standard structure and those with new structure become much smaller. The same phenomenon was observed for pilot coater made samples (Figure 53 and Figure 54). This is due to much weaker binding between CO and catalyst sites at 180°C. The performance advantages are in the range of 5 to 25 mv; on the other hand, the reduction in standard deviations for 0.5 - 0.7 A/cm² is still in the range of 40% to 50%. (Table 12)

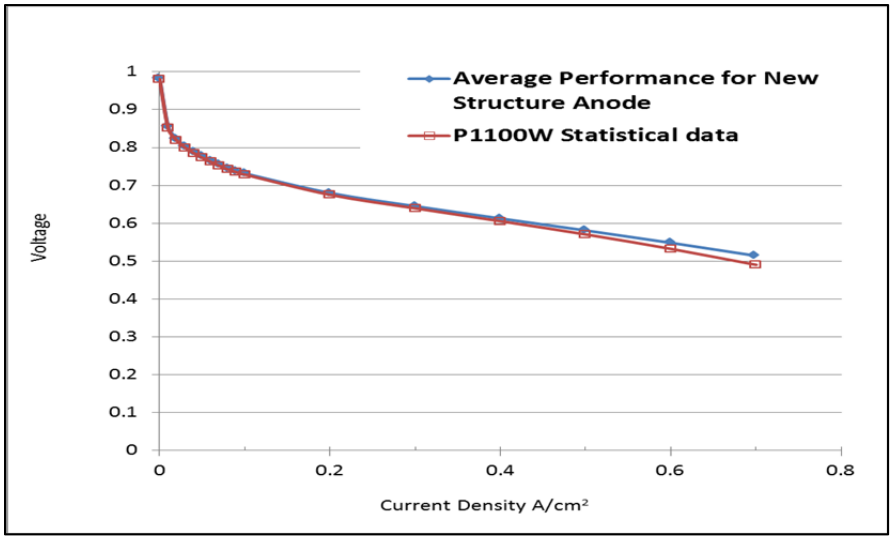

Figure 61. 180°C Reformate/Air (1.2/2) performances for anode with new structure and P1100W Standard Anode.

Table 12. Average and Standard Deviations at 180°C Reformate/Air (1.2/2) performances for anodes with new structure and P1100W standard anodes.

	Standard			New Anode Structure	
A/cm²	Avg Volts	Std. Dev.		Avg. Volts	Std. Dev.
0.2	0.675	0.006		0.680	0.005
0.5	0.571	0.010		0.581	0.006
0.7	0.490	0.018		0.515	0.009

(7) New Post Treatment for New Structure Anode

In the development of P1100W anode we found a profound influence of the post-treatment step on electrode performance, as described earlier under "Ink Stability: Full Length Coating" Sections (9) A (iii) and (iv), and "Increase GDE Throughput: Sections 4 (1) C (ii); later we found this especially true for operating at 160°C reformate. We believe this sensitivity is due to the competitive absorption of CO that can decrease the available anode catalyst sites for hydrogen oxidation. The available sites could be impacted by the post-treatment process. As elucidated in prior sections, this post-treatment step interplays with our ink selection rules, which is summarized as the solution set defined by stabilizers (additives) for ink components; minimization of residuals; and maintain key porosity and hydrophobicity.

The improved structure anodes were subjected to a new post-treatment process at the pilot scale and with standard post-treatment as a control in the same configuration. Figure 62 shows the performance comparison of 160°C reformate/air (1.2/2 stoich.) for new post-treated anode and that

for the control- standard post-treated. The new post treatment not only led to better average performances, but also resulted in smaller variability. Figure 63 shows the 2σ variability (95% confidence level) comparison of the two different oven treatment steps.

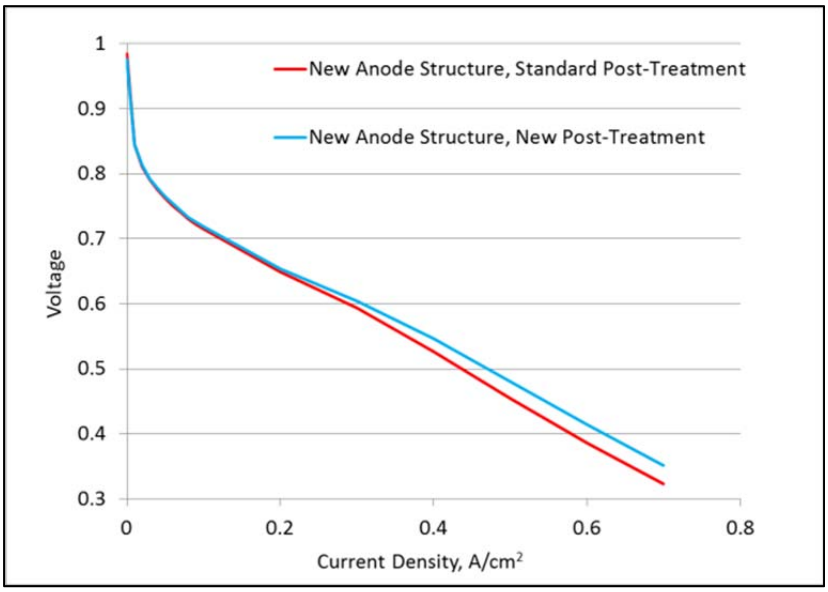

Figure 62. 160°C Reformate/Air (1.2/2) average performance comparison for new anode structure with standard post-treatment and new post treatment.

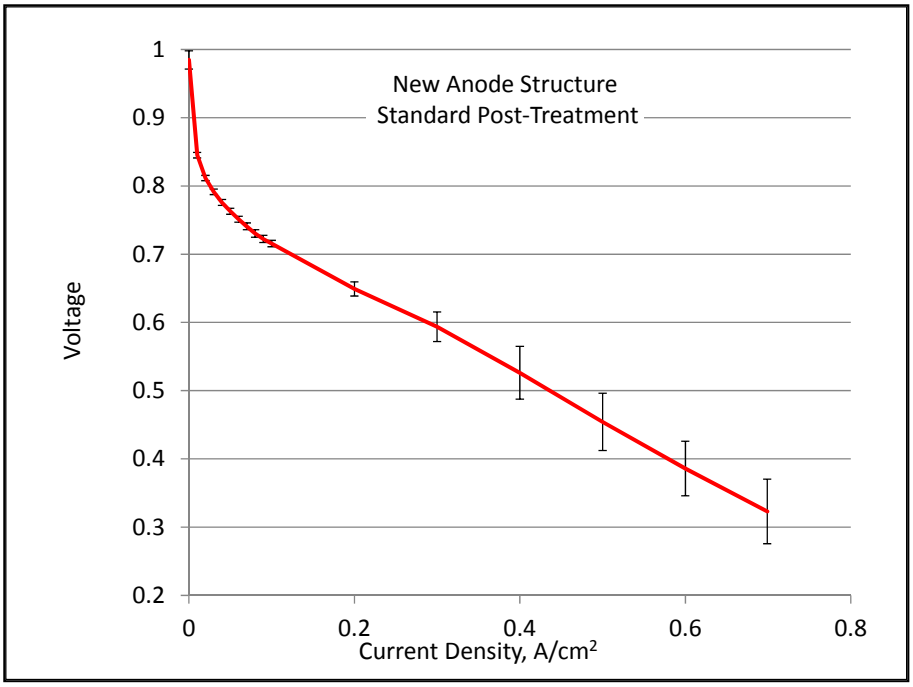

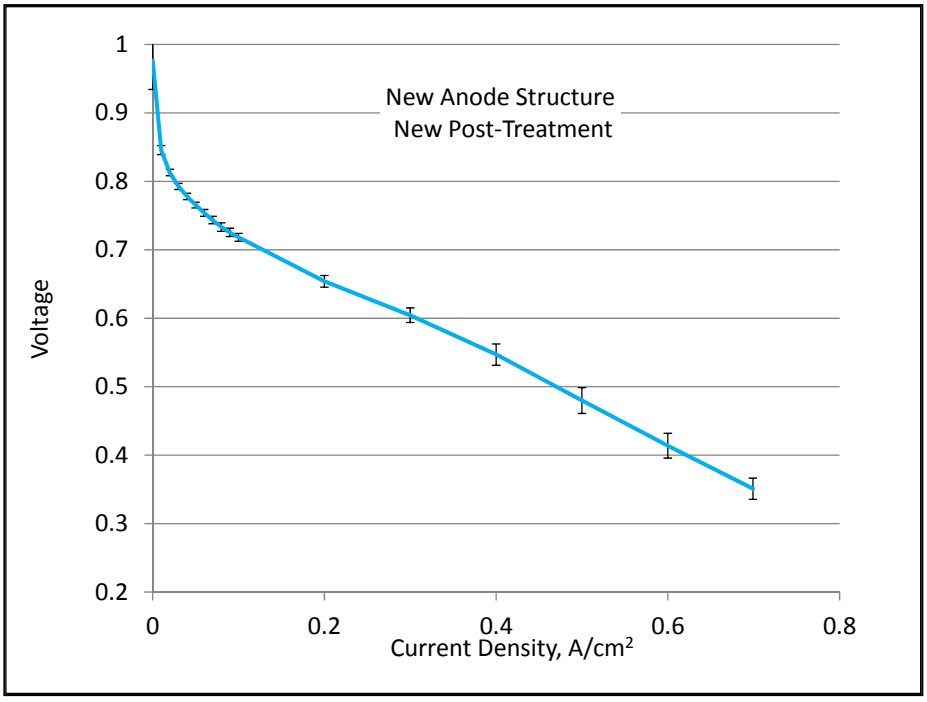

Figure 63. 2σ Comparisons for the performance curves at 160°C reformate/air (1.2/2). Variation calculated from 12 samples for each.

(8) Application of New Anode Structure to Paper Based Electrodes

As will be discussed in upcoming sections, this program has expanded our focus on paper based electrodes to further reduce MEA cost. Therefore, the new anode structure technology that holds potential for reduction of precious metal content was also explored on the paper based electrodes for next generation low cost products.

A series of anode experiments were conducted whereby the same standard paper based cathodes (Paper2) were used. Similar to the standard paper cathodes, the anodes were prepared with a new formulation so only 1-2 coats were needed to achieve the standard precious metal loading. Moreover, the paper electrode post-treatment employed was a different configuration than that for P1100W cloth.

In order to evaluate the anode performance accurately, one needs to eliminate the effect of cathode on air/reformate performance. We have developed a method that accounts for lot-to-lot differences in cathode performance and results in a plot that represents a comparative reformate gain, i.e., the performance loss when comparing pure hydrogen to reformate. We call this the reformate loss. Figure 64 and Figure 65 show the reformate loss at 180°C and 160 °C respectively for standard paper anode, new anode structure, and new anode structure with advanced (new) post treatment.

For both the test temperatures, one notes a lower voltage loss when comparing the two cases of new electrode structure plus the advanced post treatment to a standard anode. This is especially evident after 0.2A/cm^2, where one needs a higher degree of utilized catalyst to support greater levels of hydrogen oxidation. We also note that while the magnitude of the reformate gain may appear large, this is with 2 % CO, which contrasts markedly with the typical loss after exposure to 50-100 ppm CO found while operating low temperature PEM. Figure 64 and Figure 65 also substantiate our observation that the post treatment sequence plays a significant role in the performance of the electrode.

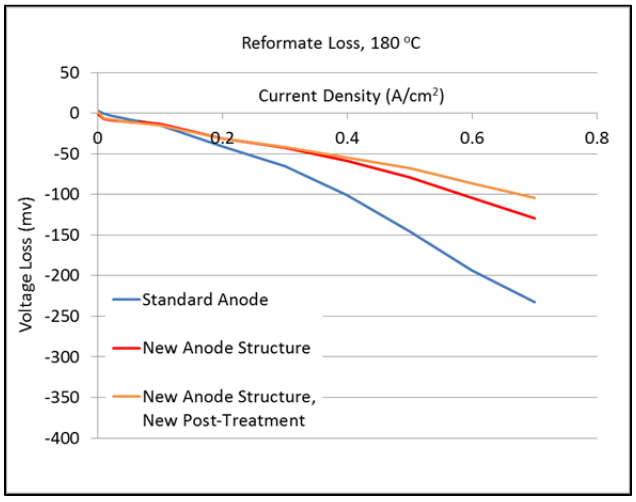

Figure 64. Reformate loss at 180°C for different anode structures or post-treatments.

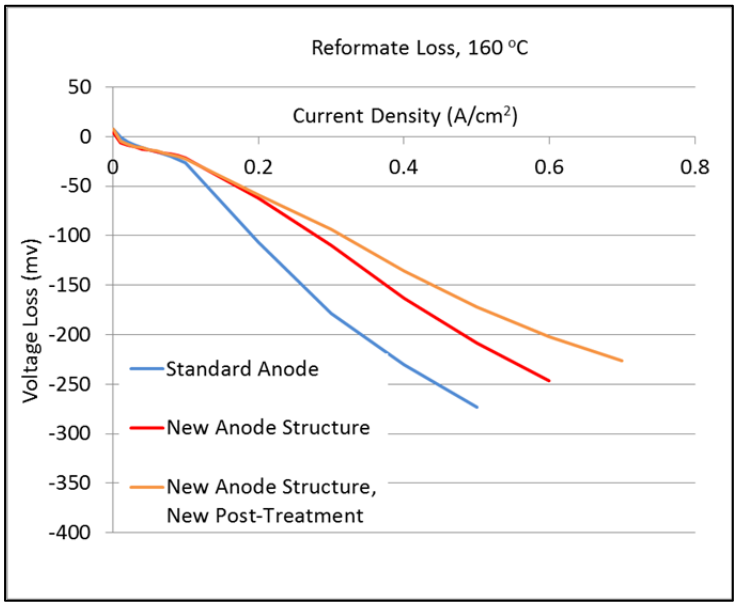

Figure 65. Reformate loss at 160°C for different anode structures or post-treatments

(9) Statistical Evaluation of New Structure Anode on Paper Substrate

Eleven MEAs were made with new structure anode (by special formulation so 1-2 coats only) with new post-treatment on paper GDL substrate along with standard paper based cathodes (Paper2) and standard membrane. The average performance and 2 standard deviation error bar is shown in Figure 66 along with P1100W spec av and min. The average is lower but the standard deviation is comparable to P1100W. When standard anodes were prepared with the same formulations, we observed 3 to 12 times of standard deviations as those for new anode structure as shown in Figure 66; moreover, a lower performance average was also observed. The results indicated again the superior property of the new anode structure. The lower average for the curve in Figure 66 is a combined effect of lower paper cathode performance, lower quality of GDL on paper and 1-2 coat process of electrode coating. These aspects need to be improved for the development of a new paper product.

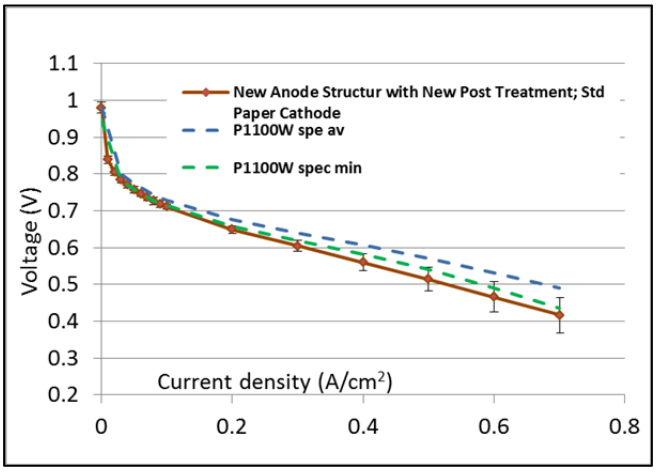

Figure 66. Reformate performance at 180°C for different anode structures or post-treatments. Ref(1.2)/Air(2.0), 2σ Error Bar

(10) New Binders in Electrodes

In "Ink Stability: Full Length Coating" Sections (9) A (iii) and (iv), and "Increase GDE Throughput: Sections 4 (1) C (ii) we have discussed the challenge of post-treatment to optimize the wet-proofing properties of gas diffusion electrodes for high temperature MEAs. Without a good wet-proofing agent, the electrodes can be easily wetted by high temperature acid because these acids are more hydrophilic than water spreading out in the electrodes of low temperature MEAs.

Post-treatment process serves the function of spreading out wet-proof agent in electrodes, so the property of the wet-proofing agent is important. It is believed that alternative wet-proofing agents may streamline the post-treatment process and reduce cost. We have chosen two alternative wet-proof agents to explore and compare them to the standard we currently use in P1100W product. This work was performed in the last quarter of this program.

All the cathodes were prepared with the same formulation and coating method as P1100W cathode. The post-treatment procedures used that for P1100W as the framework and some modifications were made according to the property of the wet-proof agent.

Figure 67 shows the average performances for these cathodes with 3 different wet-proof agents. There were 4 samples for each wet-proof agent. They showed essentially the same performances. Figure 68 shows the 2 sigma variation for the three cathodes and again the standard deviations for the three wet-proof agents are similar.

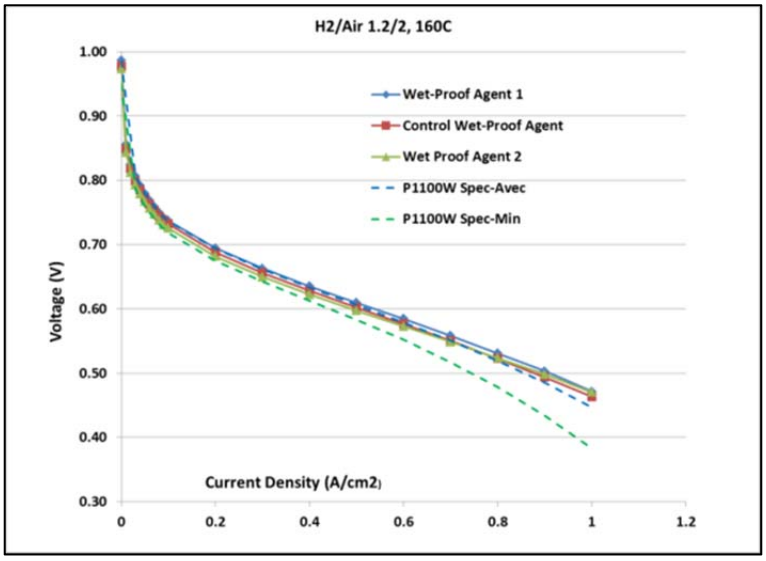

Figure 67. 160°C H_2/Air performances for cathode with different wet-proof agents.

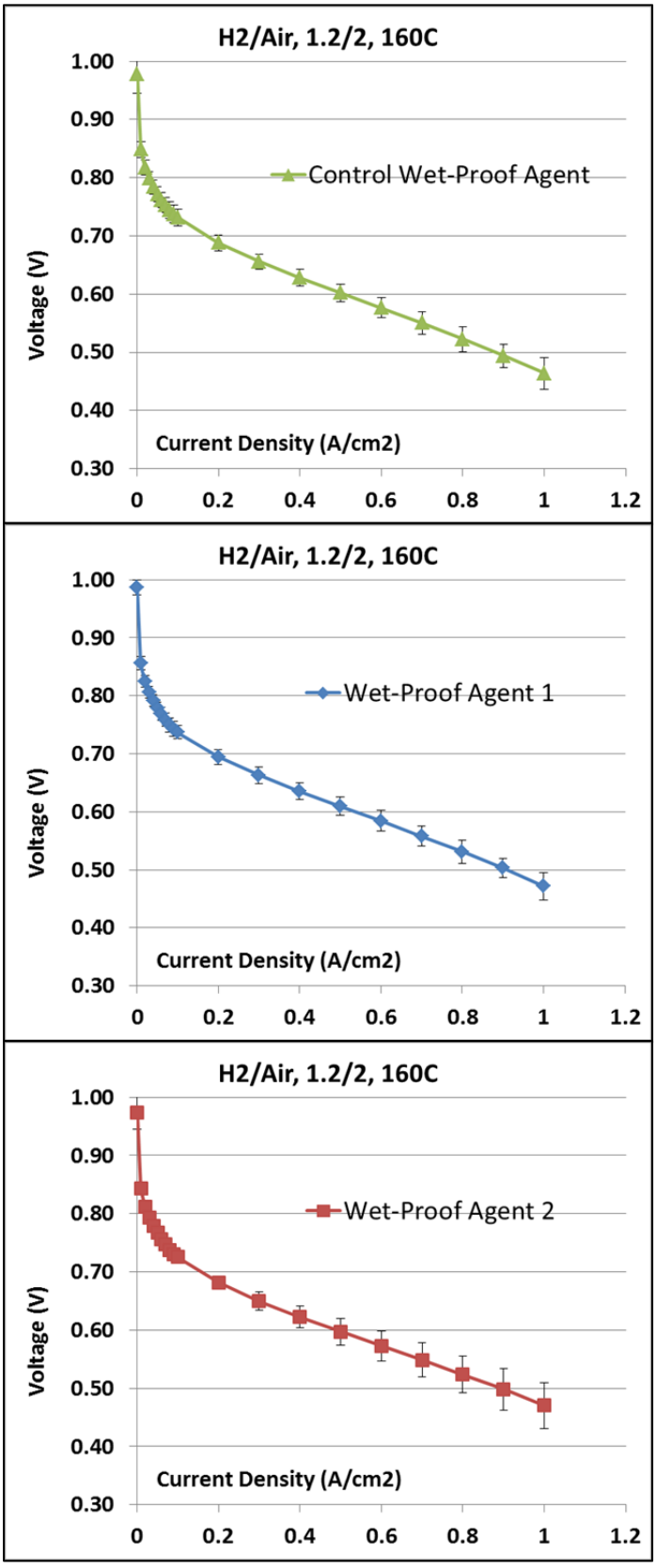

Figure 68. Two sigma variability of 160°C H_2/Air performances for cathodes with different wet-proofing agents.

Figure 67 and Figure 68 indicate that using the three wet-proofing agents in cathodes do not cause much difference in H_2/Air operation. It also implies that P1100W formulation, coating, and post-treatment processes are robust and not sensitive to component properties and has wide window of adaptability. Additional research will be needed to assess the impact of these alternative wet-proofing agents on the cost of the post-treatment cycle.

Carbon Paper Based Gas Diffusion Electrodes

(1) Background

The standard high temperature Celtec-P MEAs employs cloth based gas diffusion electrodes (GDEs). In recent years there has been growing interest in paper based GDEs. The major incentives are: (1) thinner electrodes that allows one to install more MEAs per stack and leads to higher power output; this is especially important for portable applications where small stack volume is preferred; (2) higher rigidity of paper MEAs allows shallower flow channel design and results in a further reduction of stack volume; (3) potentially lower cost; (4) more uniform thickness results in better quality control and possible elimination of some inherent cloth defects such as miss-weaves.

The carbon paper from previous supplier is not easy to hand due to its brittleness. BFC identified one carbon paper (paper 1) with much higher flexibility. Paper 1 can be easily folded and thus well matched to coater radius and linear pull requirements. Damage by handling is not an issue as that for the previous carbon paper. The cost of paper 1 is roughly about 1/3 of the carbon cloth substrate. In addition, the coating efficiency can be improved because the micro porous layer (MPL) for carbon paper requires less coating passes as there is no large size straight pores to fill.

While the main thrust of the program is to reduce the cost in cloth-based GDE, the strategy of this task is to apply the ink formulations and processes to the paper based electrode preparation. Figure 69 illustrates the morphology differences between the paper and cloth. Figure 70 compares the pore size distributions between paper 1 and cloth. The major difference between paper and cloth substrate is: the woven type carbon cloth contains large straight pores. These pores must be filled before forming a continuous coating layer. However, it provides an additional interfacial area between the substrate and the MPL to form a strong bond. On the other hand, the structure of carbon paper is more compact with smaller average pores. The paper substrate has therefore limited bonding with micro porous layer.

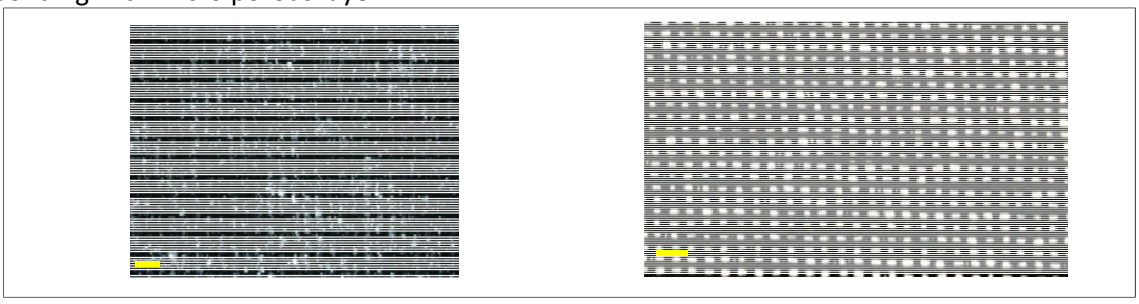

Figure 69. The carbon paper (paper 1) substrate (left) and the carbon cloth substrate (right) on light table; scale bar: 1 mm.

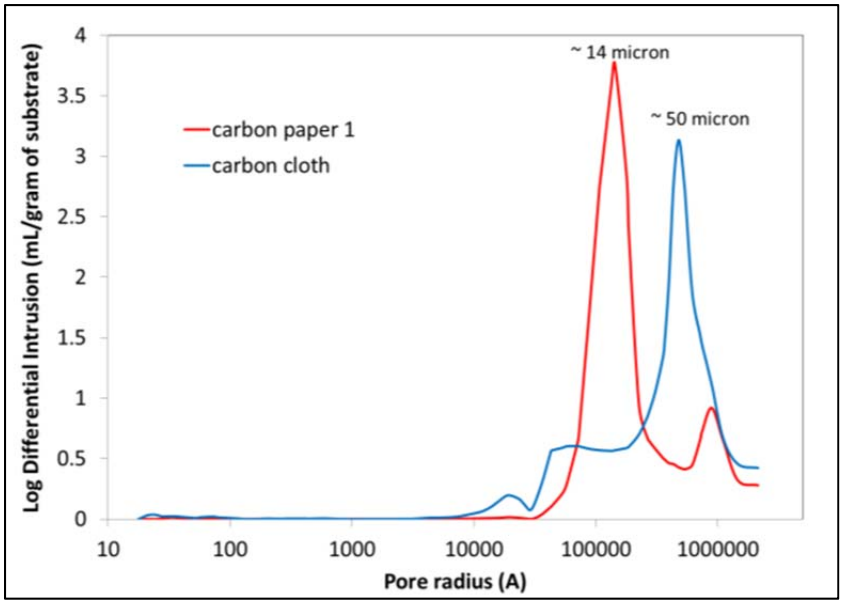

Figure 70. The pore size distribution of paper 1 and cloth substrates from mercury intrusion.

Figure 71 shows the beginning of life performance of paper 1 based cathode made with the pre-program cloth cathode and MPL formulation. The performance is slightly higher compared to the average cloth cathode. However, the paper 1 based electrode and GDL show poor coating quality. The coating on paper is less uniform with severe adhesion problem as shown in Figure 72. The coating quality issues are the results of the poor ink homogeneity. They become pronounced on low surface roughness paper substrate. Other proofs include large amount of agglomeration collected from the ink circulation; low yield due to surface agglomerates; limited ink shelf life, etc.

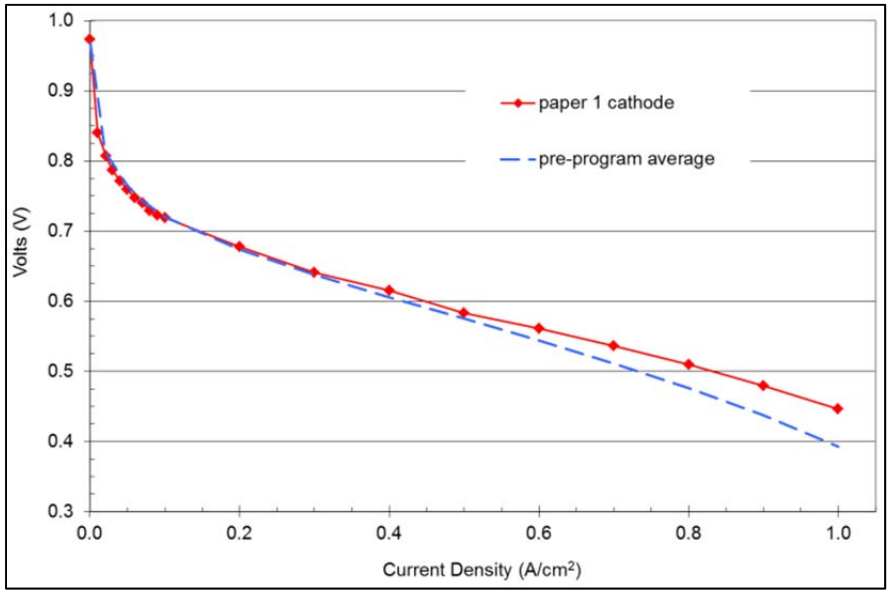

Figure 71. Beginning of life performance of carbon paper 1 based cathode made from standard P1000 ink formulations; MEA is assembled with standard PBI membrane and pre-program cloth anode; operating condition: H_2/air, 160°C, stoich 1.2/2.0, ambient.

Microscopically, the carbon black particles used in the MPL ink are homogenous in surface chemistry. So the ink homogeneity issue is more likely caused by insufficient dispersion and / or non-stabilizing dispersants. Although the GDL image shows negligible mud cracking in MPL, the rough coating surface indicates the ink is precipitating during the coating.

The catalyst ink is more complicated since the platinum or platinum alloy catalysts and the carbon support are different in surface chemistry. Therefore, it can be difficult to have a true (microscopic) homogenous ink and form crack-free coating surface. However, the anode and cathode images in Figure 72 show a "river" pattern with severe flaking problems. Such coating quality usually suggests that the ink has additive or application issues.

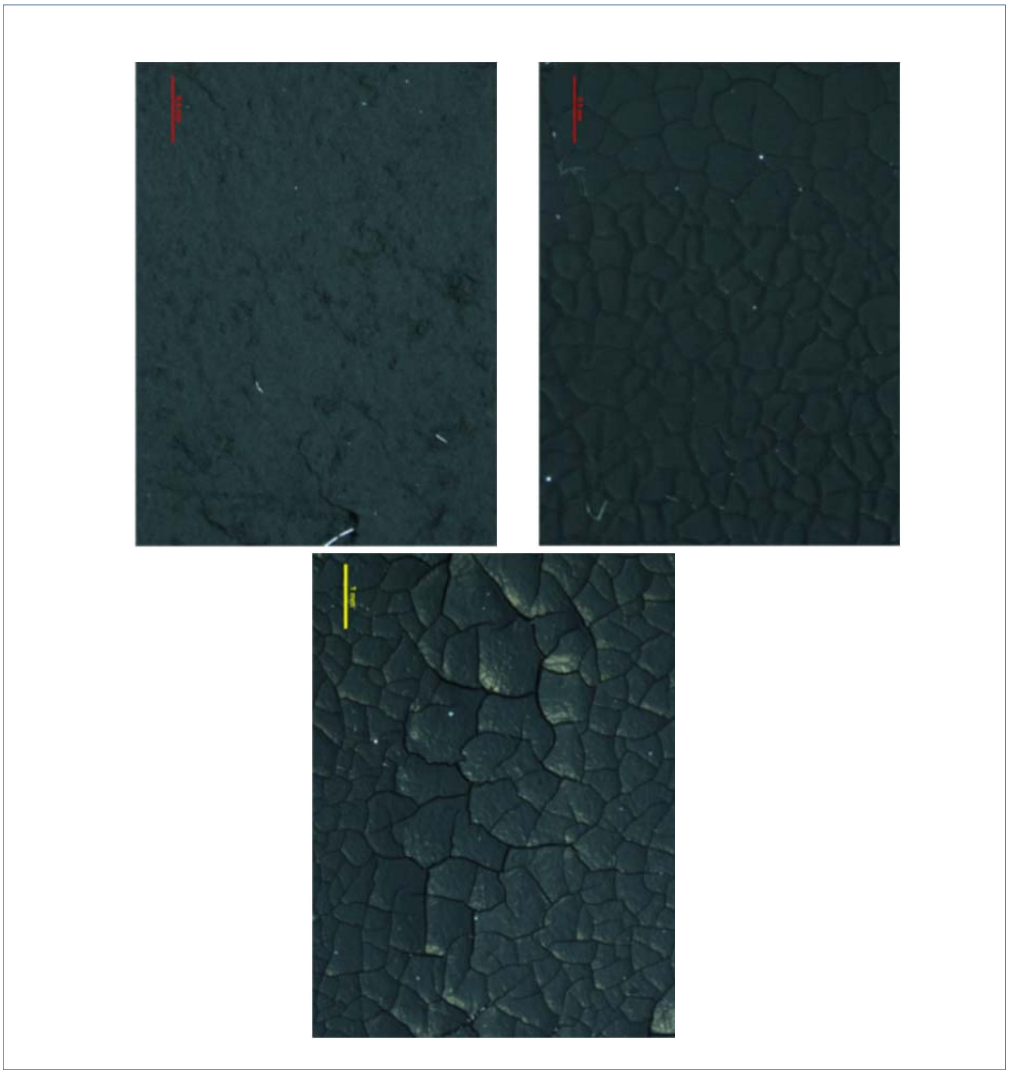

Figure 72. The surface quality of carbon paper 1 based MPL (left), anode (middle), and cathode (right); Scale bar: 0.5 mm for GDL and anode; 1.0 mm for cathode.

We note the paper cathode coating quality is more severe than the anode. The cathode catalyst is sintered at high temperature to form the Pt alloy. The process removes the surface hydroxyl groups on carbon support. The finished catalyst support not only becomes more hydrophobic, but also has

fewer sites to bond with additives. As a result, a dispersant that works with the anode may have great difficulties with cathode ink formulations.

In summary, we are facing serious coating issues that prevent process scale-up. The main challenges are to obtain sufficient ink homogeneity and maintain it with proper additives. The formulations for pre-program GDEs are inferior when applied to paper. The new formulations are needed.

(2) New ink approach

The pre-program inks had inherent limitations that can impact the ink homogeneity. The limitations include:

1. The catalyst cannot be properly dispersed with low energy mixing equipment
2. The catalyst is dispersed without dispersant, the dispersion cannot be stable
3. When mixed with PTFE dispersion, the catalyst will compete with PTFE for its surfactant; This impairs the PTFE dispersion

It is clear that appropriate ink homogeneity cannot be sufficient with this approach. The electrode catalyst utilization is low because insufficient dispersion energy cannot create enough exposed surface area. The coating agglomerates and limited shelf life are evidences of insufficient ink homogeneity.

(3) High energy dispersion for carbon paper formulations

The first designed experiment is to introduce a new approach to improve the ink homogeneity. The major process differences from the pre-program ink approach are:

1. The high energy dispersion is used for catalyst dispersion
2. Dispersants are added from the beginning of the dispersion
3. The ink concentration is doubled
4. Mix catalyst dispersion with PTFE dispersion,

There is no change in additives. The catalyst / PTFE ratio and the catalyst / additives ratios are kept the same as pre-program formulations. For comparison, the same batch paper 1 GDL is used to make cathodes from the pre-program ink formulations.

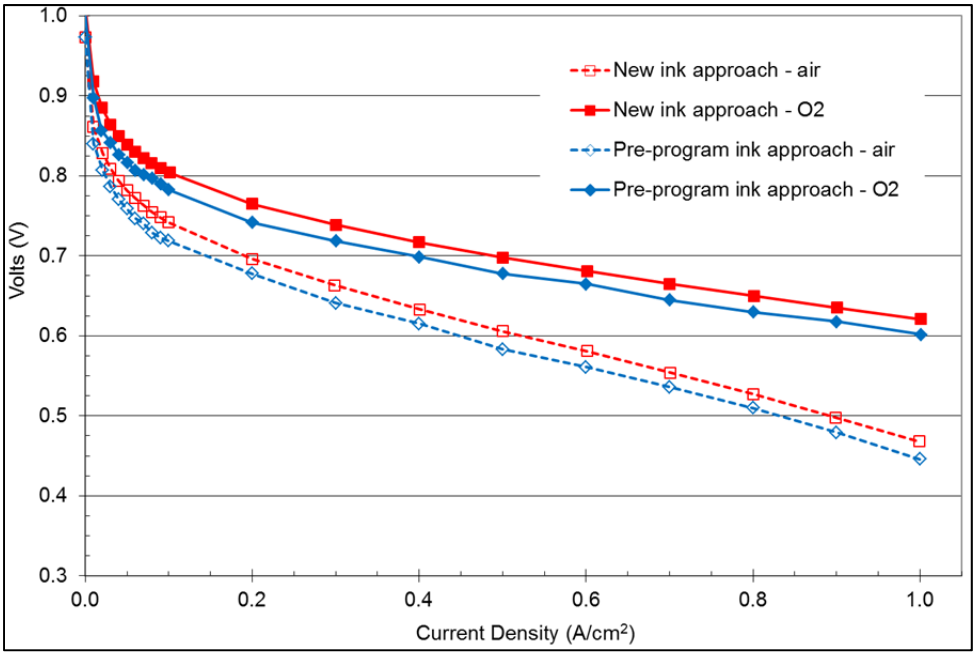

Figure 73. Beginning of life performance of carbon paper 1 based cathode made from the new ink approach and the pre-program cloth approaches; operating conditions: H_2/air or O_2, 160°C, stoich 1.2/2.0 (air) or 9.5(O_2), ambient.

Figure 73 compares the beginning of life performance of the paper 1 cathode made from the new and the pre-program ink approaches. The new ink approach greatly improved the cathode performance. There is about a 30mV gain at 0.2A/cm^2 with the new ink approach. Given the typical Tafel slope of -90mV/dec for PBI type MEA at 160°C, the MEA performance is doubled with the new ink approach. The H_2/O_2 polarization curves of cathodes made from new and pre-program ink approach are parallel. This parallelism indicates that the major difference between the new and cloth ink approach is the degree of catalyst utilization which may be due to an increase in electrochemical interfacial area (ECA). Low ECAs are often observed when the catalysts are not dispersed properly as in pre-program ink approach.

The ink's shelf life is greatly improved by the new ink approach. The grind gage is used to inspect the dispersion quality and the ink stability. Figure 74 compares the grind gage test at day 1 (fresh ink) and day 8. The coating quality and the amount of agglomerates are similar after a week. Figure 75 compares the beginning of life performances of paper 1 cathodes made from same ink on day 1 and day 8. The polarization curves of cathode made from fresh ink and 8 days old ink nicely overlaps each other. The electrodes for this ink stability test were machine coated. We did not observed any ink agglomerations during the coating process.

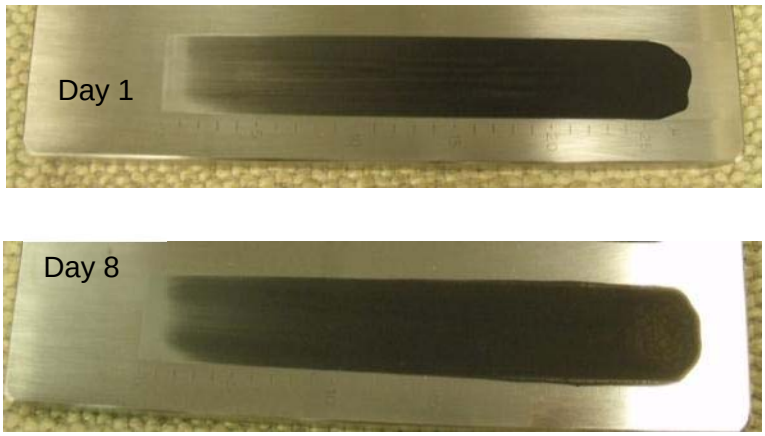

Figure 74. The cathode catalyst ink coated on the grind gage; No visible difference between fresh and 8 days old ink.

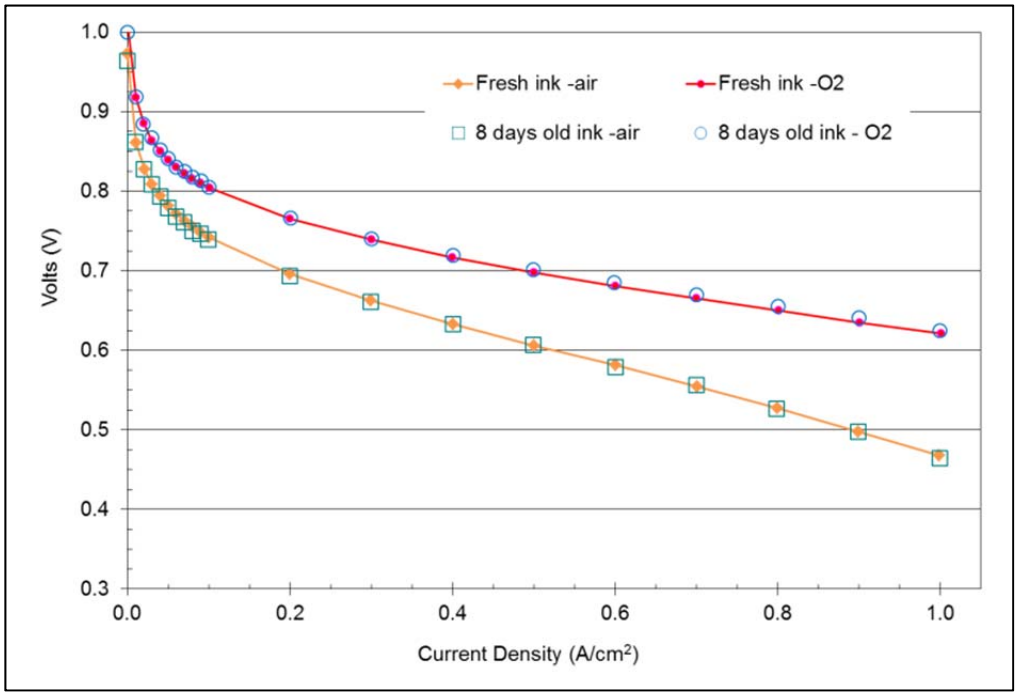

Figure 75. Beginning of life performance of carbon paper 1 based cathode made from fresh and 8 days old ink, operating conditions: H_2/air or O_2, 160°C, stoich 1.2/2.0 (air) or 9.5(O_2), ambient.

The performance improvement from the new ink approach is very encouraging. However, there remain issues to be solved before the process can be scaled-up. Some additives were not suitable for catalyst and MPL formulations. In addition, use of high energy dispersion introduces foaming and heat generation problems.

(4) Dispersant hydrophobic-lipophobic balance

The high energy dispersion can break the pigments (catalyst or carbon black) down to desired aggregate size. However, proper dispersant is needed to keep these aggregates from re-agglomeration and precipitation. The hydrophilic or lipophilic part of the dispersant must form stable bonding with the pigment. The so called hydrophilic-lipophilic balance (HLB) is one of the most important parameter to guide the surfactant selection.

The catalyst surface oxidation layer, e.g. Pt-OH, may bond the hydrophilic group of the dispersant. Catalyst particles only contribute to 20-25% of total surface area. It is the bonding between the dispersant and the carbon support that determines the quality and the shelf life of the catalyst ink dispersion. The structure of the carbon black affects the amount of dispersant to be used. The surface chemistry of the carbon black determines the type of the dispersant to work properly.

The anode catalyst is deposited on regular carbon black, which contains a large amount of hydroxyl groups. On the other hand, the cathode catalyst process has a high temperature alloying step. We believe the hydroxyl groups on carbon support are mostly removed after this high temperature step. The more graphitic carbon black used in the MPL formulation contains even lower amount of surface groups for the dispersant.

Because the carbon black properties of the three inks are different, we will have problems if the same dispersants are used in all three formulations like in pre-program case. Figure 76 shows the cathode ink has great wetting difficulties from the second coating pass. Figure 72 shows the poor MPL coating qualities.

The low process temperature of the anode catalyst process probably allows the carbon black to remain some of the surface hydroxyl groups. Consequently, high HLB dispersants in standard pre-program formulations could work well in the anode formulation. Due to the cathode catalyst process however, low HLB dispersant is necessary to achieve a similar dispersion quality. Figure 77 shows the above mentioned cathode wetting issues being solved with the introduction of low HLB dispersants. The MPL formulation is less complex because of the homogenous surface chemistry of carbon black. A low HLB dispersant can work well with graphitized carbon black. Figure 78 shows the new ink approach with proper dispersant greatly improves the MPL coating quality.

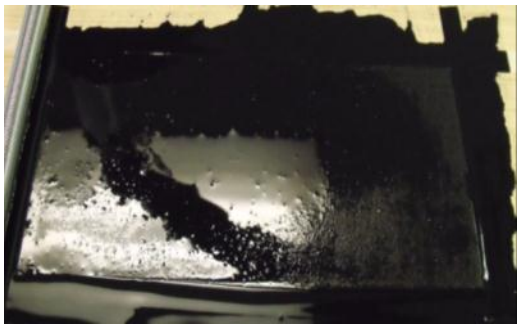

(a) First coating pass (wet)

(b) First coating pass (dry)

(c) Second coating pass (wet)

(d) Second coating pass (dry)

Figure 76. Cathode coating trial with new ink approach but same dispersants as pre-program cathode formulation; the second coating pass shows ink wettability issue.

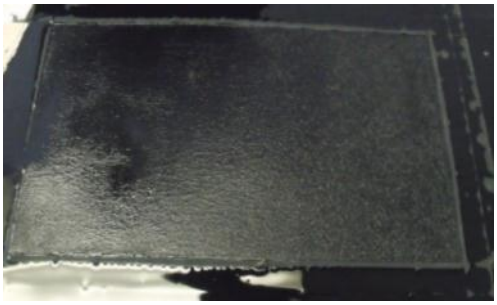

(a) First coating pass (wet)

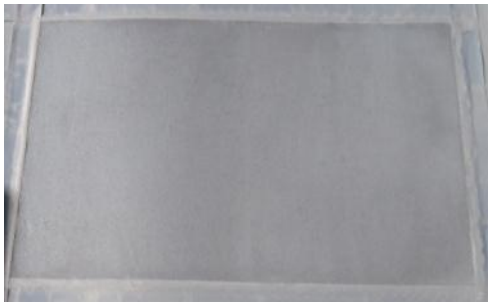

(b) First coating pass (dry)

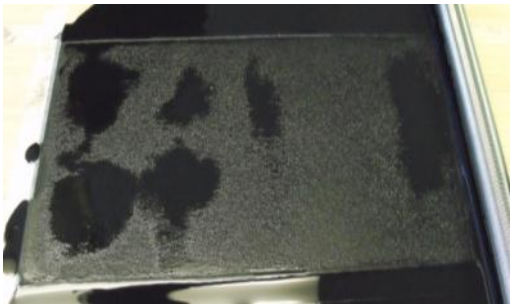

(a) Third coating pass (wet)

(b) Third coating pass (dry)

Figure 77. Cathode coating trial with new ink approach and low HLB dispersants; No ink wettability issue observed after second coating pass

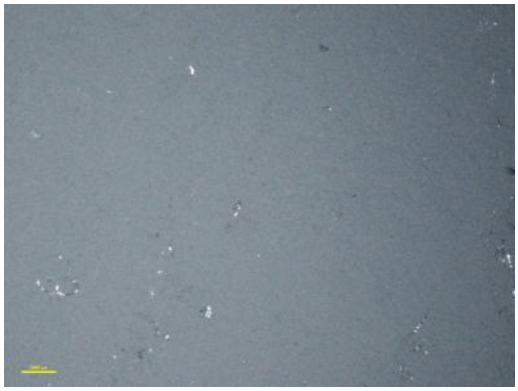

Figure 78. Surface quality of the MPL made from new ink approach and low HLB dispersant.

(5) The foaming and heat issue

Use of high energy dispersion equipment could introduce foam and heat generation issues. The foam can be several times the original ink volume when high HLB dispersants are used in the formulation. Our tests show many defoamers can effectively remove the foam, but are ineffective in preventing foam generation. However, some manufacturers premix dispersant and defoamer to prevent foaming from the beginning of dispersion. This approach has advantages in process and quality control over the typical method of adding defoamer after generating a large amount of foam.

The defoamer forms small insoluble droplets in the dispersed system to break the foam. The dispersion efficiency becomes lower with foam generation. Therefore, adding defoamer for a real time control is better in dispersion quality control, but greatly increases the process complexity. Adding defoamer after dispersion is simplified in equipment and process, but may suffer from the inconsistent dispersion quality. By preventing foaming generation with a selected dispersant, we can avoid such a tradeoff.

It is not surprising that the ink temperature increases during high energy dispersion. However, the dispersant may not work properly if the temperature is close to its cloud point. Our approach is to select a dispersant with a cloud point substantially higher than the maximum temperature the ink will reach under high energy dispersion. The ink temperature in lab test is normally below 50^{o}C. We have not loss in dispersant functionality due to temperature change. For process scale-up, there are reliable temperature control solutions.

(6) Filming and leveling control

Filming and leveling control is critical in forming a smooth, uniform, integral coating layer. Lack of filming and leveling control can cause more quality issues on the paper substrates as they are smoother than carbon cloth. We have showed that good coating quality can be obtained with proper dispersants. However, the coating quality could further benefit from filming and leveling control. Figure 79 shows the ink coating on grind gage with or without leveling agent. Clearly the filming and leveling agent brings some fine tuning of the surface quality. We have not observed the impacts on performance from the use of filming and leveling agent.

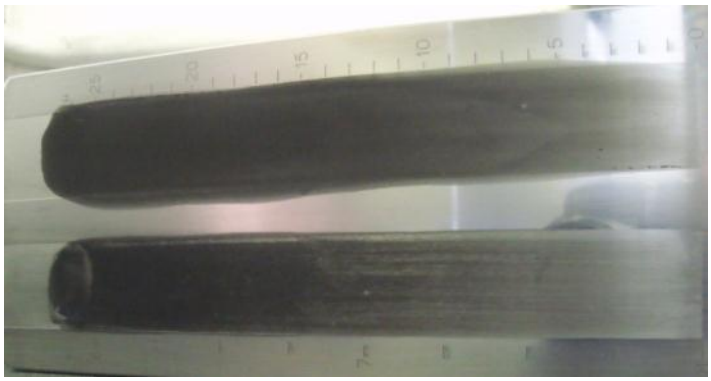

Figure 79. The cathode catalyst ink coated on the grind gage; Top: ink with filming and leveling control; bottom: same ink without filming and leveling control.

Summary

To summarize the ink formulation work, we have introduced a new ink approach, which utilizes high energy dispersion for catalyst and carbon black. This process maximizes the catalyst utilization by providing more uniformity and interfacial area; we have demonstrated the correlation between the catalyst or carbon black surface chemistry and the HLB of the dispersants. This correlation is used to guide the dispersant selection; we have established an optimal method for foam control; the filming and leveling control is introduced to the ink formulation. The final formulation is developed based on these considerations. The formulations show good ink quality and shelf life. A minimum of three $2m^2$ scale machine coating pilot trials have been carried out before finalizing the formulation. Figure 80 shows the coating quality of a paper 1 based cathode with the new formulation. The coating quality has been greatly improved compared to the images in Figure 72.

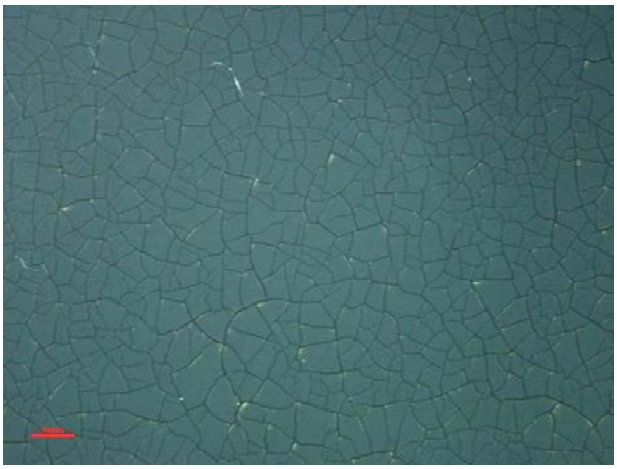

Figure 80. The surface quality of carbon paper 1 based cathode made with new formulation; scale-bar = 1mm.

(7) Performance and optimization

Carbon paper has been widely used in low temperature fuel cells as the GDL substrate. Most low temperature fuel cell MEAs are made by decal transfer method, in which the GDL is not involved in MEA's hot press assembly. So the mechanical properties of the paper are less relevant to the MEA performance.

Unlike in many low temperature proton exchange membrane, the proton conduction in a phosphoric acid- PBI membrane is only through the phosphoric acid, which can be >90% by weight. The low content PBI functions as a polymer matrix. It holds the phosphoric acid by hydrogen bonding, thus the membrane has weak mechanical strength and integrity. The high liquid content inhibits catalyst bonding to the membrane. Therefore, the MEAs using PBI membrane are better fabricated by GDE approach. Phosphoric acid has to be introduced into the electrode to form the three phase boundary. The assembly process should have minimum damage to the electrode structure, and allow proper amount of acid in the electrode's catalyst layer to form three phase boundary.

In our MEA fabrication process, phosphoric acid is squeezed from membrane into electrode during hot pressing. The carbon cloth substrate is far more flexible and stronger than paper, so its

assembly condition may not be suitable to paper. The assembly pressure is higher than paper's maximum allowed pressure for a reversible compression. Figure 81 shows the mercury intrusion accumulated volume as a function of intrusion pressure for paper 1 anode. It turns out the volume difference between two intrusion pressures is quite small. The paper 1 MEA assembled at lower pressure performs slightly better. We have not observed the structure collapse at the standard assembly pressure. It is possible the intruded phosphoric acid may provide support to prevent structure collapse.

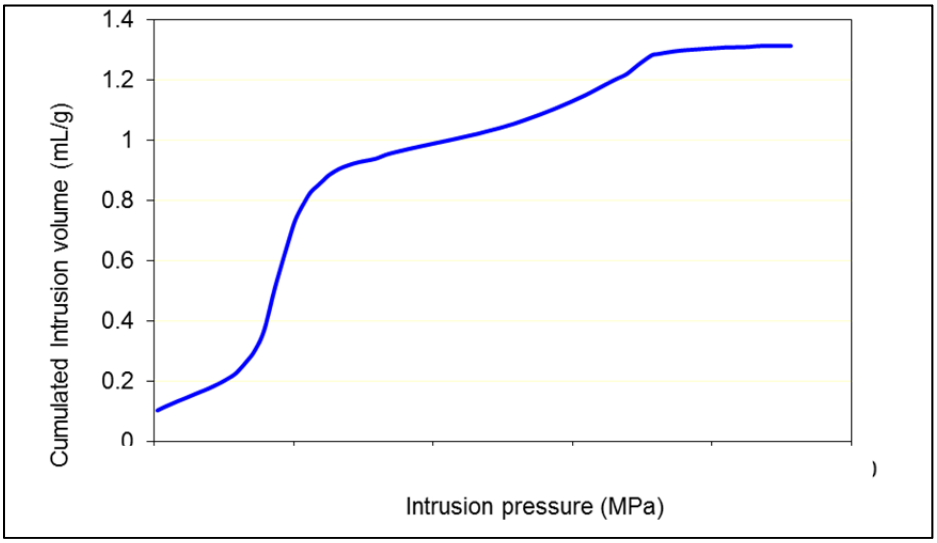

Figure 81. Mercury intrusion of paper1 based anode.

(8) Electrode structure optimization

The microscopic structure of a porous electrode cannot be directly controlled to provide specific surface area, porosity, and tortuosity. Therefore, a good three phase boundary is obtained by having optimal phase volume fractions and sufficient dispersion of each phase.

In low temperature fuel cells, the volume fractions can be better controlled because components to form the electrode matrix phase and the electrolyte phase are quantified in the ink formulation. The optimization often illustrates the trade-off among kinetic, ohmic, and mass transport losses based on the electrode's ionomer content.

Unfortunately for high temperature PBI MEAs, the electrolyte release into the electrode is during MEA assembly, and we do not have a technique to measure the amount of phosphoric acid in electrode after assembly. However, we adjust the electrode matrix phase in order to guide the introduction of electrolyte in electrode. The structure of the electrode matrix phase is formed by bonding the catalyst with PTFE. The amount of PTFE not only determines the matrix phase structure, but also provides the electrode hydrophobicity, affects the available catalyst active surface area, controls the total volume for electrolyte and gas channels. The PTFE distribution affects the amount and the distribution of phosphoric acid in electrode. Therefore, the optimization that illustrates the trade-offs is based on the amount of PTFE in the electrode.

In the optimization experiment design, the PTFE contents in MPL, anode and cathode catalyst layer varies from 15% to 50%. Only one PTFE content is changed at each time. The cell voltage at 0.2A/cm^2, 0.7A/cm^2 for anode, and 1.0A/cm^2 for cathode are used to evaluate the impact of PTFE on performance. Presumably, the higher the performance, the closer the electrode structure to its optimal.

The MEA performances as functions of the PTFE content in cathode MPL are plotted in Figure 82(a) and (b). The polarization curves are obtained from hydrogen fuel and air oxidant at 160^{o}C. Data show the PTFE content in cathode MPL has little impact on the cell performance. Because the PTFE content in anodes or cathodes is kept the same, it is reasonable to assume that the three phase boundary conditions in all MEAs are similar. The product water is in vapor form at 160^{o}C. There is no demand for hydrophobicity to prevent the retention of liquid water. The gas diffusion coefficient is about 10^{-2} to 10^{-1} cm^2/s, which is sufficient for the operational current density. Similarly, the MEA performance is not sensitive to the PTFE content in anode MPL either.

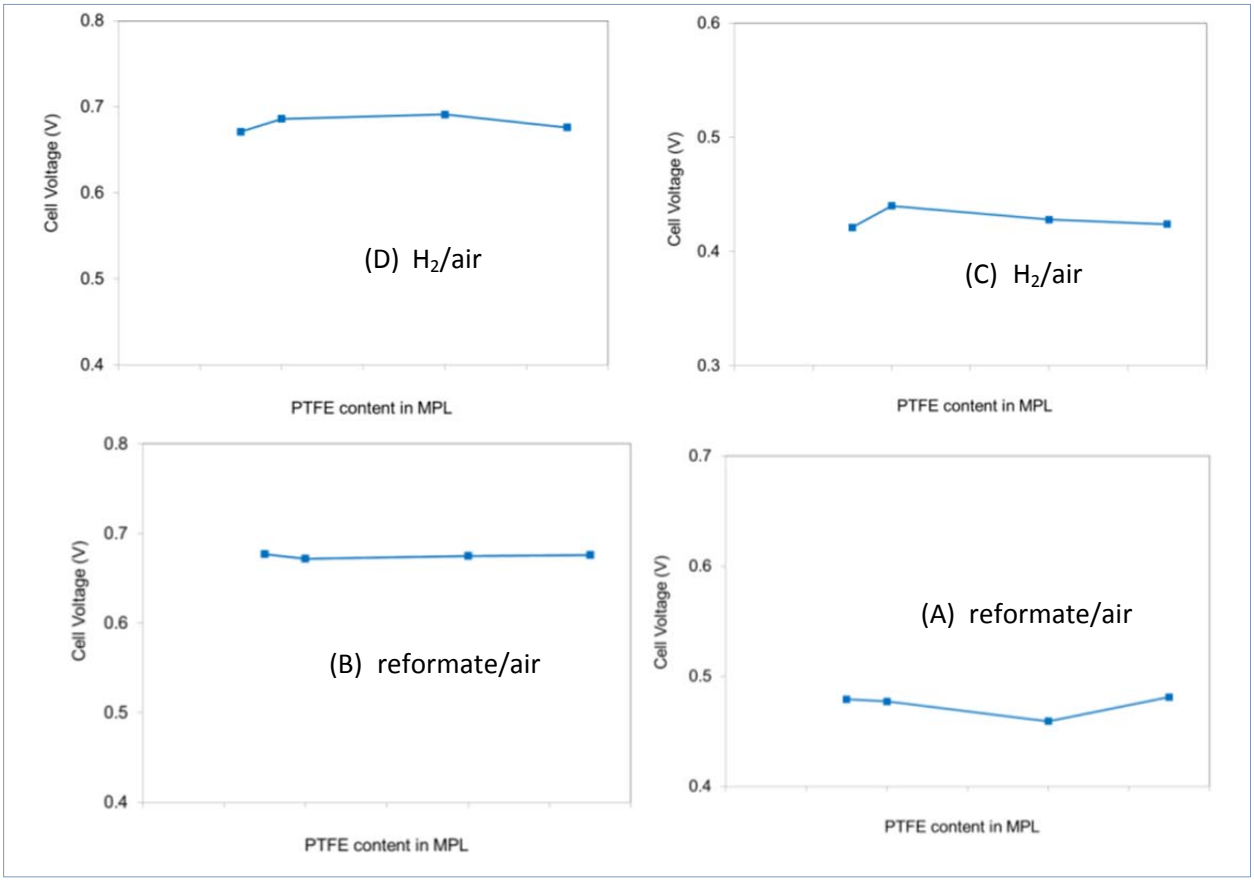

Figure 82. Impacts of the PTFE content in MPL on the MEA beginning of life performance; (a) Cell voltage at 0.2A/cm^2 with H_2/air at 160^{o}C; (b) Cell voltage at 1.0A/cm^2 with H_2/air at 160^{o}C; (c) Cell voltage at 0.2A/cm^2 with reformate/air at 180^{o}C; (d) Cell voltage at 0.7A/cm^2 with reformate/air at 180^{o}C; For all: stoich 1.2/2.0, ambient

In the series of experiments for cathode catalyst layer optimization, the PTFE content in the cathode catalyst layer varies from 15% to 50%. The PTFE content in anode and both MPLs are kept

unchanged. The polarization curves are obtained from hydrogen fuel and air or oxygen oxidants at 160°C. The polarization curves are plotted in Figure 83. The cell voltage comparison at 0.2A/cm^2 is plotted in Figure 84.

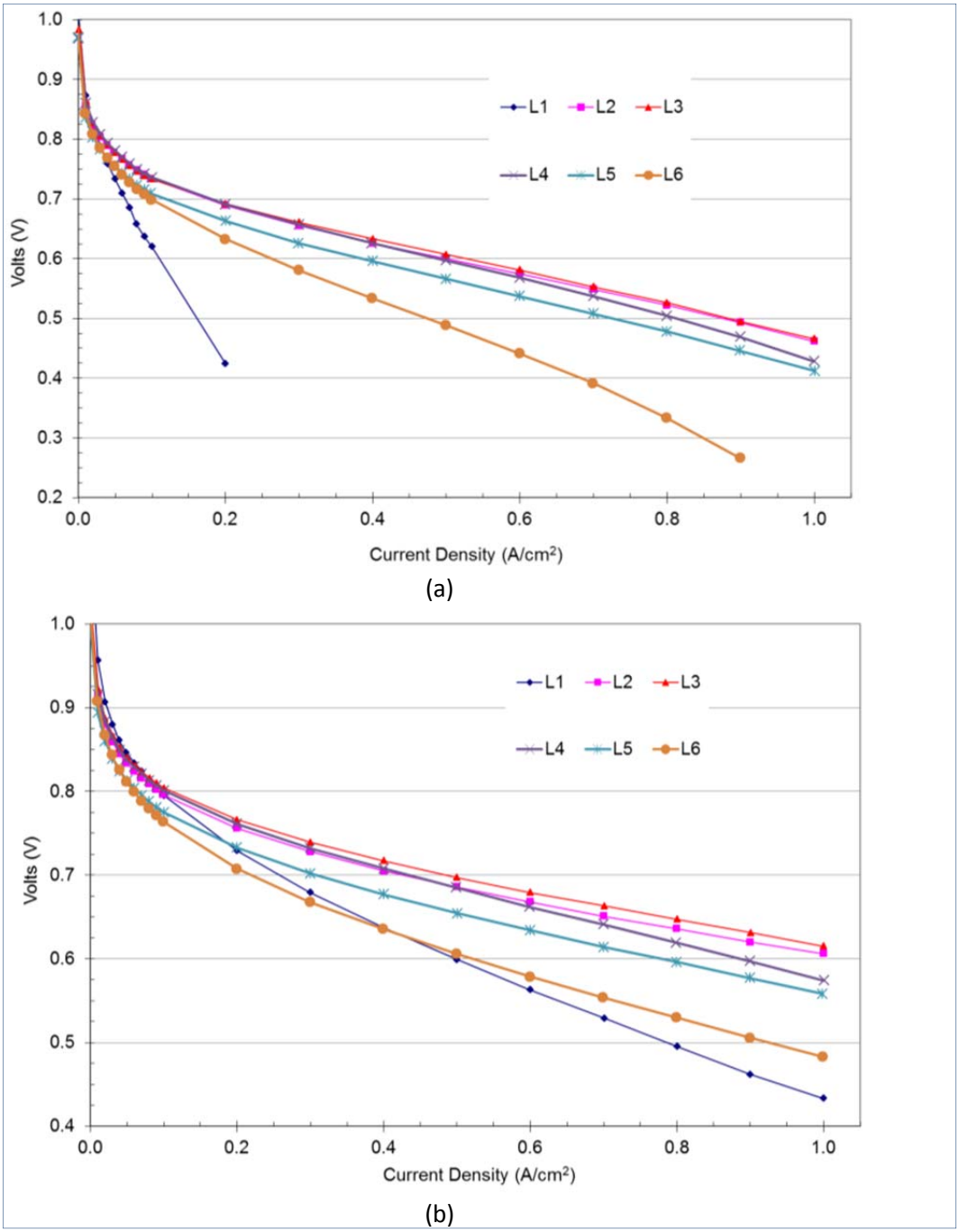

Figure 83. MEA beginning of life performance as a function of the PTFE content in cathode catalyst layer; operating conditions; (a) H_2/air at 160°C, stoich 1.2/2.0, ambient; (b) H_2/O_2 at 160°C, stoich 1.2/9.5, ambient.

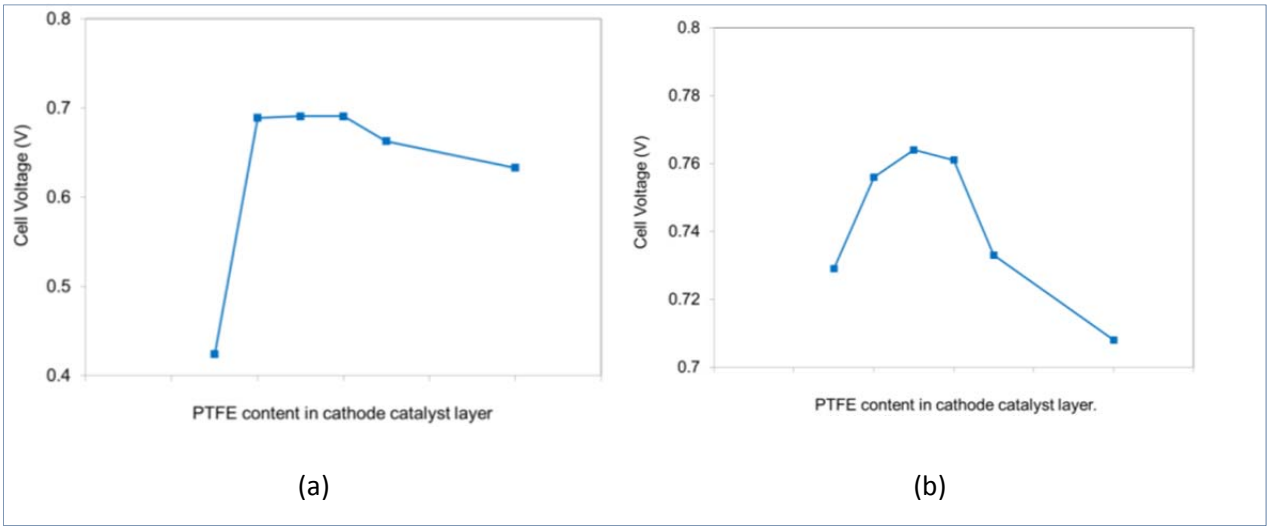

Figure 84. Impacts of the PTFE content in cathode catalyst layer on the MEA beginning of life performance at 0.2A/cm^2; operating condition: (a) H_2/air, 160^{o}C, stoich 1.2/2.0, ambient; (b) H_2/O_2 at 160^{o}C, stoich 1.2/9.5, ambient.

It turns out the PTFE content in catalyst layer greatly affects the electrode performance. The trade-off between kinetic and mass transport losses is quite clear. For example, the cathode with Level 1 (L1) PTFE content shows extremely poor performance with air oxidant. However, its catalyst utilization seems to be the highest at very low current density, e.g. less than 0.05A/cm^2.

If the PTFE content is too low, the electrode structure is not strong enough due to insufficient binder. But there is less catalyst surface blocked by PTFE. On one hand, there could be large interfacial area between catalyst and acid. On the other hand, the void volume could be greatly reduced after MEA assembly, which results in significant mass transport problem with air oxidant as show in Figure 83 (a).

More than enough PTFE not only blocks the catalyst surface, but also reduces the total void volume. Figure 83 (a) and (b) show that the cathode with Level 6 (L6) PTFE has the lowest catalyst utilization and substantial mass transport loss at high current density.

The practical operation current density for the PBI MEA should be less than 0.5A/cm^2. The optimal PTFE content is from Level 2 (L2) to Level 4 (L4). This relatively large window has great process advantages. It provides a larger tolerance for the ink scale-up quality control.

The impact of PTFE content in anode catalyst layer is similar to that in cathode. But the optimal PTFE content is slightly different. Figure 85 and Figure 86 compares the anode performance with reformate fuel and air oxidant at 180^{o}C. It turns out anodes with PTFE content in catalyst layer from L1 to Level 3 (L3) show similar performance. If the PTFE content in anode catalyst layer is increased to L4 or higher, the performance will be greatly reduced. Hydrogen transport is less likely to be the limitation for the anode. Because of the CO poisoning effect, the anode is sensitive to the active surface area. Large activated catalyst surface area is necessary for good reformate oxidation. Therefore, the anode catalyst layer with L1 PTFE content could work well. But L4 PTFE content may block too much catalyst surface, and results in low performance with the increase of current density.

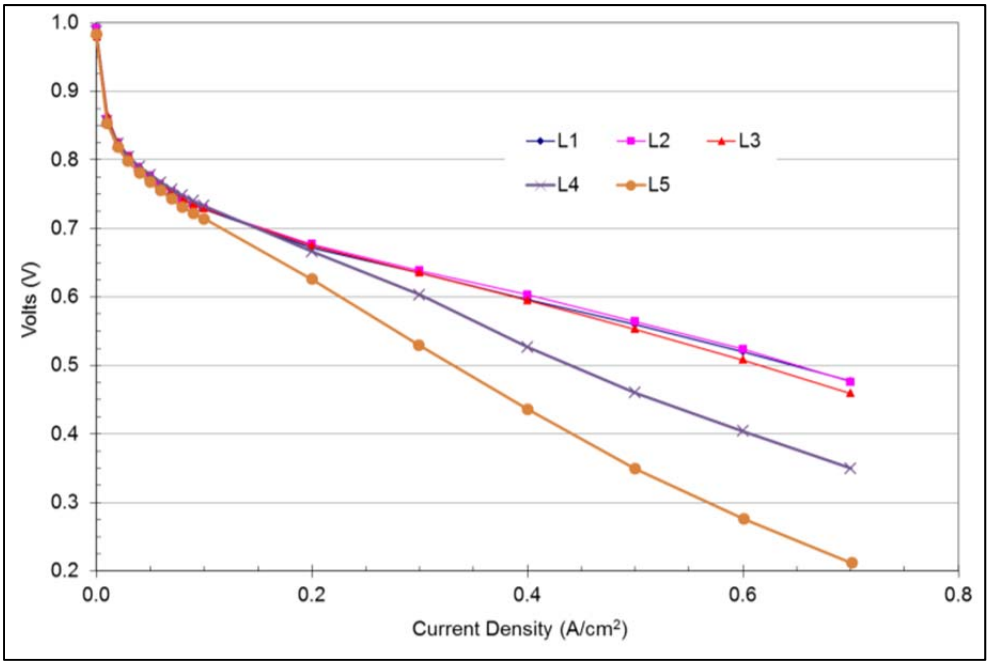

Figure 85. MEA beginning of life performance as a function of the PTFE content in anode catalyst layer; operating conditions: Reformate/air at 180°C, stoich 1.2/2.0, ambient

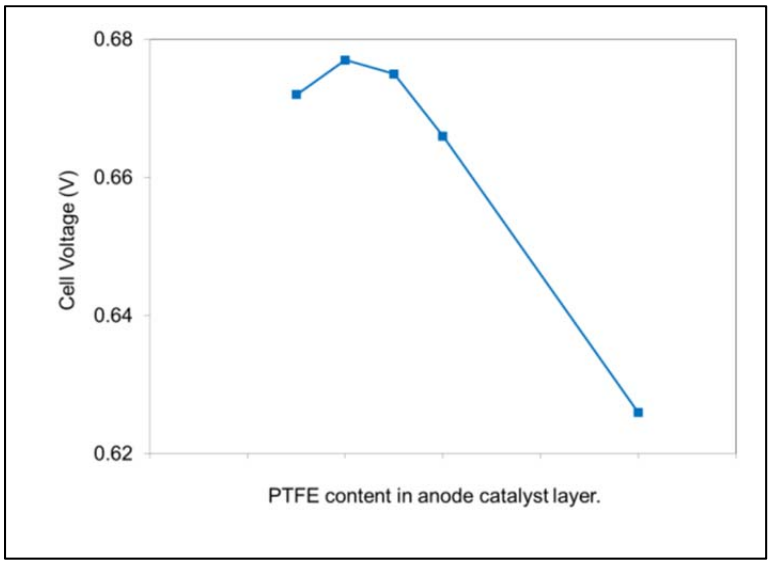

Figure 86. Impacts of the PTFE content in anode catalyst layer on the MEA beginning of life performance at 0.2A/cm^2; operating condition: Reformate/air, 180°C, stoich 1.2/2.0, ambient

It is necessary to point out the optimal PTFE content for catalyst layer is obtained from the beginning of life performance. The electrode structure could change as time progress. The life time of PBI MEA is significantly impacted by the electrolyte distribution in electrodes. It is possible the optimal window will be narrowed down by the life time test results.

(9) Membrane parameters

The three phase boundary is formed by introducing phosphoric acid into the electrode. On one hand the electrode structure has to be optimized to allow better electrolyte distribution. On the other hand, the assembly has to ensure proper amount of phosphoric acid is retained in the electrode.

The membrane contains PBI, phosphoric acid, and water. Because of the low polymer content (<5wt%) and its weak bonding with phosphoric acid, it is safe to neglect PBI when evaluating the phosphoric acid intrusion and distribution into the electrode. The optimization is designed as:

1. Assemble MEAs using membrane of same thickness, but different phosphoric acid content;
2. Assemble MEAs using membrane of same phosphoric acid content, but different thickness.

The compression level for all MEA assembly is kept the same. The typical electrode porosity is about 0.65-0.7. Calculation shows that if assuming only membrane is compressed, the thickness change of the electrode is negligible. The void volume in the electrode is more than enough to accommodate the acid and water losses from the membrane. The electrode matrix phase may be kept intact after assembly. Thus, the membrane parameters could be correlated to the volume fraction of the electrolyte in the GDE.

For series 1, the membrane acid content varies from Acid Level 1 (AL1) to Acid Level 5 (AL5). For series 2, the membrane acid content is fixed at Acid Level 3 (AL3), the thickness varies from thin to thick.

The purpose of the experiment series is to correlate the membrane properties with paper MEA performance, determine the optimal membrane parameters, and. maximize the electrode performance. Figure 87 compares the iR free performance obtained from hydrogen fuel and oxygen at 160^{o}C. It turns out the best performed MEA is the one assembled with AL3 acid content membrane. The MEAs assembled with AL4 or AL5 acid content membrane show lower catalyst utilization. Their polarization curves are parallel to that of MEA made with AL3 acid content membrane, but are about 5mV and 15mV lower respectively. On the other hand, the MEA assembled with AL1 or AL2 acid content membrane show good catalyst utilization at low current density (<0.3A/cm^2). But the performance decreases quickly as current density increased. It seems the acid distribution is good as it provides sufficient interfacial area between electrolyte and catalyst. However, the amount of acid may not be sufficient enough so the proton transport in the electrode may incur high resistance.

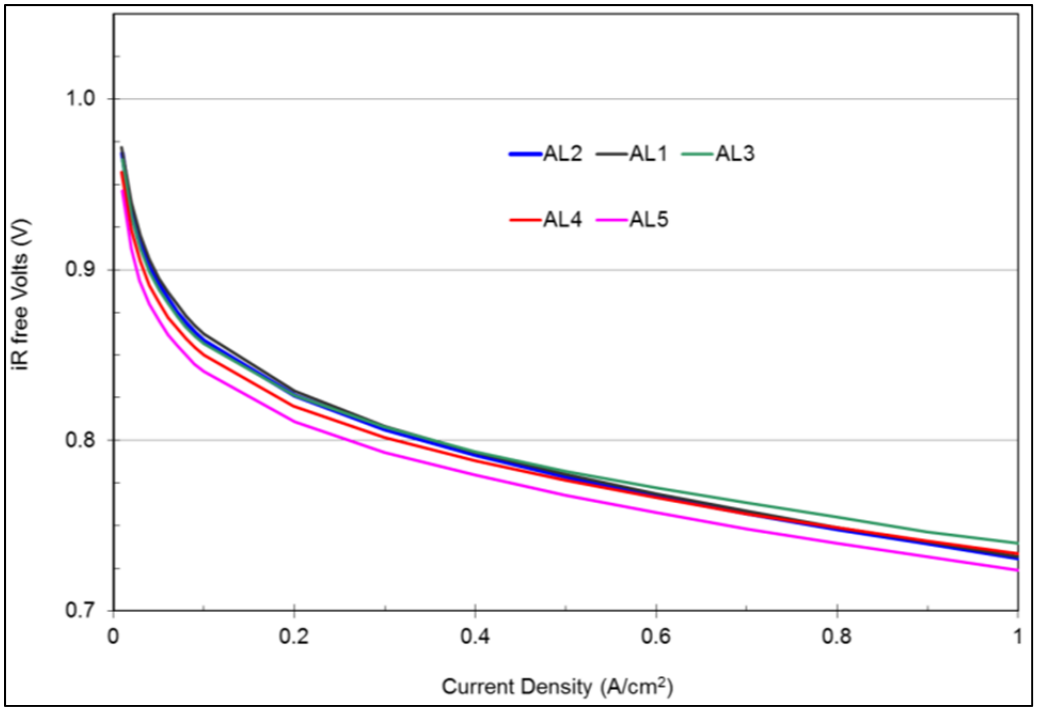

Figure 87. IR free beginning of life performance of MEA assembled with different acid content membrane; operating condition: H_2/O_2, 160°C, stoich 1.2/9.5, ambient.

We do not have techniques to quantify the amount of phosphoric acid and water in catalyst layer, MPL, and the substrate. Therefore, it is difficult to illustrate the differences in electrode structure after assembled with different acid content membranes. One would expect that assembly with high acid content membrane could introduce more acid into the electrode, thus provides more interfacial area to catalyst. However, the experiment series 1 suggests the reality may be more complicated. The inversed correlation between membrane acid content and the catalyst utilization implies there may be difficulties for MEA assembly with high acid content membrane to achieve good acid distribution in the electrode. This is probably due to the water playing an important role in the electrolyte distribution. It might also help bridge the catalyst surface and phosphoric acid molecules to activate the interfacial area. On the other hand, it seems low acid content membrane could result in a large proton transport issue. Figure 88 and Figure 89 show the polarization curves obtained from air oxidant and reformate fuel. Similar conclusions could be drawn from these curves.

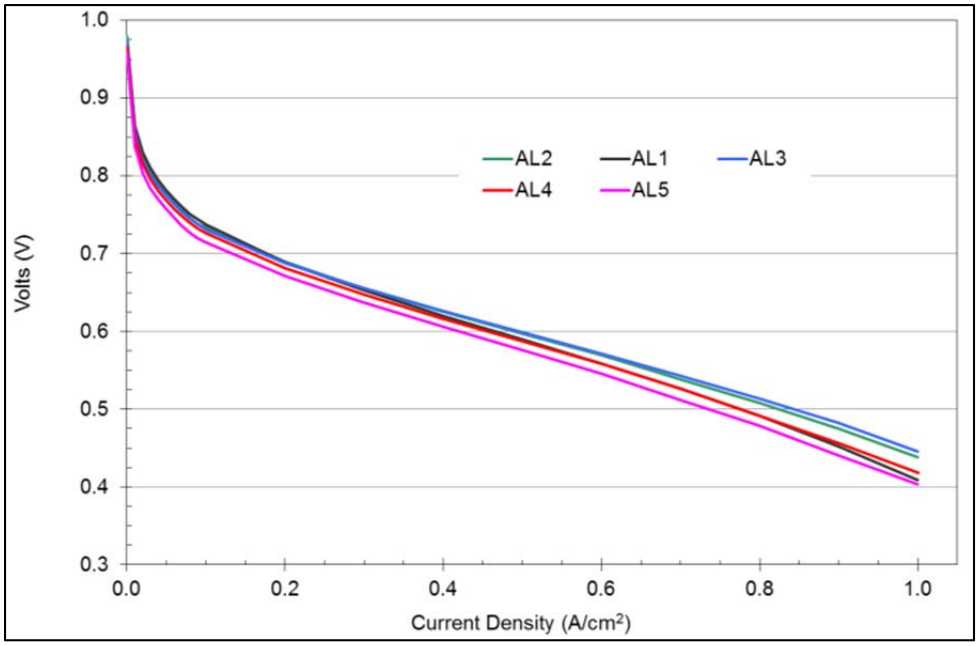

Figure 88. Impact of membrane acid content on MEA beginning of life performance; operating condition:H_2/air, 160°C, stoich 1.2/2.0, ambient

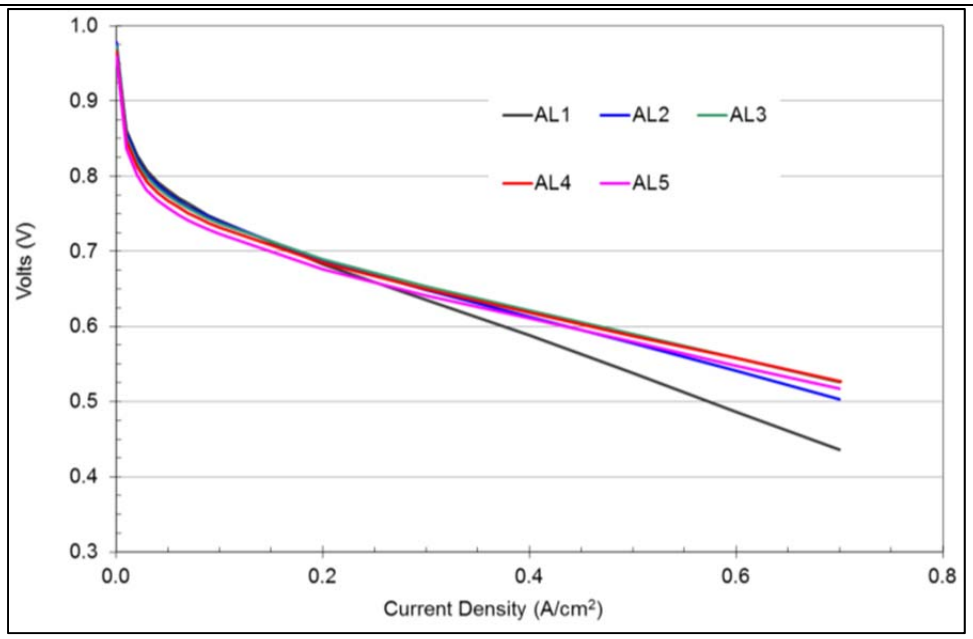

Figure 89. Impact of membrane acid content on MEA beginning of life performance; operating condition: Reformate/air, 180°C, stoich 1.43/5.0, ambient.

Based on the conclusion from experiment series 1, the AL3 acid content membranes are used in experiment series 2. Figure 90 shows the polarization curves from experiment series 2. The oxygen polarization curves seem to suggest the catalyst utilization decreases with the membrane thickness. The MEAs assembled with base membrane performs better than those assembled with thick membrane.

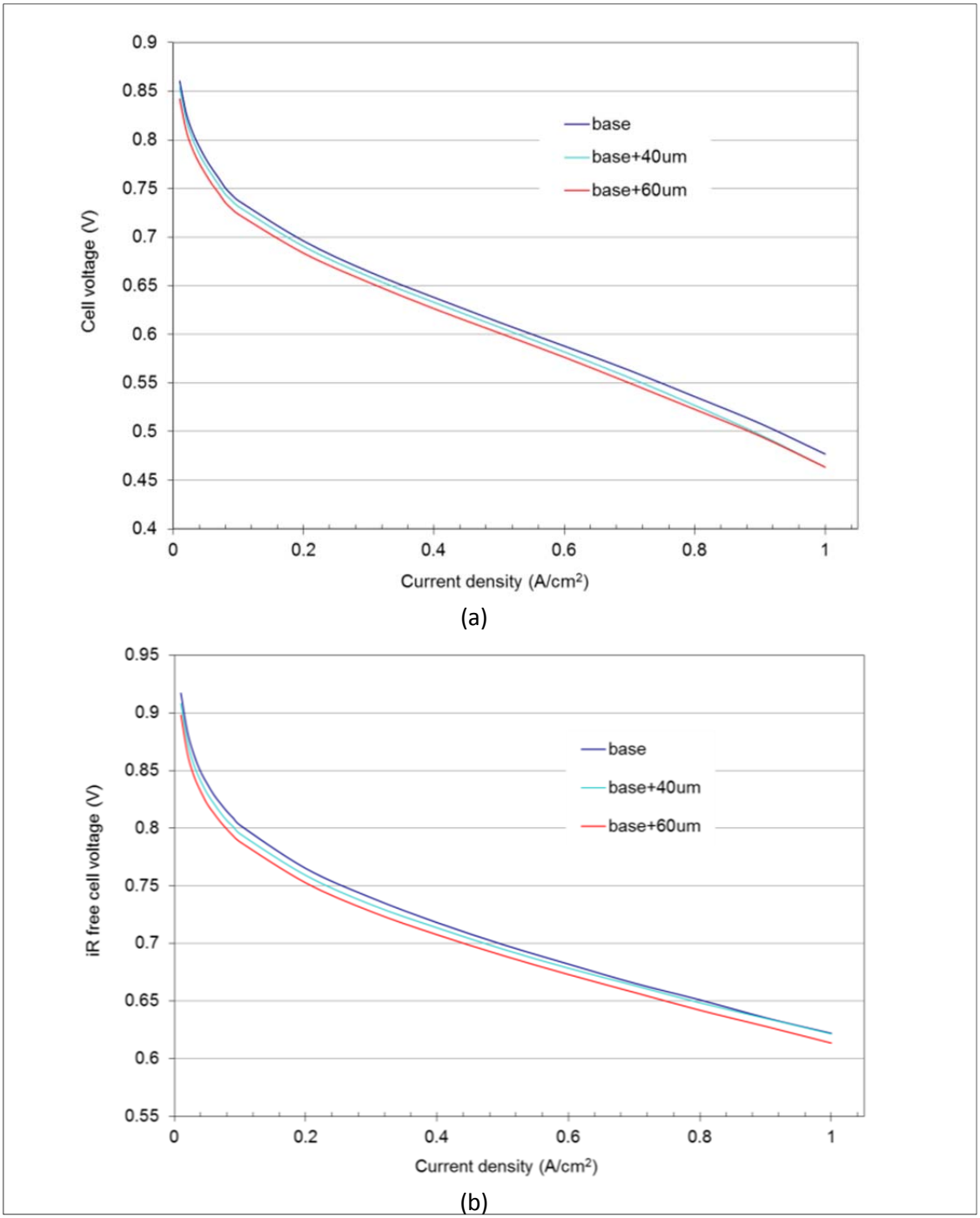

Figure 90. Impact of membrane thickness on MEA beginning of life performance ;operating conditions: (a) H_2/air, 160°C, stoich 1.2/2.0, ambient; (b) H_2/O_2, 160°C, stoich 1.2/9.5, ambient

The membrane thickness difference in experiment series 2 is relatively large compared the average catalyst layer thickness. It is reasonable to assume MEAs assembled with thicker membrane will introduce more electrolyte into the electrode. Thus the electrode could be “overdosed” with acid after assembly with base+40µm or higher membranes. Surprisingly, the excess amount of electrolyte does not increase the total area interfaces catalyst. This is different from what observed in low temperature fuel cell.

During assembly, phosphoric acid and water could penetrate the catalyst layer and enter the MPL and substrate. Such penetration is expected to start from large pores and spread into small pores. So the acid intrusion into the MPL and catalyst layer may start simultaneously. These phenomena may depend on the level of penetration. The electrolyte distribution in catalyst layer may not to be uniform. Experiment series 2 suggests such penetration has a negative impact on the catalyst layer. Again, we have difficulties to illustrate the fundamental differences in electrode structure after assembled with different membranes. We do not have enough long term data to provide insights on the electrolyte migration and how it impacts the performance.

(10) Impact of Water

We have discussed in previous section that water could play an important role in the electrolyte distribution in the GDE. In this section, we will demonstrate the water control is critical to the performance of paper based MEA.

It is well known that the PBI membrane leaches acid with the present of liquid water. In our design of the experiments, we would like to investigate if water vapor may have any negative impact on the MEA's performance and durability. In a series of experiments, the MEAs are burned-in for same duration but at different current density. Thus the MEAs have been exposed to different amounts of the water vapor after break-in. The difference in the beginning of life performance could be correlated to the amount of water it has been exposed.

The standard break-in condition is 0.2A/cm^2 constant current for 15 hours at 180^{o}C with hydrogen fuel at stoichiometry of 1.2, air oxidant at stoichiometry of 2.0. The total generated water vapor the MEA has exposed after break-in is calculated to be 1.37 standard liter /cm^2. For comparison, the break-in current has been increased to 0.6A/cm^2 and 1.0A/cm^2. The MEAs are correspondingly exposed to 3 or 5 times more water vapor during break-in.

When break-in occurs at high current density, the gas flows rates are correspondingly higher. To separate the impact of different gas flow, the reference MEAs are burned-in at standard 0.2A/cm^2 current density, but with gas flow rates equal to that of 0.6A/cm^2.

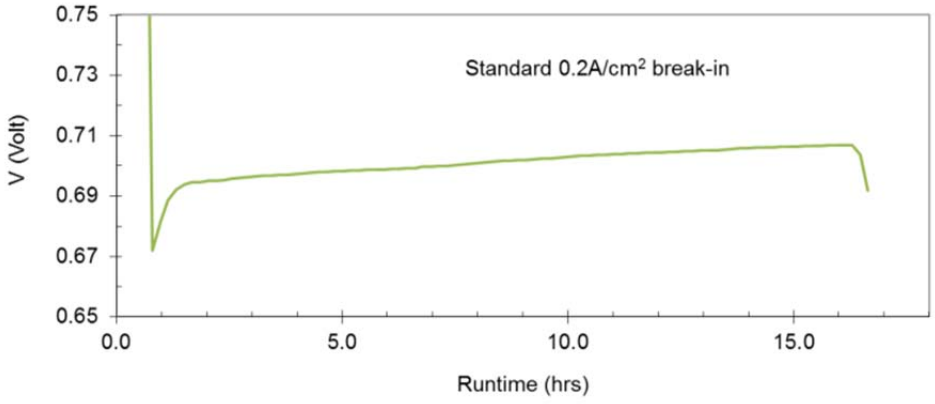

(a)

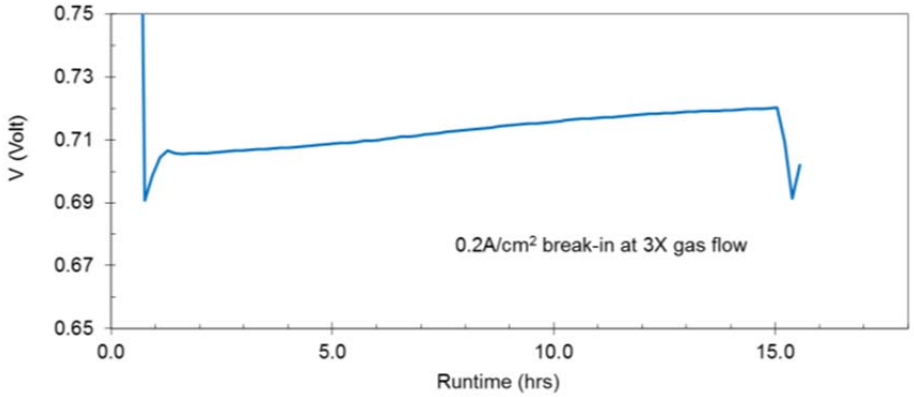

(b)

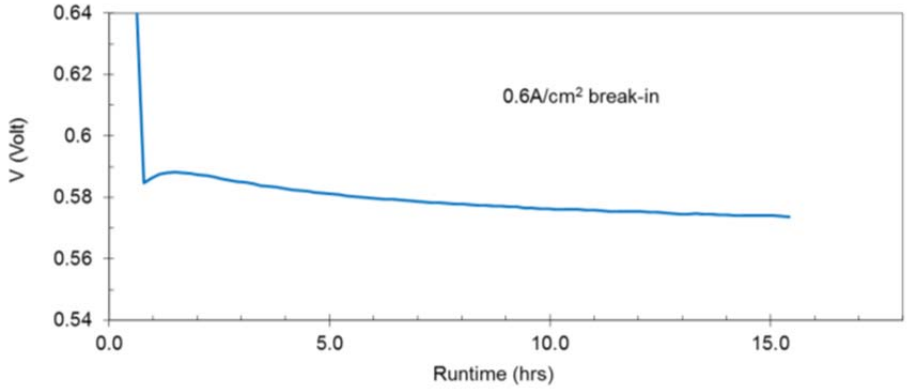

(c)

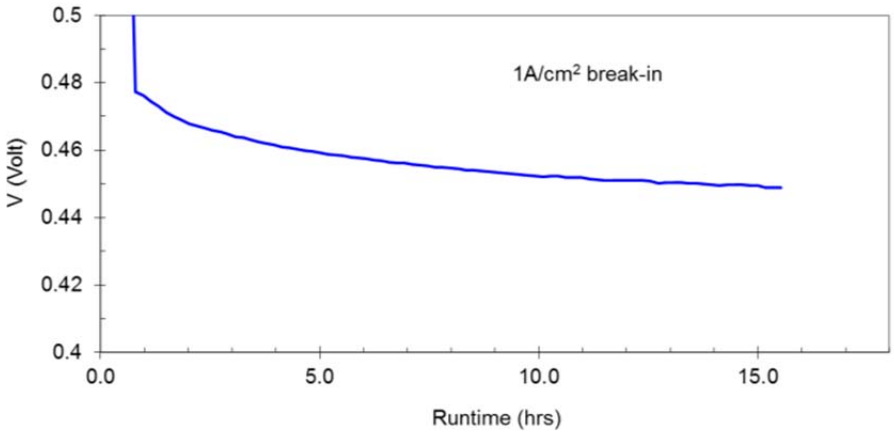

(d)

Figure 91. The MEA break-in behavior at different conditions;(a) standard 0.2A/cm^2, 180^{o}C, stoich 1.2/2.0 ambient; (b) 0.2A/cm^2, 180^{o}C, stoich 3.6/6.0 ambient; (c) 0.6A/cm^2, 180^{o}C, stoich 1.2/2.0 ambient; (d) 1.0A/cm^2, 180^{o}C, stoich 1.2/2.0 ambient.

Figure 91 shows the cell voltage response during the break-in. The break-in current density has significant impacts on MEAs break-in behavior. Figure 91(a) shows the cell voltage increases with

time, which suggests the electrode three-phase-boundary is gradually improved with the low current density break-in. The cell voltage roughly gains about 15mV after break-in. The MEA could achieve higher beginning of life performance with this break-in condition as shown in Figure 92.

Figure 91(b) shows the MEA break-in behavior at 0.2A/cm^2 current density, but with gas flow rate equal to that at 0.6A/cm^2. Its break-in behavior is very similar to that of the standard break-in. However, the MEA performs lower after break-in as shown in Figure 92. It does not show evidence of loss of catalyst utilization, as the performances at 0.1A/cm^2 or less are identical. The performance decrease rapidly with current density increased, which seem to be associated with high proton transport losses.

Figure 91(c) and (d) show different break-in behaviors at higher current densities. With 0.6A/cm^2 break-in current density, the cell voltage increases for first 30 minutes and then starts to decrease. The voltage at the end of break-in is about 15 mV lower than the peak value. The cell voltage decreases from the beginning with 1A/cm^2 break-in current density. But the rate of decrease slows down after several hours. The overall voltage loss after 1A/cm^2 break-in is close to 30 mV. The beginning of life performance after 0.6A/cm^2 and 1A/cm^2 are almost the same. Both show loss of catalyst utilization compared to that after 0.2A/cm^2 break-in.

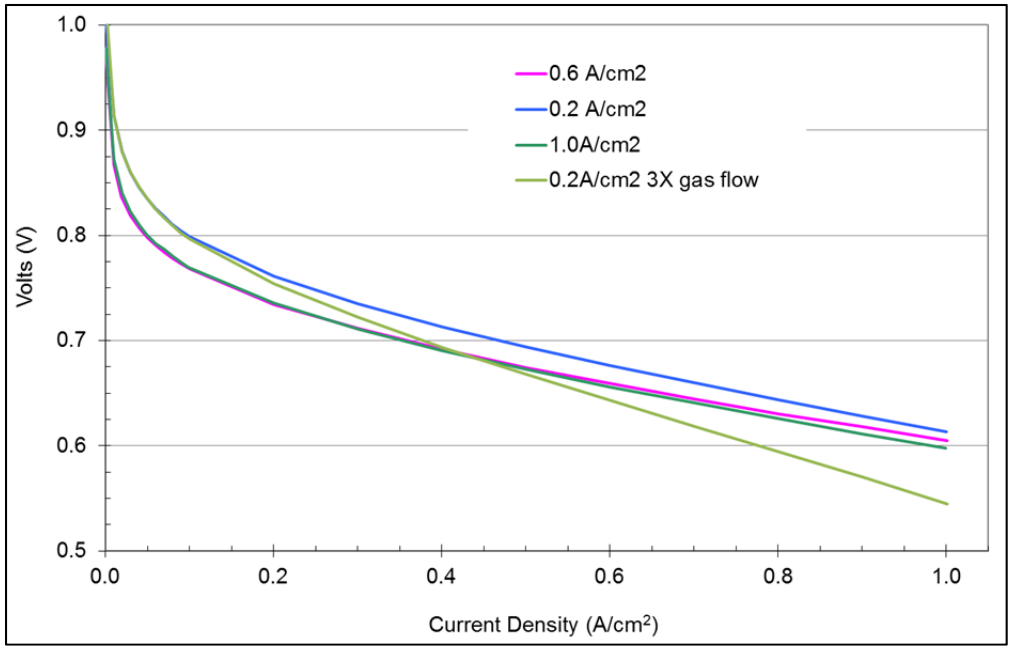

(a)

(see next page for legend)

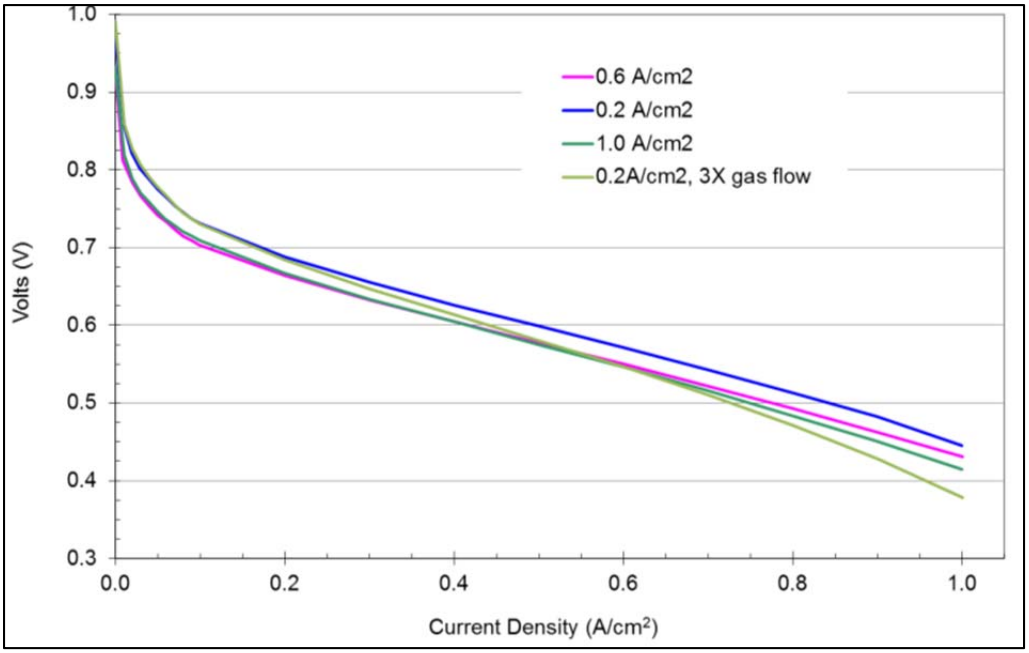

(b)

Figure 92. The beginning of life performance of MEA after different break-in conditions, operating condition: (a) H_2/O_2, 160°C, stoich 1.2/9.5, ambient; (b) H_2/air, 160°C, stoich 1.2/2.0, ambient

The water generation is proportional to the current density. Thus the break-in condition shown in Figure 91(b) could have an interface between electrolyte and the catalyst similar to the standard break-in. The change in electrolyte distribution may be negligible. However, the electrolyte in large pores may be lost at high gas flow due to low capillary pressure. Electrolyte loss in large pores results in mainly the high ionic resistance in the GDE. The polarization curve seems to indicate the typical characteristics for high ionic resistance: good catalyst utilization in the very low current density region, rapid decrease in performance as the current density increases, and no obvious mass transport losses.

Large water generation at high break-in current density could lower the phosphoric acid content in the electrolyte phase. Because the phosphoric acid is fluid, accumulated water generation may impair its interface with catalyst, which results in accelerated loss in catalyst utilization. The local low acid content electrolyte provides driving force for diffusion and electrolyte redistribution. The phosphoric anion migrates towards anode under potential, which may results in the total electrolyte loss in cathode. All results in the loss of cathode catalyst utilization. Depending on the current density, the MEA shows different performance losses after break-in. The break-in behavior, as an example, shows the impact of water on MEA. This observation supports the conclusion that a PBI system is better operated at low current density steady state conditions, which is well suited to µCHP.

(11) Remove impurities

Additives must be used in preparation of the catalyst and MPL inks. However, any additives retained in the electrode lower the electrode performance and durability. For this reason, only the more easily removed additives are selected for the ink formulation. The paper electrode is sintered

with the same program developed for cloth based GDEs. The sintering program is simulated in the thermo gravimetric analyzer (TGA) to evaluate the additive residues after sintering. The TGA weight loss is compared with the theoretical value calculated from the ink formulation. The comparison suggests a negligible amount of residues catalyst layer after sintering, but the additives used in MPL formulation may have 20-30% residue in the GDL. Since we have not seen unusual mass transport losses from the polarization curves, the sintering program is not a priority for paper electrode development.

In summary, electrolyte amount, distribution, and retention in the electrodes are no doubt the most critical part for the PBI MEA optimization. The optimization is achieved by control the electrode matrix phase and the membrane. Our data indicates that optimal electrode structure could be formed by the control of the PTFE content. But at the same time, the membrane thickness and acid content must be in a proper range. We also find the water management is critical for the MEA performance, even at its vapor form.

(12) Scale-up

The paper electrode scale-up is divided into two steps. The first step is from small scale (1m^2) to intermediate scale (5-10m^2) on the pilot coater. The second step is from the pilot coater to the production coater. Each step requires minimum of three trials. We have successfully finished the production trials of MPL coating up to 110 linear meters. Due to availability and manufacturing schedules, the catalyst coating trials on the production coater was not conducted. The large scale catalyst coating trials on pilot coater has been finished.

The scale-up of MPL has two focuses. One is to evaluate the feasibility of the scale-up. The other is to investigate the number of coating passes required for the MPL coating.

The pilot coater and the production coater use the same applicator method. But the control parameters are not completely the same. We note the coating process is quite smooth after some slight adjustment of coating parameters.

The MPL target solid loading on carbon paper is less than half of that on carbon cloth, as there are no large pores to fill up. Thus the number of coating passes can be greatly reduced. It is possible to meet the target solid loading in just one coating pass. However, since the ink penetration is in the first coat, and because the paper substrate may have the flatness issue, the surface quality is hard to compete with that from the multicoated product. Moreover, the additional drying time for a thick coating layer will force the machine to run at lower speed. Therefore, there are economic and quality trade-offs when comparing single pass verse multi pass coating. Even in economic point of view, the MPL might be better applied in a multi-coats approach.

Figure 93. MPL surface morphology of the GDL made in production coating trial; the scale bar is 1 mm

The production trials show excellent MPL surface quality and good process control could be obtained from 2 or 3 coating pass process. Figure 93 shows the surface quality of a MPL production coating trial sample. The surface is smooth, uniform, without visible surface cracks.

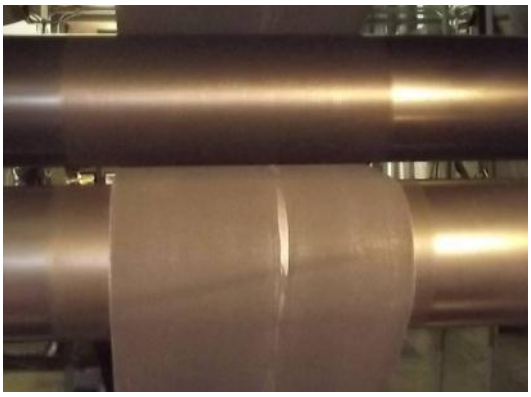

Figure 94. The typical defect of uncoated island in production trials

The uncoated island is the major defect in production trial. The production coater is not equipped with specific devices to maintain the flatness of the substrate. Such a device is not necessary for cloth due to its flexibility and softness. Most uncoated islands on paper substrate can be coated in the second coating pass. But manual adjustment may be necessary for some part of the substrate with serious flatness issue. Figure 94 shows a typical uncoated island after the first coating pass.

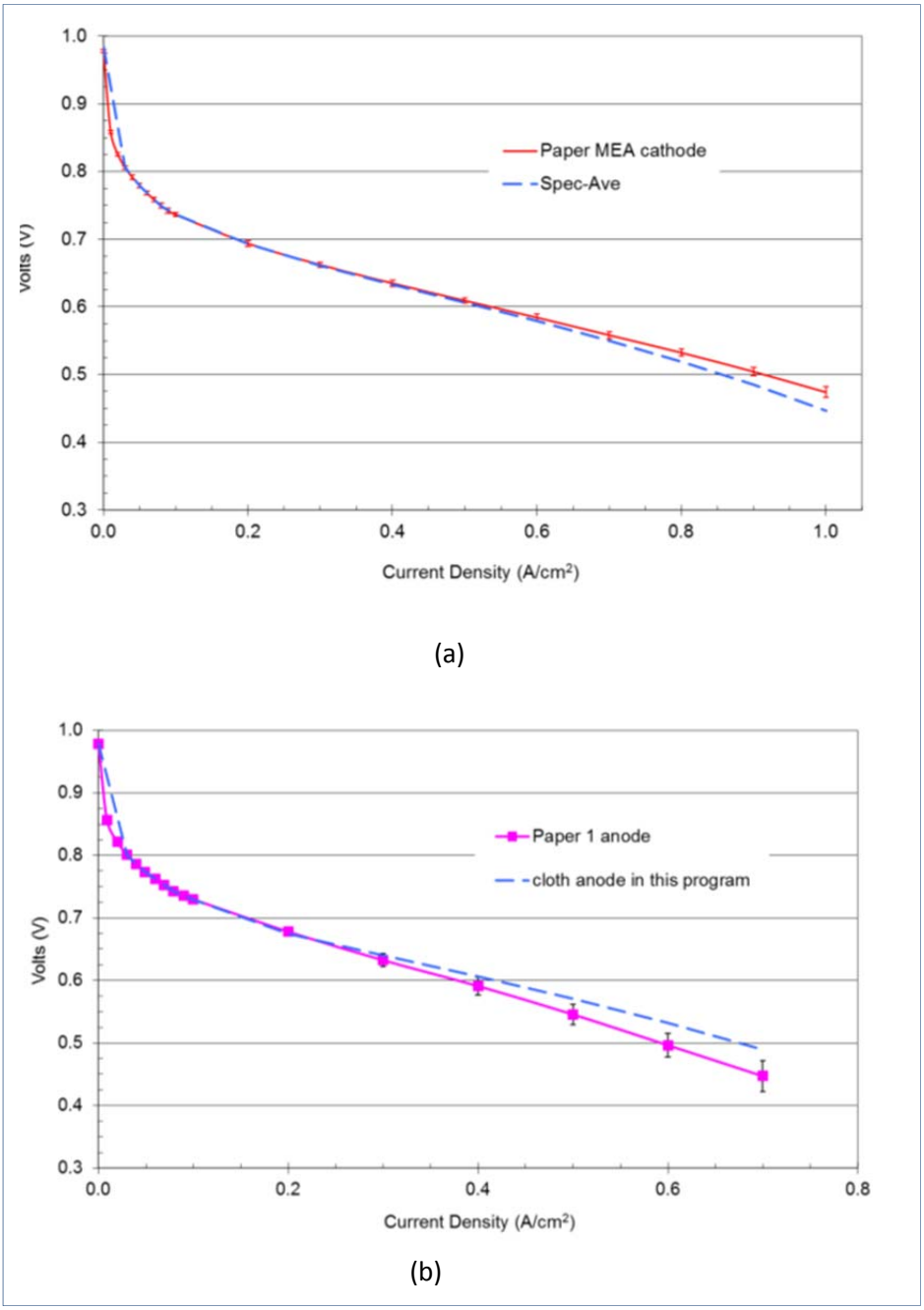

Figure 95. The average paper 1 MEA beginning of life performance.; operating conditions: (a) H_2/air, 160°C, stoich 1.2/2.0, ambient; (b)Reformate/air, 160°C, stoich 1.2/2.0, ambient

The catalyst coating scale-up is carried out on the same pilot coater. The intermediate scale can provide sufficient electrodes to prepare paper based MEAs for customer sampling. The ink batch for the intermediate scale is about 5-10 kg. We have not observed any coating issue during the scale-up. Figure 95 shows the average anode and cathode performance of the intermediate trials. The polarization curves are plotted against the best cloth materials developed in the program, which is about 30 mV higher than the pre-program cloth materials. The paper 1 based anode and cathode perform similar to the new cloth electrode from this program.

(13) Improving coating efficiency

The paper 1 based electrode has demonstrated good beginning of life performance, acceptable lifetime, and customer acceptance for fit and form of MEAs produced with this material. However, the overall coating efficiency needs further improvement.

While the coating passes for MPL is two or three, the average catalyst coating passes can be as many as six depending on the ink properties and loading requirement. It is not realistic to meet the loading target in just one or two passes with a low viscosity and easy flowing ink. However, the goal might be achievable if the ink viscosity is increased.

We have developed a high viscosity paste formulation. The paste coating has negligible amount of penetration into the substrate. Its bonding with paper 1 substrate is quite weak. However, a new substrate candidate paper 2 could form acceptable adhesion with the paste. Paper 2 is made from a different process. It has lower density and higher surface roughness than paper 1. The average pore size is about 35µm. Paper 2 is also thicker than paper 1. Figure 96 shows the beginning of life performance of paper 2 based cathode. The MPL and catalyst layer are prepared on pilot coater with ink formulations developed for paper 1 electrodes. It turns out the performance difference between paper1 and paper2 cathode is not significant. It might be eliminated with further optimization.

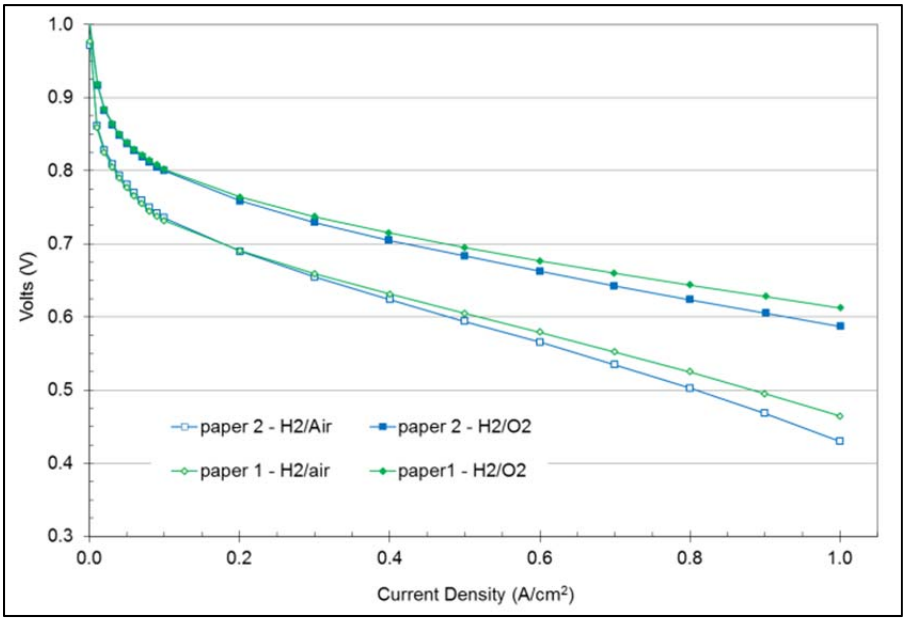

Figure 96. Comparison of the beginning of life performance of paper 1 and paper 2 based MEA. Electrodes are made from same ink formulation; operating condition: H_2/air or O_2, 160°C, stoich 1.2/2.0(air) or 9.5 (O_2), ambient

Figure 96 compares the beginning of life performance of paper 2 cathodes made from ink and paste formulations. Although the cathode made from paste formulation performs relatively lower, the difference at operation current density 0.2A/cm^2 is not big. Considering the efficiency improved by one coating pass. The trade-off might be worthwhile. Figure 97 compares the surface morphology of paper 2 cathode made from the paste formulation to the paper 1 cathode made from an ink

formulation. The surface quality of the paste cathode is not as good as that of an ink cathode. This difference is not significant.

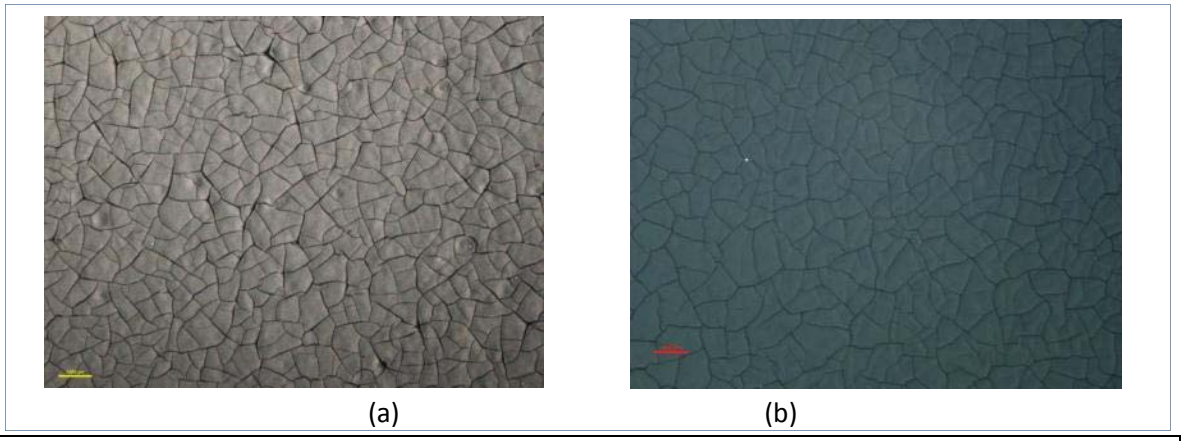

(a) (b)

Figure 97. The surface quality of paper 2 cathode made from paste formulation (a); and paper 1 cathode made from ink formulation (b); scale bar is 1 mm

We have recently implemented the corrosion resistant Pt alloy catalyst into the ink and paste formulations. The coating quality is found comparable to the cathode made with regular Pt alloy catalyst. The performance of Paper 2 cathode with corrosion resistant catalyst is plotted in Figure 98 The average performance of paper 1 cathodes and the paper 2 cathode with regular alloy catalyst are plotted as references. The paper 2 cathode with corrosion resistant catalyst performs lower than the reference, but may be still within the acceptable range. The durability performance of all paper based cathode will be discussed in durability section.

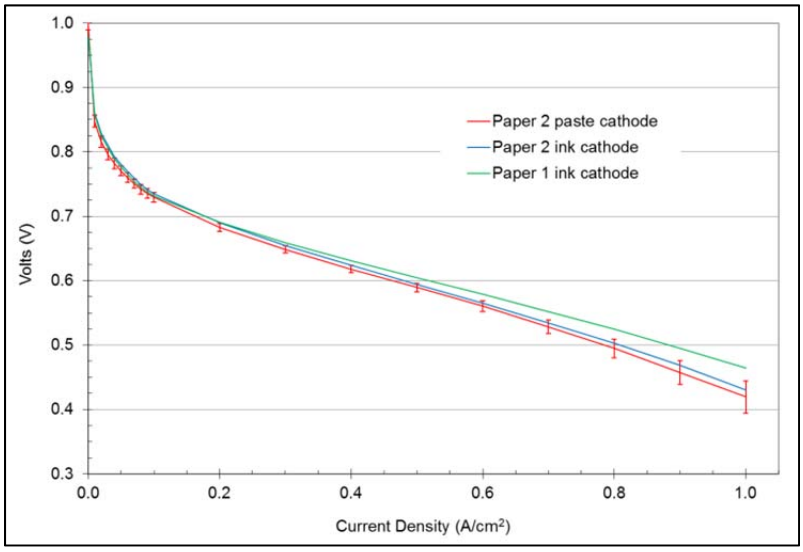

Figure 98. The beginning of life performance of the paper 2 cathode made from "single pass" paste formulation and corrosion resistant catalyst versus prior "multi pass" formulation; Paper 2 paste cathode uses corrosion resistant alloy catalyst, the reference ink cathodes use standard alloy catalyst; Operation condition: H_2/Air, 160°C, stoich 1.2/2.0, ambient

(14) Durability

There are two major degradation mechanisms for PBI based MEAs. One is from the catalyst degradation, which may be similar to those observed in low temperature fuel cells. The other is the loss of the phosphoric acid in electrode and membrane. This mechanism may be similar to those observed in the phosphoric acid fuel cells.

We use two durability test protocols to simulate the actual operation. The life time protocol is to simulate the continuous operation. The 50cm^2 single cell MEA is kept at constant current density of 0.2A/cm^2 at 160^{o}C, with hydrogen fuel and air oxidant, until the cell voltage is below the minimum requirement. The cycle test protocol is to simulate the portable application with frequent starts and stops. To start a cycle, the MEA is set at 160^{o}C, 0.2A/cm^2 with hydrogen fuel and air oxidant for 2 hours; After a short nitrogen flush, the MEA is cooled down to 40^{o}C and stay for 2 hours with no gas supply; the final step of the cycle is to heat the MEA up to 160^{o}C under hydrogen and air, in which the 0.2A/cm^2 constant current is applied after the cell temperature reaches 120^{o}C. The cycle test uses 50cm^2 single cell MEA.

The challenges for the electrodes in these two test protocols are different. In the life time test, the steady state operation condition helps the electrolyte distribution reach equilibrium. The acid loss is a gradual progress. In this mode, the impacts from the catalyst degradation can be differentiated. The cycle test is more aggressive. It combines the load cycle and the temperature cycle and puts more stress on catalyst stability and electrolyte retention. The dramatic voltage change associated with load cycling could cause the catalyst particle dissolution and redeposition, which is known as a major cause for catalyst degradation. The temperature cycle causes water condensation, evaporation, and acid dissolution. It is thermodynamically in favor of acid leaching. The MEA's electrolyte retention ability may become the overwhelming factor to survive the cycle test.

Figure 99 shows the life time performance of paper 1 cathode. The best new cloth cathode materials from this program are used as reference. Both paper 1 cathode and the cloth cathode use standard Pt alloy catalyst. We note the MPL solid loading on paper 1 is less than half of that on cloth. The pores in cloth, after filled with coating, are still larger than the pores in paper 1 substrate.

The life time data suggest that paper1 MEAs could have durability at least as good as the cloth materials if not better. Although the tests were stopped after about 3000 hour operation due to test station availability, there is sufficient data to support these conclusions.

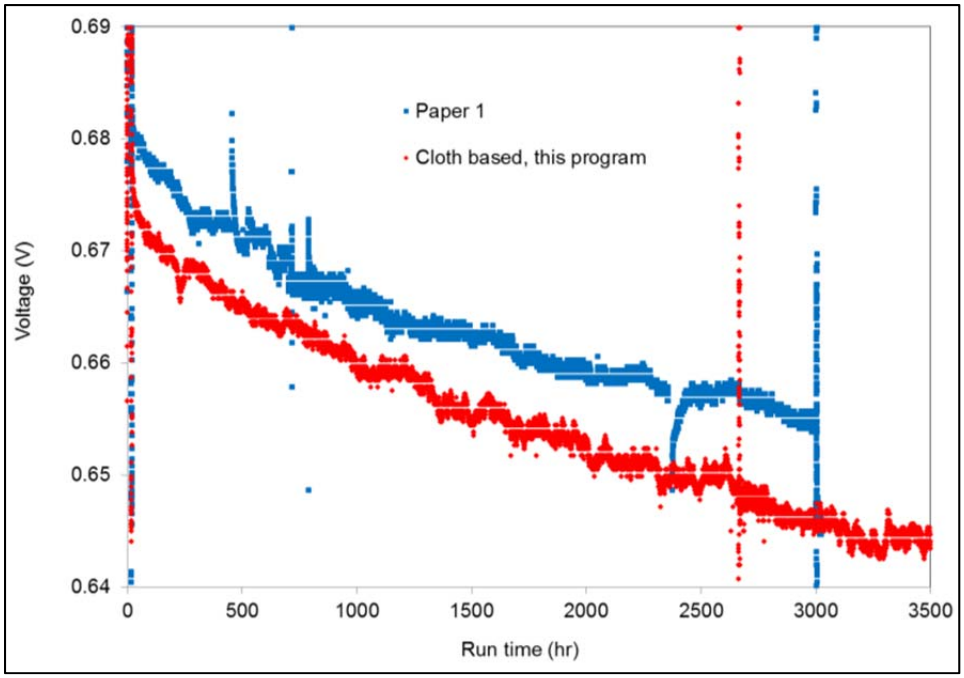

Figure 99. The life time test for paper 1 MEA; 50cm^2 MEA in a single cell hardware; operation condition: 0.2A/cm^2, H_2/air, 160^{o}C, stoich 1.2/2.0, ambient

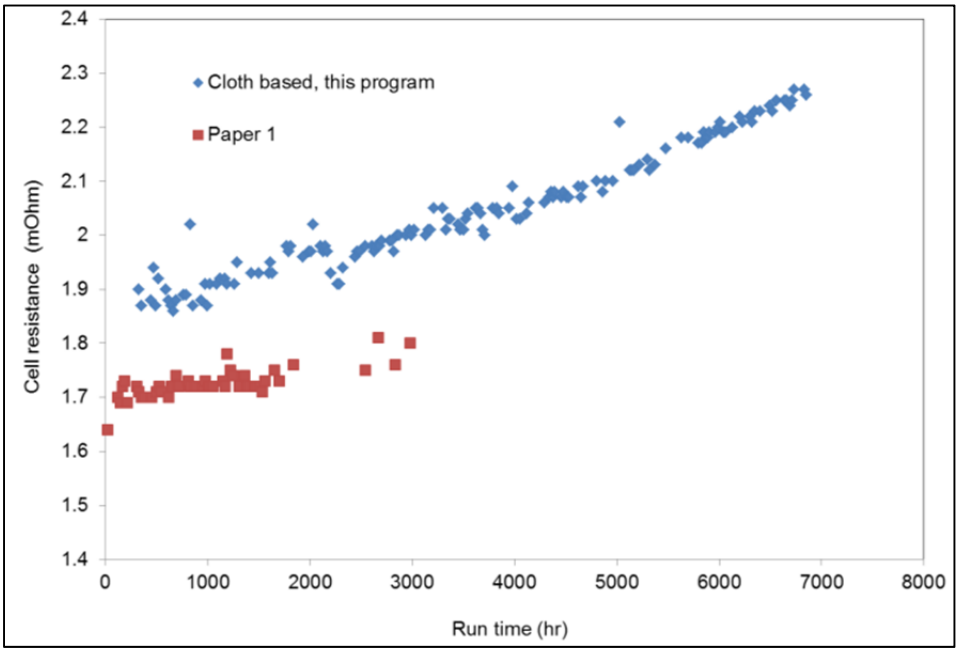

Figure 100. The paper 1 MEA cell resistance in life time test; 50cm^2 MEA in a single cell hardware; operation condition: 0.2A/cm^2, H_2/air, 160^{o}C, stoich 1.2/2.0, ambient

The cell voltage drops quickly during first few hundreds hours. This earlier stage voltage decay could be associated with the phosphoric acid dissociation and redistribution. It may also be due to an initial saturation of the bipolar plate with phosphoric acid.

Figure 100 compares the cell resistance change during the life time tests. The relatively low initial cell resistance of paper1 MEA supports that the initial decay is more electrolyte redistribution through the MEA and less outright electrolyte loss from the membrane. Although we do not have the initial cell resistance data of the particular cloth MEA used for life time test, the average value of the cloth MEAs is typically lower than the resistance monitored during the durability tests.

Paper 1 and cloth MEAs have same beginning of life performance. Figure 99 shows that Paper1 MEAs demonstrate less voltage drop during the initial few hundred hours. Such a voltage difference between Paper1 MEA and cloth MEA is maintained as time progresses. This behavior suggests that the paper1 MEA could have improved durability as both MEAs have similar voltage decay rates and that the voltage decay mechanism due to electrode structure could be fundamentally different when comparing paper to cloth based MEAs. From Figure 99 the voltage decay rate within the steady controlled period ranges is around 5μv/h.

Because the dissociation and migration of the phosphoric acid can be potential related, the equilibrium of such liquid electrolyte distribution may be sensitive. Figure 99 shows that after the accidental power loss and uncontrolled shutdown at about 2500 hours. Figure 100 shows the corresponding increase of cell resistance. Similar phenomena have been observed for the cloth MEAs during power interruption at ~2500hour and 4000 hour. In Figure 100 the paper1 MEA shows a slightly lower increase in cell resistance gain with time. Due to substrate structural differences, the paper1 electrode could have better integrity and uniformity on the micro porous layer and catalyst layer compared to the carbon cloth based MEA. This material uniformity may result in improved electrolyte distribution control. Due to the limited run time of paper1 MEA, we have not observed the accelerated cell resistance gain as in the cloth MEA. However, it is reasonable to expect the Paper1 MEA to have a better lifetime compared to the cloth one.

Figure 101 shows the life time performance of paper 2 cathode made in paste formulation with corrosion resistant catalyst. The life time performance of paper 1 cathode with regular catalyst is plotted as reference. It turns out the corrosion resistant catalyst does help the MEA's life time performance. The cell voltage decay is slowed down after about 1000 hours run time. The decay rate after 1200 hours is about 2.5μv/h, which is only half of the paper 1 cathode in the same run time period. Figure 102 shows that as the cell voltage of paper 2 cathode becomes stable after 1000 hours, the cell resistance is also stabilized. The electrolyte distribution could be very close to the equilibrium.

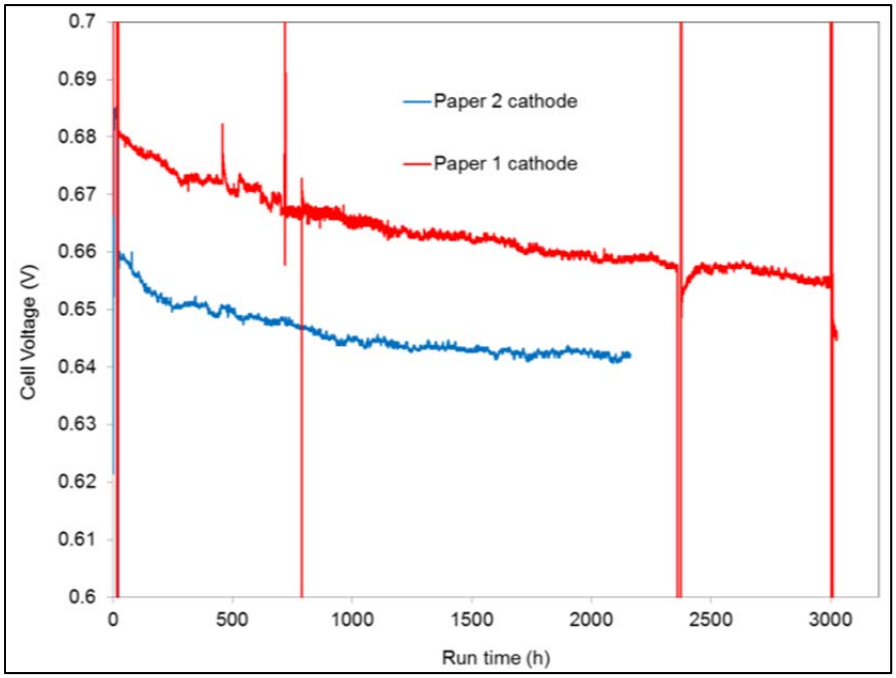

Figure 101. The life time test for paper 2 MEA;50cm^2 MEA in a single cell hardware; operation condition: 0.2A/cm^2, H_2/air, 160^{o}C, stoich 1.2/2.0, ambient; the paper 2 cathode was made by paste approach with corrosion resistant alloy catalyst; the paper 1 cathode was made by ink approach with standard alloy catalyst

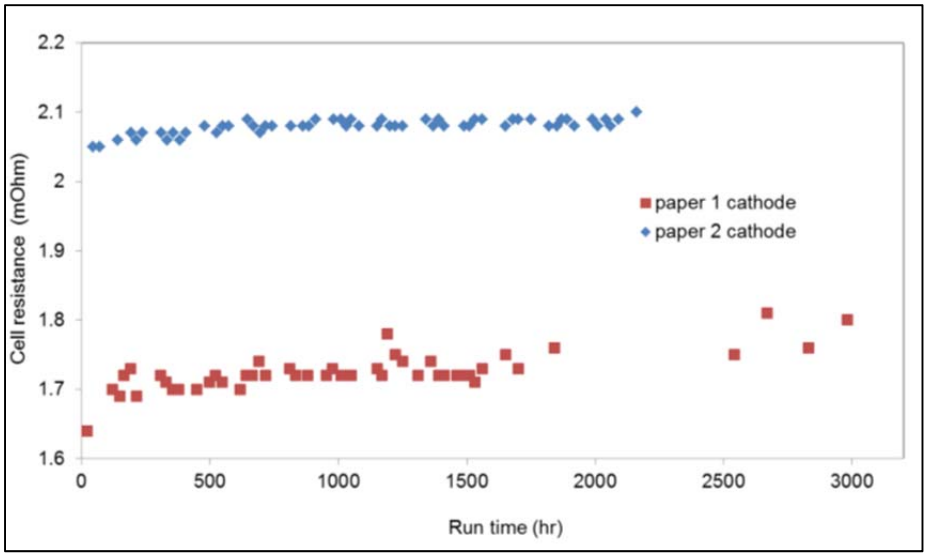

Figure 102. The paper 2 MEA cell resistance in life time test;50cm^2 MEA in a single cell hardware; operation condition: 0.2A/cm^2, H_2/air, 160^{o}C, stoich 1.2/2.0, ambient; the paper 2 cathode was made by paste approach with corrosion resistant alloy catalyst; the paper 1 cathode was made by ink approach with standard alloy catalyst

Paper 1 cathode decay rate becomes stable after about 600 hours. But paper 2 cathode needs more than 1000 hours to reach steady state. It is not clear why paper 2 cathode needed longer time to reach the equilibrium. It is also not clear why the benefit of corrosion resistant catalyst has not been observed in the first 1000 hour operation. According to the life time plot in Figure 33, paper 1 and paper 2 are almost parallel before paper 2 cathode is stabilized.

The electrode structure could be the reason for different stabilization time. Mercury porosimetry indicates paper 1 and paper 2 cathodes have different pore structure in the catalyst layer and MPL. For better comparison, the pore volume in substrate has been subtracted, only the pore volume generated by coating is plotted in Figure 103. In both electrodes, most pore volumes with small pore radius are in catalyst layer only. The pores in MPL for both electrodes are larger. It is clear that the catalyst layer and MPL in paper 2 cathode have a narrower pore size distribution. Paper 1 cathode has a broader pore size.

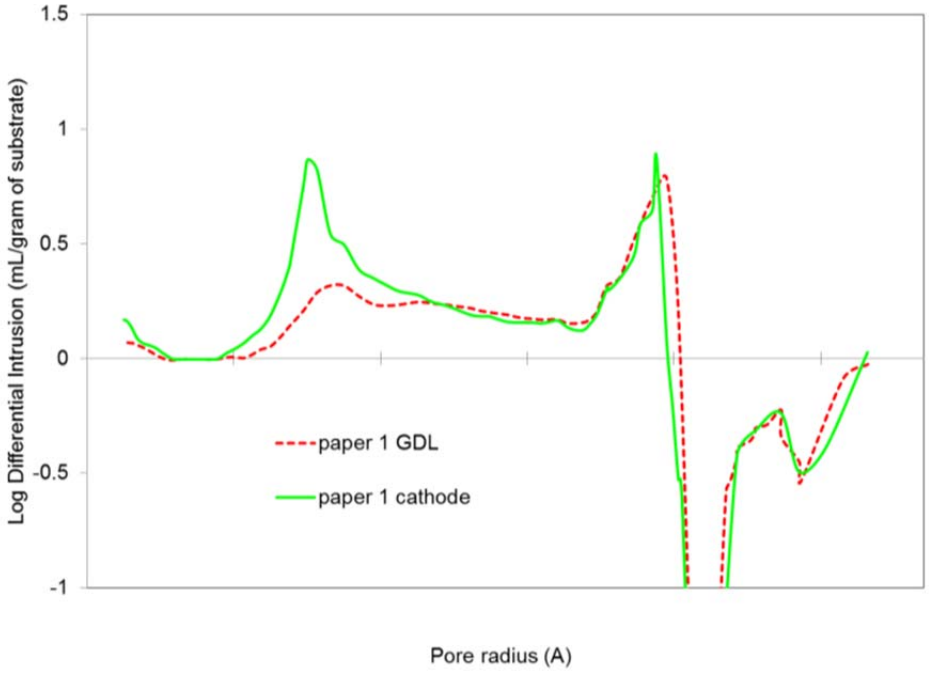

(a)

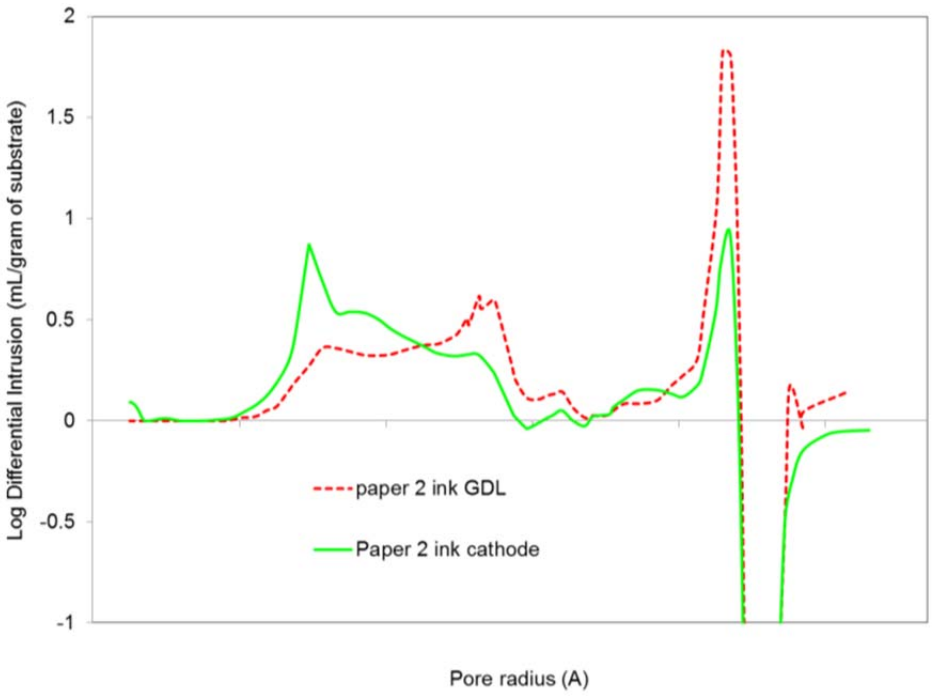

(b)

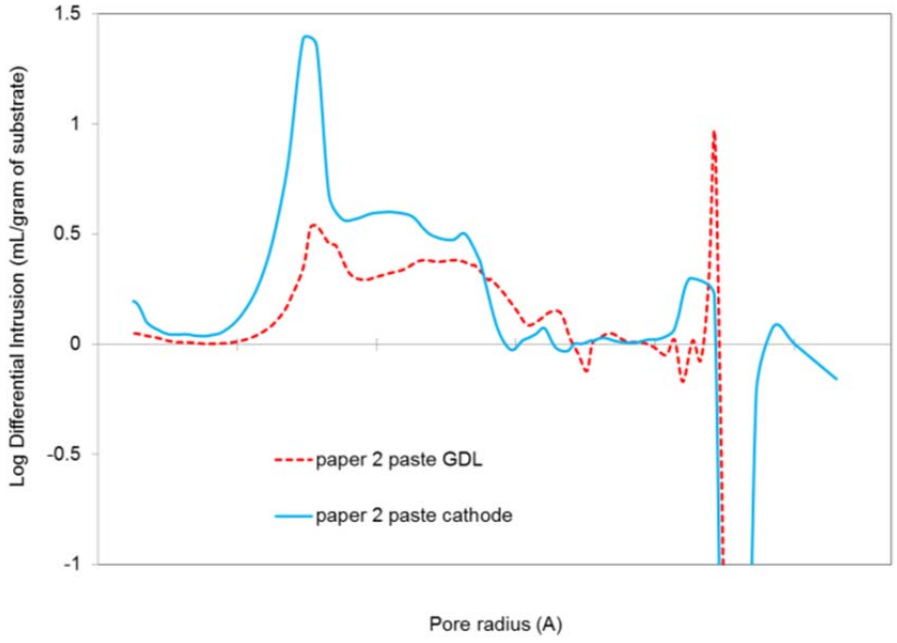

(c)

Figure 103. The pore structure and volume gains for paper 1 and paper 2 substrates after the MPL and the catalyst layer coating;(a) paper 1 substrate with ink MPL and catalyst layer coating; (b) paper 2 substrate with ink MPL and catalyst layer coating; (c) paper 2 substrate with paste MPL and catalyst layer coating.

The catalyst particle has a hydrophilic surface. This makes the pores formed in catalyst layer less hydrophobic. On the other hand, the more graphitic carbon and PTFE makes the pores formed in MPL more hydrophobic than pores in either catalyst layer or the substrate.

By comparing the pore distribution of MPL and the catalyst layer, one can conclude that the intermediate pores in paper 1 cathode are mainly from the MPL, and are almost unchanged after catalyst layer coating. They could function as a hydrophobic barrier in the electrode that prevents the electrolyte from leaving the neighboring smaller and less hydrophobic catalyst pores. Their hydrophobicity might also facilitate the water transport through these pores. Thus helps stabilize the electrolyte distribution in the electrode.

Paper 2 cathode does not contain any intermediate pores from MPL after catalyst coating. It may have more catalyst pores in direct connect with large pores. These less hydrophobic large pores have compromised the ability to prevent the electrolyte from leaving the small catalyst pores. Therefore, the electrolyte loss through the large pores may be easier. The electrolyte distribution may approach equilibrium with more difficulties.

Figure 104 shows the paper 2 cathodes performance decay during the cycle test. The paper 2 ink cathode is made with ink formulation developed for paper 1 with regular Pt alloy catalyst. The paper 2 paste cathode is made from the paste formulation with corrosion resistant Pt alloy catalyst. The cloth cathode from this program is also plotted as reference. Only the cell voltage at $0.2A/cm^2$ 160^oC is plotted to illustrate the performance decay.

As discussed above, the cycle test is more aggressive test protocol. Therefore, its performance at $0.2A/cm^2$ show higher decay rate. The decay rate for paper 2 ink cathode is about 350μv/cycle or 50μv/hr (each cycle takes 7 hours). This rate is similar to that of the cloth cathode from this program. However, the paper 2 paste cathode with corrosion resistant catalyst performs poor in cycle test. Its decay rate is as high as 910μv/cycle or 130μv/hr. Figure 103(b) show the pore structure of paper 2 ink cathode. The paper 2 ink cathode has considerable amount of hydrophobic intermediate pores . These pores may greatly improve the electrode's ability to hold the electrolyte under temperature cycling. As mentioned above, the paper 2 paste electrode does not have an effective hydrophobic barrier in its structure. Its poor electrolyte retention ability is well highlighted in the cycle test.

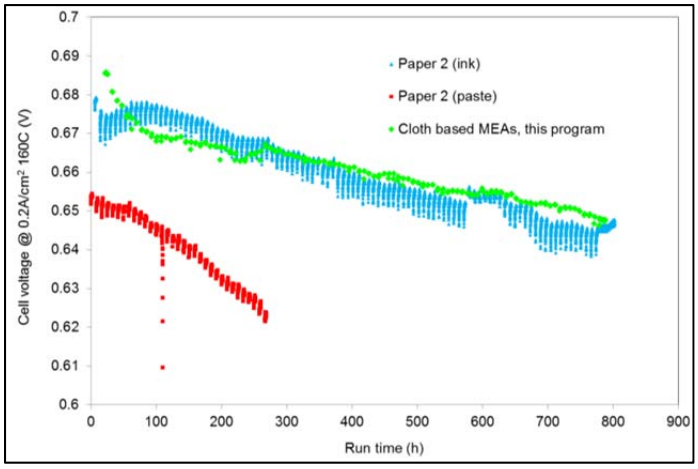

Figure 104. The paper 2 cathode performance at 0.2A/cm2 160oC in cycle test;50cm^2 MEA in a single cell hardware; the paper 2 paste cathode was made with corrosion resistant alloy catalyst; the paper 2 ink cathode and the cloth based cathode were made with standard alloy catalyst

In summary, we have seen the durability of paper 1 and paper 2 electrodes made with ink formulation are as good as the best cloth based MEAs developed in the program. However, the paper 2 electrode made from paste formulation has a different structure. Such differences greatly impair the electrode's ability to hold the electrolyte.

(15) Overall summary for paper GDE development

We have developed complete solutions for carbon paper based gas diffusion electrode production. The paper 1 based electrode has demonstrated good beginning of life performance, good lifetime performance, and received positive feedback in customer sampling. The scale-up trials show it has potential to be produced at lower cost than current cloth based electrode. The ink approach and formulation can be transfer to other substrates. We have shown the paper 2 based electrode made with this formulation show similar beginning of life performance and good cycle test performance.

We have also developed the paste approach for paper based electrode. The paste approach allows the coating to be finished in "single pass". But the electrode structure still needs optimization.

Creating a specification based on six-sigma methodology

As part of the overall objective of this work, we developed a specification based on six-sigma methodology to support the release of a new product. The gas diffusion electrodes for the Celtec® P1100W, released in March of 2012, are partially based on the improvements made in this program. A manufacturing specification was created whereby multiple tests (>250) on anode and cathode coatings on the carbon cloth were performed, and then averaged. The variation is calculated, and lower and upper limits of three sigma are set based on this reference set of materials. Figure 105 is a summary plot showing the +/-three sigma limits. When new cathode materials are fabricated, an average (of three to five fuel cell tests) is plotted against the average reference line in Figure 105 as

well as a two-sigma variation. A cathode gas diffusion electrode is passed when the average-two sigma of the test material is greater than the average-three sigma of the reference material. The same methodology is used for anode gas diffusion electrodes. This principal is illustrated in Figure 106 and Figure 107. In Figure 106, one notes the average performance of this batch of cathode is above the lowest cut off (dotted line), yet, when the variation is considered there will be a fraction of the material that will fall below the minimum based on the variation after 0.6A/cm^2. Thus, this material is considered not acceptable since some of the material is beyond the six-sigma limit. In Figure 107, one notes the average trace for this batch of cathode is only slightly below the specification average line but more importantly, the variation is very small throughout the polarization curve so the material as a whole is well above the cut-off dotted line. Figure 108 is the reference curve for anodes. By using this average minus two sigma criterion, we are utilizing both an absolute value (average of test material must be comparable to the average of the reference material) and the variation of that material as guides to quality. This way, material that is passing based on average values may actually fail if the coating is not uniform and has high variation (Figure 106 example). The +/- three sigma curves shown in Figure 105 and Figure 108 show substantially less variation then the prior P1000 product that has served as a benchmark in this program. The high variation of P1000 led to substantial rejection of material in order to "cherry pick" materials that perform reasonably in our customer's systems. The cut-off lines of Figure 105 and Figure 108 represent our manufacturing capability.

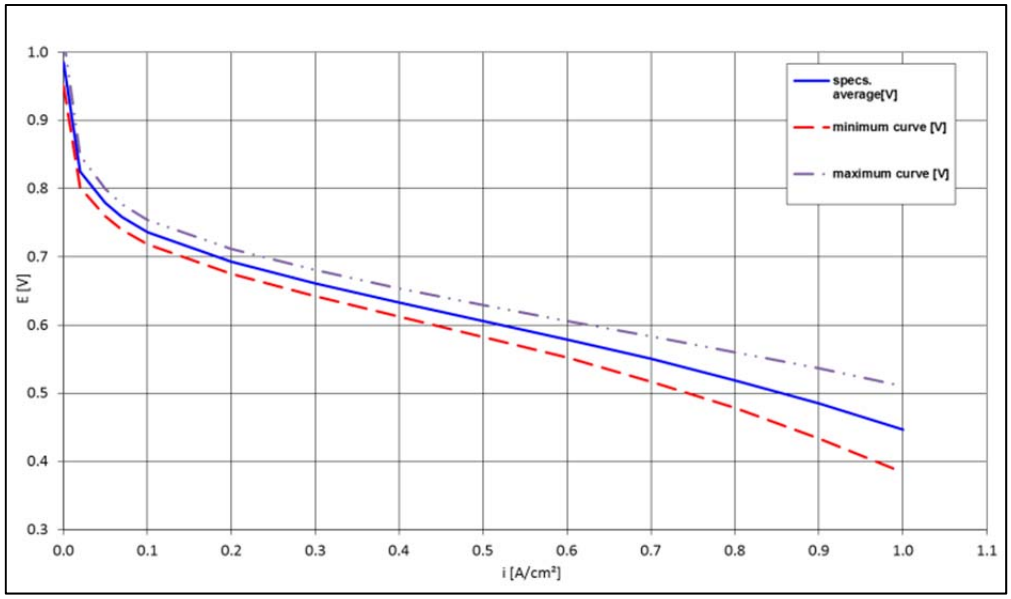

Figure 105. Cathode reference plot showing six sigma (+/-three sigma), n=250, T=160°C pressure=1 bar$_a$, stoich: 1.2/2

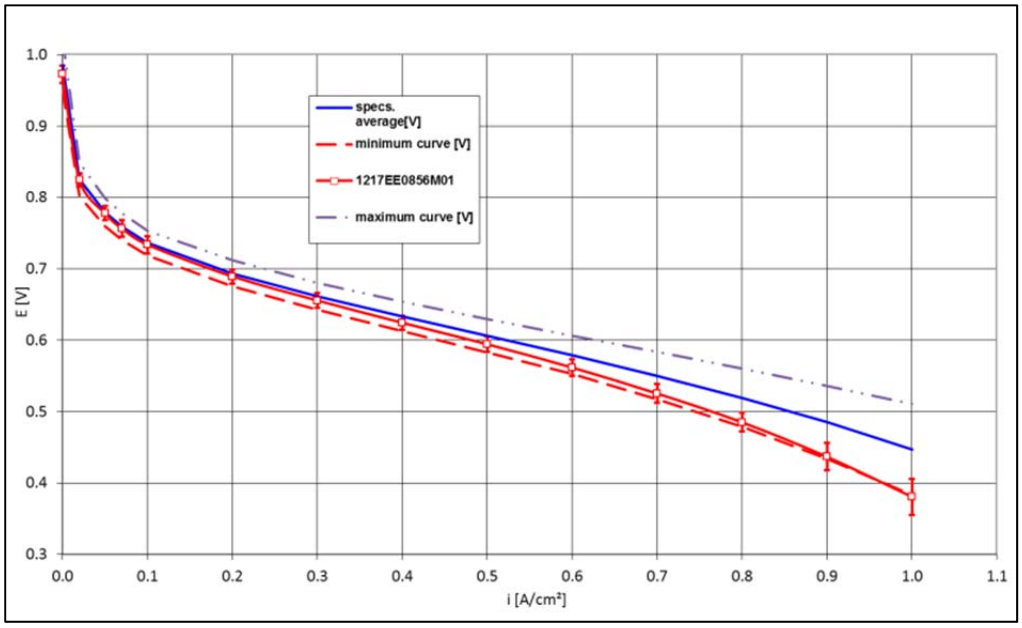

Figure 106. Example of "rejected" material due to lower bars of variation being below minimum curve at >0.6A/cm^2. Error bar is +/-2σ. Same operating conditions as Figure 105.

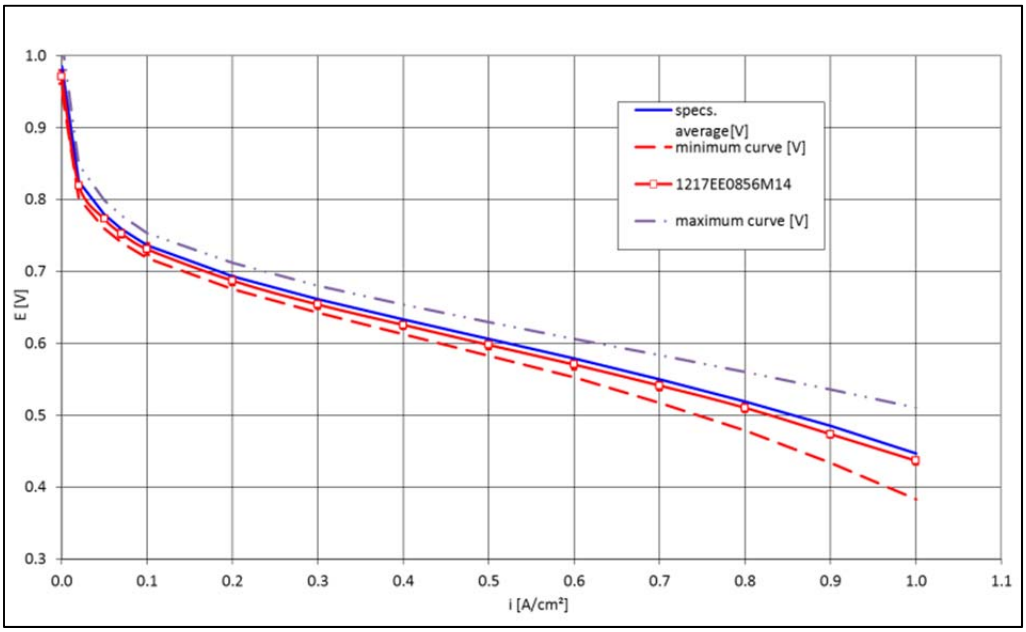

Figure 107. Example of "accepted" material due to lower bars of variation being above minimum curve. Error bar is +/-2σ. Same operating conditions as Figure 105.

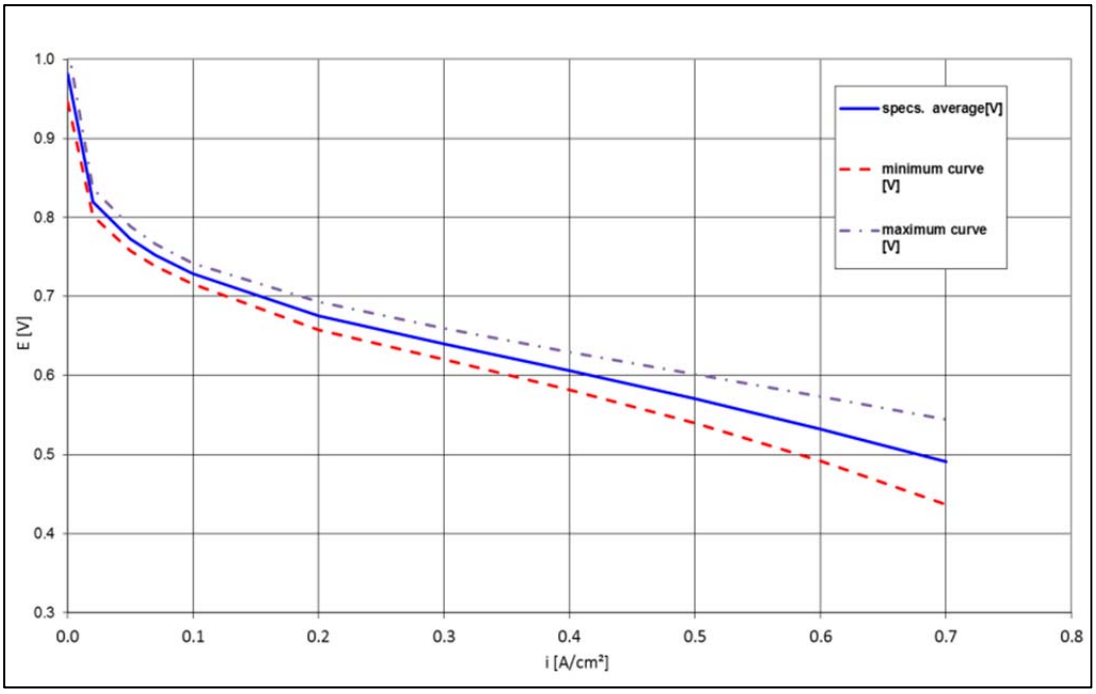

Figure 108. Anode reference plot showing six sigma (+/-three sigma), n=250, T=180°C Pressure =1 bar_a, Ref/air stoich: 1.2/2. Reformate = 70% H_2, 2% CO, 28% CO_2

Conclusions and Future Directions

We have achieved DOE's milestone 1.6 for direct coating of catalyst on gas diffusion media, and exceeded our program goal of three fold improvement in material throughput for carbon cloth based media. This improvement has led to a 75% reduction in labor cost to manufacture and produced very uniform, lower defect materials. A well-received new product (Celtec® P1100W) was launched based on this program. Through the gain in our understanding of formulating these materials in aqueous suspensions, we developed a new set of inks (MPL, anode catalyst, cathode catalyst) for use on carbon paper substrates and project an additional 30% savings over that achieved with cloth substrates. The development of an on-line X-ray fluorescent scanning instrument for measuring catalyst applications on gas diffusion media meets DOE milestone 1.1 - continuous in-line measurement for MEA component fabrication.

New Product Release

In March of 2012, BASF Fuel Cell launched a new high temperature membrane electrode assembly based on the cloth substrate materials developed in this program. This new product is called Celtec® P1100W. Customer response has confirmed our findings – namely that the MEAs are more uniform, higher quality, and consistently deliver higher power.

Special Recognitions & Awards/Patents Issued

1. 2013 DOE Hydrogen and Fuel Cells Program R&D Award for reducing the cost of manufacturing gas diffusion electrodes (May Annual Merit Review).

Publications/Presentations

Joerg Belak, "Improved Membrane Electrode Assemblies for High Temperature PEM Fuel Cells." ACS Meeting (Division of Polymer Chemistry): Advances in Materials for Proton Exchange Membrane Fuel Cell Systems, Feb. 17 - 20th, 2013, Asilomar Conference Grounds, Pacific Grove, California.

Collaborations

During the development of materials in this program, BASF Fuel Cell developed several collaborations. They are summarized here.

- ClearEdge Power: testing full scale materials developed in this program at the stack (5kW) level for uCHP applications.
- X-ray Optical Systems: although initially a subcontractor, the staff at XOS also provided high resolution XRF maps of GDEs that contained induced defects. This activity was not part of the sponsored program.
- NREL: BASF Fuel Cell provided both membrane and GDE materials for NREL's defect detection program.

Acronyms

GDE	Gas Diffusion Electrode
GDL	Gas Diffusion Layer
MEA	Membrane Electrode Assembly
MPL	Microporous Layer
µ-CHP	micro-Combined Heat and Power
XRF	X-ray Fluorescence

References

[1] L. Xiao, H. Zhang, E Scanlon, L.S. Ramanathan, E-W Choe, D. Rogers, T. Apple and B.C. Beniecewicz: "High-Temperature Polybenzimidazole Fuel Cell Membranes via a Sol-Gel Process", *Chem. Mater,* 17, pp. 5328-5333 (2005)

[2] T.J. Schmidt and J. Baurmeister: "Properties of High-Temperature PEFC Celtec®-P 1000 MEAs in Start/Stop Operation Mode", *Journal of Power Sources*, 176, pp.428-434 (2008)

[3] Q. Li, R He, J-A Gao, J. O. Jensen, and N. J. Bjerrum, *J. Electrochem. Soc.*, 150, pp.A1599-1605 (2003)

Financial Summary

Quarter	From	To	Estimated Federal Share of Outlays	Actual Federal Share of Outlays	Estimated Recipient Share of Outlays	Actual Recipient Share of Outlays	Cumulative
3Q09	7/1/2009	9/30/2009	223,295	223,295	120,236	120,236	343,531
4Q09	10/1/2009	12/31/2009	158,380	158,380	85,281	85,281	587,192
1Q10	1/1/2010	3/31/2010	133,299	133,299	71,776	71,776	792,267
2Q10	4/1/2010	6/30/2010	164,336	164,336	88,488	88,488	1,045,091
3Q10	7/1/2010	9/30/2010	150,012	150,012	80,776	80,776	1,275,878
4Q10	10/1/2010	12/31/2010	133,297	133,297	71,775	71,775	1,480,950
1Q11	1/1/2011	3/31/2011	212,341	212,341	114,337	114,337	1,807,628
2Q11	4/30/2011	6/30/2011	95,077	95,077	51,195	51,195	1,953,900
3Q11	7/1/2011	9/30/2011	116,837	116,837	62,912	62,912	2,133,650
4Q11	10/1/2011	12/31/2011	101,415	101,415	54,608	54,608	2,289,673
1Q12	1/1/2012	3/31/2012	87,418	87,418	47,071	47,071	2,424,161
2Q12	4/1/2012	6/30/2012	54,298	54,298	29,238	29,238	2,507,697
3Q12	7/1/2012	9/30/2012	58,892	58,892	31,712	31,712	2,598,301
4Q12	10/1/2012	12/31/2012	27,824	27,824	14,982	14,982	2,641,106
1Q13	1/1/2013	3/31/2013	14,793	14,793	7,965	7,965	2,663,864
2Q13	4/1/2013	6/30/2013	167,813	167,813	90,361	90,361	2,922,037
FINAL	7/1/2013	9/30/2013	7,999	7,999	4,307	4,307	2,934,344
TOTALS			**1,907,324**	**1,907,324**	**1,027,020**	**1,027,020**	